PSFC/RR-98-2

Introduction to Gas Discharge Plasma Physics: Lecture Notes

S. I. Krasheninnikov

Five lectures given at
Independent Activities Period
January 1998

Plasma Science and Fusion Center
Massachusetts Institute of Technology
Cambridge, Massachusetts 02139 USA

This work was supported by the US Department of Energy, Grant No. DE-FG02-91ER54109. Reproduction, translation, publication, use, and disposal, in whole or in part, by or for the US Government is permitted.

Important Note:

This document serves as "notes" for the participant, rather than as a formal presentation of research findings. As such, many of the pages are askew and illegible.

Introduction to Gas Discharge Plasma Physics*

Sergei Krasheninnikov

MIT Plasma Science and Fusion Center

(Notes of the lectures given on January 27-30, 1998 during IAP at the MIT Plasma Science and Fusion Center)

Abstract

The basic physics of gas discharge plasmas, including atomic processes, electron kinetics, waves and instabilities, and chemical reactions are considered.

* Sponsored by the MIT Plasma Science and Fusion Center and Nuclear Engineering Department.

Lectures outline

L1. Introduction and atomic processes in weakly ionized plasmas

L2. Electric breakdown of a gas and steady state gas discharges

L3. Electron and vibrational kinetics in non-equilibrium plasmas

L4. Waves and instabilities in gas discharge plasmas

L5. Plasma-chemical processes in non-equilibrium weakly ionized plasmas

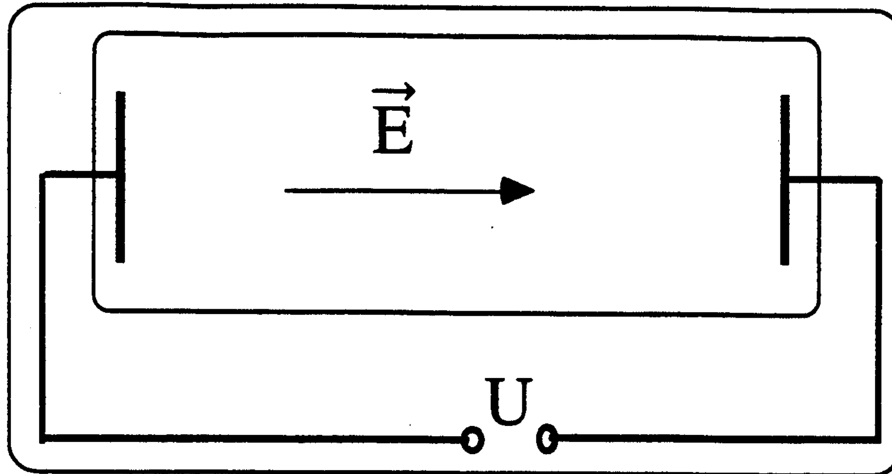

$$m\frac{d\vec{v}}{dt} = -e\vec{E} + (\text{collisions})$$

$$\frac{d\, mv^2/2}{dt} = -e(\vec{E}\cdot\vec{v}) + (\vec{v}\cdot(\text{collisions}))$$

- Gaining the energy from electric field electrons can start to ionize neutrals ⇒ rapid increase in plasma density ⇒ electric breakdown of gas ⇒ gas discharge
- However, what is the role of collisions?

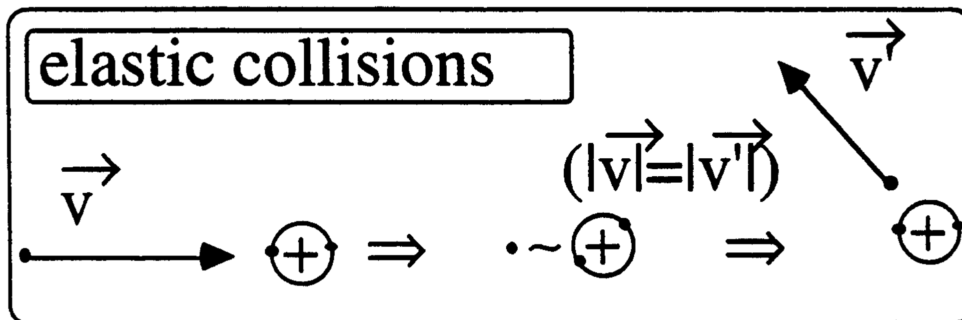

- Energy gain, ε_E, between elastic collisions:

$$\left\langle \frac{d\left(mv^2/2\right)}{dt} \right\rangle = -e\left\langle\left(\vec{E}\cdot\vec{v}\right)\right\rangle \equiv -e\left(\vec{E}\cdot\vec{V}_E(t)\right)$$

$$\vec{V}_E(t) = -e\vec{E}\,t/m$$

$$\varepsilon_E \equiv \delta\left\langle mv^2/2\right\rangle = -e\int_0^{\tau_{col}}\left(\vec{E}\cdot\vec{V}_E(t)\right)dt = \left(eE\tau_{col}\right)^2/2m$$

- Energy loss, ε_{loss}, due to elastic collisions

$$\varepsilon_{loss} \sim \varepsilon_T(m/M) << \varepsilon_T \equiv \left\langle mv^2/2\right\rangle$$

- From energy balance, $\varepsilon_E = \varepsilon_{loss}$, we find

$$\varepsilon_T \sim (M/m)\varepsilon_E >> \varepsilon_E; \quad V_E << V_T = \sqrt{\varepsilon_T/m}$$

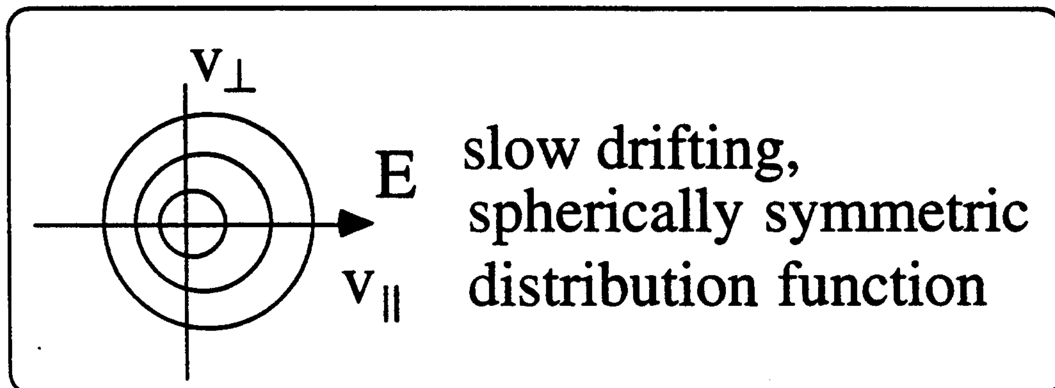

- $\tau_{col} \approx \lambda_{col}/v_T \approx 1/(N\sigma_{el}v_T)$, σ_{el}=?
- Polarization interaction of electron with a neutral particle

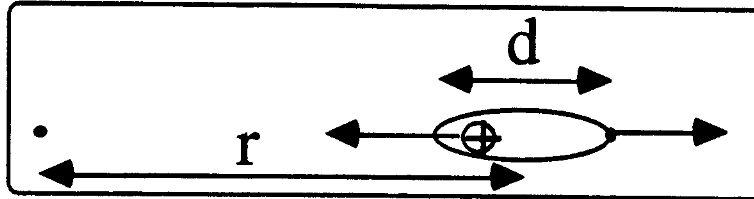

$$d = \tilde{\alpha}E \equiv \alpha\left(r_b^3/e\right)E$$

here α is dimensionless parameter and $E \approx e/r^2$

α:	4.5	1.4	160	14	7
Atom:	H	He	Li	C	N

- Electron-atom interaction potential at large r

$$\varphi_{e-A}(r) \approx e^2 d/r^2 \approx \alpha\varepsilon_b(r_b/r)^4, \quad \varepsilon_b = e^2/r_b = 27 \text{ eV}$$

- Estimates for σ_{el} and $\sigma_{el}v_T$

$$\varphi_{e-A}(r_{el}) \sim \varepsilon_T \Rightarrow \sigma_{el} \approx \pi(r_{el})^2 \approx \pi(r_b)^2\sqrt{\alpha\varepsilon_b/\varepsilon_T}$$

$$\sigma_{el}v_T \approx \pi(r_b)^2\sqrt{\alpha 2\varepsilon_b/m} \approx 10^{-7} \text{ cm}^3/\text{s}$$

- However, in practice there are also inelastic collisions of electrons with neutrals and ions, e. g.

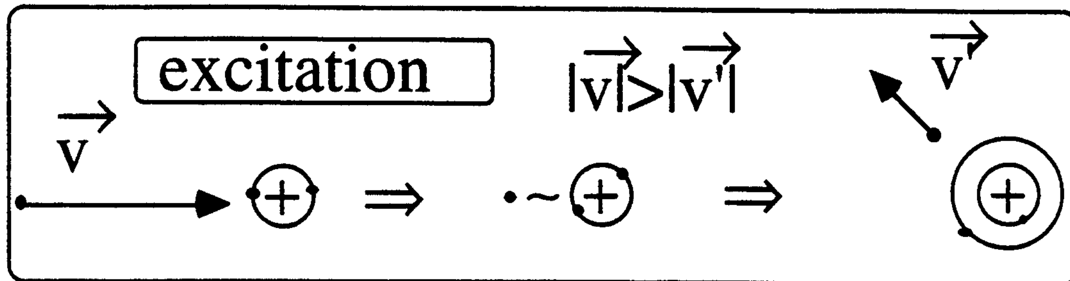

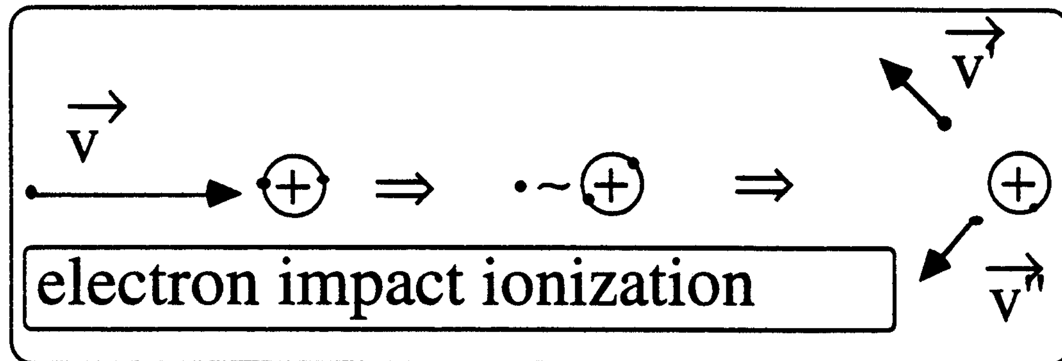

- For these processes $\varepsilon_{loss} \sim 10$ eV >> $\varepsilon_T(m/M)$ and in practice they are determining ε_T and neutral ionization, excitation and other plasma-chemical processes

I. Atomic processes in gas discharge plasmas

i. Elastic collisions

- Usually $\sigma_{el}(v)v \approx 10^{-7}\ cm^3/s$, $\sigma_{el} \approx 10^{-15}\ cm^2$ for ~ 1-10 eV electrons (less for helium)
- However, for some cases $\sigma_{el}(v)$ has a strong non-monotonic velocity dependence in some velocity range

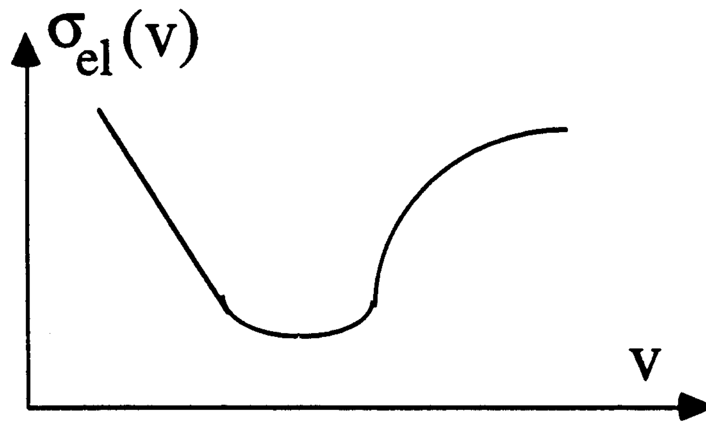

- This behavior is caused by Ramsauer's effect

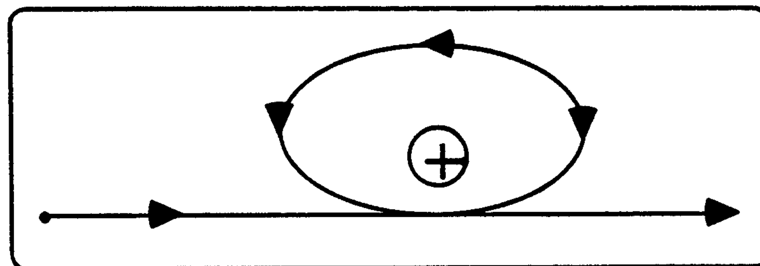

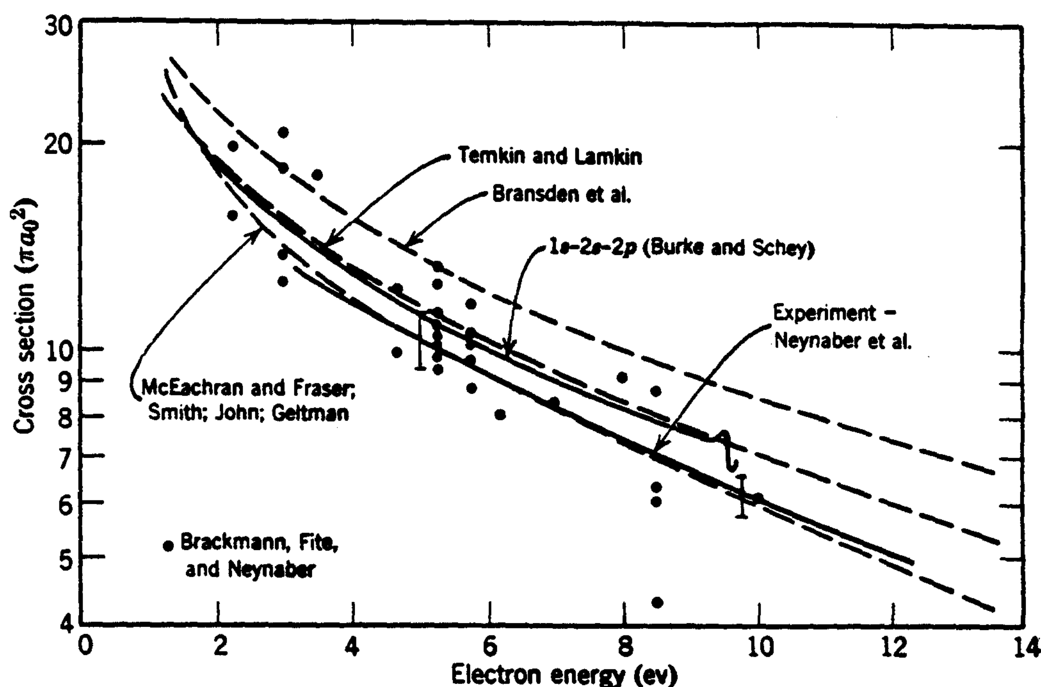

FIG. 4-1-9. Elastic scattering cross sections for electrons on atomic hydrogen, takei from the paper by Burke and Schey.[29] The experimental data of Neynaber and hi co-workers[20] refer to elastic scattering only at electron energies below the first excitatioi energy of the hydrogen atom, 10.15 ev. The solid dots denote cross sections compute by Neynaber et al. from measurements by Brackmann et al.[21] The remaining dat represent the results of theoretical calculations: Bransden, Dalgarno, John, an Seaton[23] employed a variational calculation containing both *s*- and *p*-wave scatterin; Temkin and Lamkin[24] calculated *s*-, *p*-, and *d*-wave scattering by the method of polarize orbitals. McEachran and Fraser,[25] Smith,[26] and John[27] employed numerical methoc with exchange approximations (see end of Section 4-4). Geltman[28] used a variation: method in which a trial function allowed for the virtual excitation of the 2*s* and states. Burke and Schey[29] utilized a close-coupling approximation in which the tot wave function is expanded in hydrogen eigenstates, and only terms corresponding the 1*s*, 2*s*, and 2*p* states are retained. Note the resonance at 9.61 ev shown on the cur of Burke and Schey. For a general discussion of the scattering of low-energy electro by hydrogen atoms, see P. G. Burke and K. Smith, *Rev. Mod. Phys*. **34**, 458 (196

The principal limitation to the recoil method is the relatively poor detecti efficiency for most neutral atoms. However, the alkalis can be detect with exceptionally high efficiency by using surface ionization (see Secti 13-6). This method possesses certain advantages over the method c scribed above, in which observations are made on the scattered electr beam. In the recoil method one is not concerned with the trajectories of t scattered electrons, and consequently it is not necessary to use a higl collimated electron beam. This fact permits the use of a simple electr gun design, as well as an axial [illegible] he beam. Al the problems associat [illegible] w energies

and usually requires ... measurements are to be made. Some of these techniques were introduced around 1930.[7] They have been greatly extended and improved in recent years and are now being used in many laboratories for various types of experiments. In this section we shall describe first the crossed-beam apparatus used by Neynaber and his colleagues for electron scattering studies and present some of the experimental data obtained on the elastic

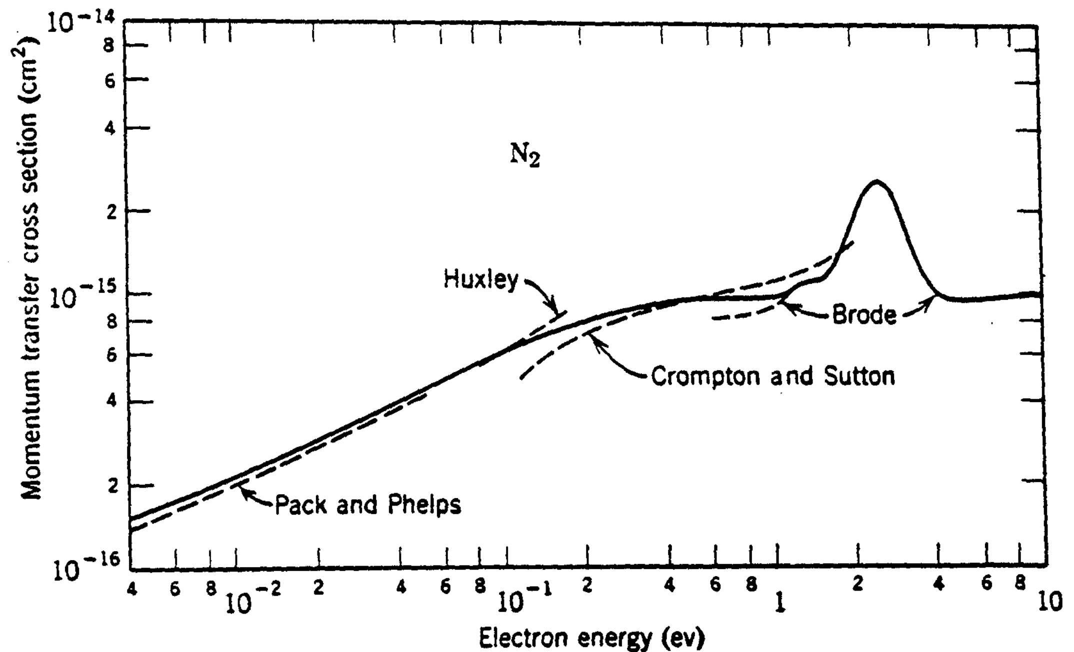

FIG. 4-1-7. Momentum transfer cross sections for electrons in nitrogen, as derived by Frost and Phelps[19] (solid curve). Also shown are data of J. L. Pack and A. V. Phelps, *Phys. Rev.* **121**, 798 (1961); L. G. H. Huxley, *Australian J. Phys.* **9**, 44 (1956) and *J. Atmospheric Terrest. Phys.* **16**, 46 (1959); R. W. Crompton and D. J. Sutton, *Proc. Roy. Soc.* (London) **A-215**, 467 (1952); and R. B. Brode, *Rev. Mod. Phys.* **5**, 257 (1933).

scattering of electrons by atomic hydrogen, oxygen, and nitrogen. Then we shall describe the atomic beam recoil techniques used by Bederson's group for studies of electron scattering by alkali atoms.

The technique used by Neynaber et al.[20] for measuring the scattering cross sections of atoms normally present in molecular form is the following. The number of electrons scattered from a region defined by the intersection of a dc electron beam and a modulated (i.e., mechanically interrupted) molecular beam is compared with the number scattered when the beam is partially dissociated. The molecular dissociation is accomplished in a radio-frequency discharge, and the degree of dissociation (typically about 30%) is measured with a mass spectrometer. From the scattering and

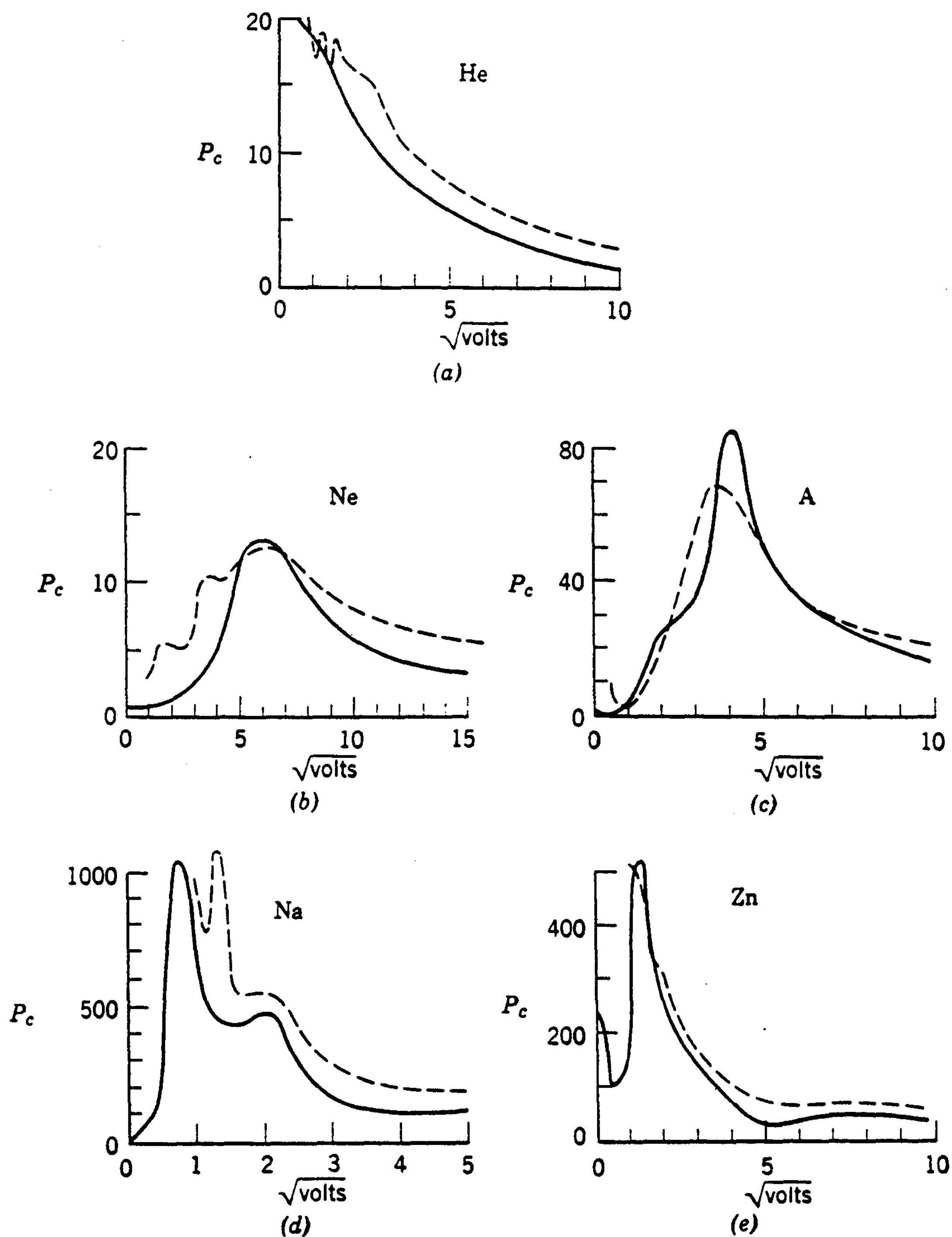

FIG. 4-4-1. Comparisons of the theoretical results of Allis and Morse (solid curves) with experimental observations (dashed curves) on electron scattering.

Although we are not giving a thorough coverage of the scattering theory, one additional point must be brought out here: the necessity of considering the possible effect of *electron exchange* on the scattering. This exchange refers to the changing of position of the incident electron with one of the orbital electrons of the target particle, which is then the one observed in the scattering. The probabilities of direct and exchange scattering cannot be added directly, since the wave amplitudes and not

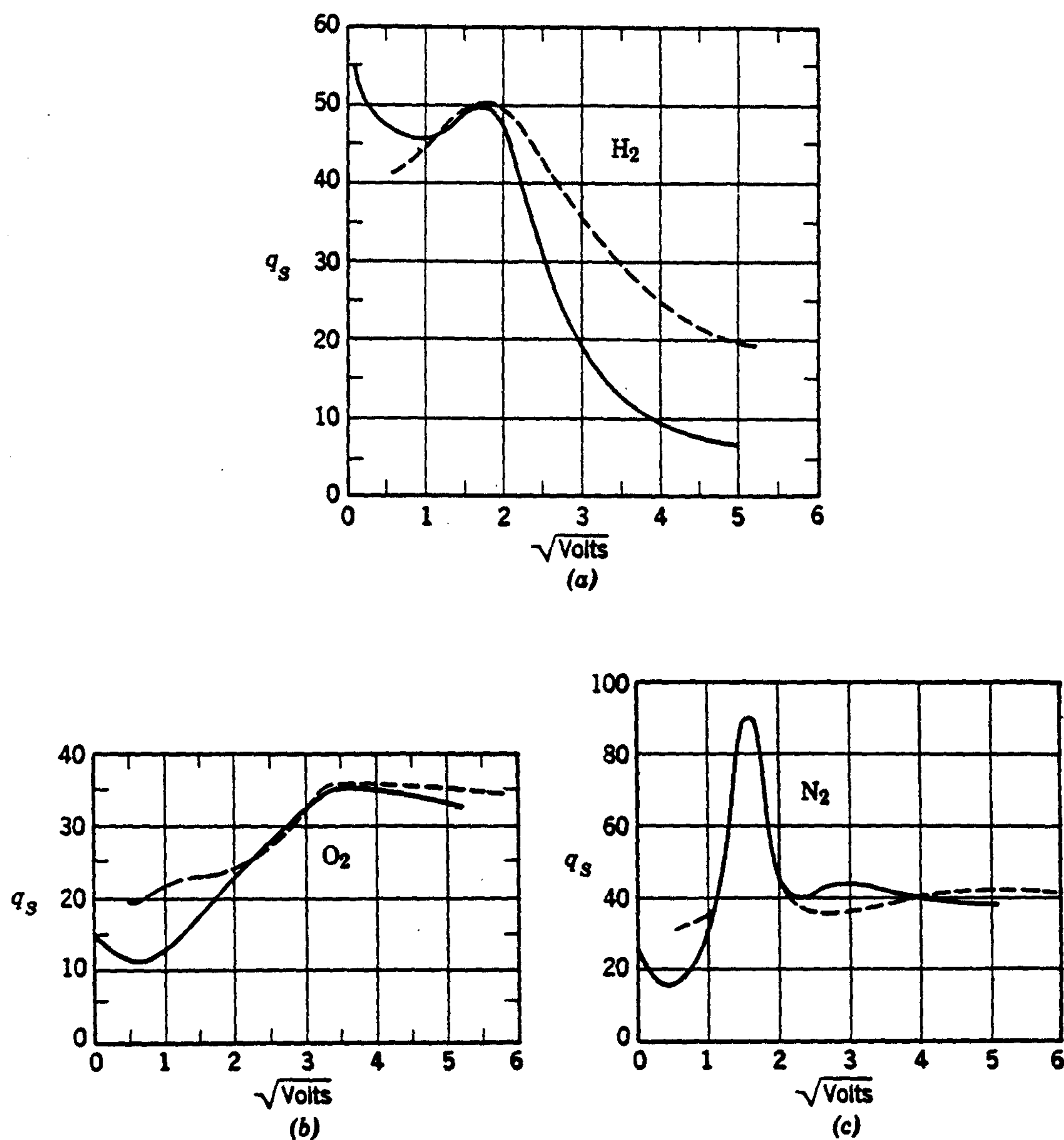

FIG. 4-4-2. Elastic scattering cross sections for electrons calculated by Fisk (solid curves) compared with experimental results (dashed curves). In this figure the cross sections are given in units of a_0^2.

the intensities are the quantities to be combined (see Section 6-13-B). For light atoms and low bombarding energies electron exchange appears to be an important effect, as shown by Fig. 4-4-3. Rubin, Perel, and Bederson[45] have performed an atomic beam recoil experiment for direct study of the exchange scattering of slow electrons by potassium atoms.

PART $\mathscr{B}$. THE ELASTIC SCATTERING OF HEAVY PARTICLES

There are several incentives for studying the elastic scattering of ions, atoms, and molecules. Perhaps the strongest comes from the possibility

ii. Ionization

- Electron impact ionization, $e + A \rightarrow 2e + A^+$, is an important mechanism of neutral ionization

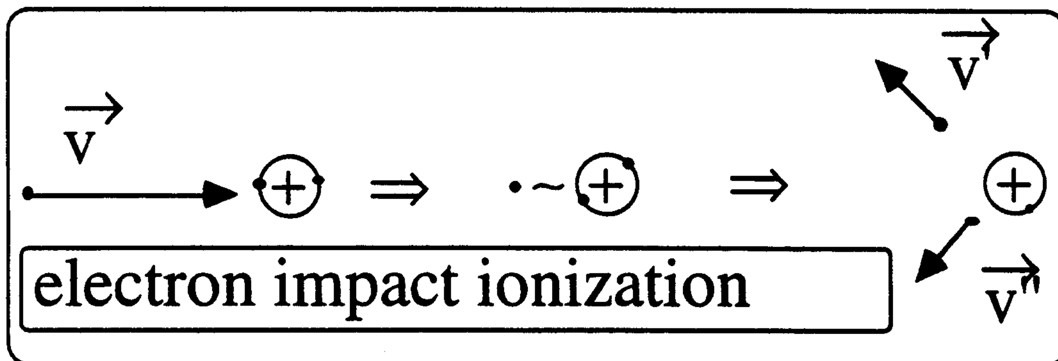

- Thomson's estimation for $\sigma_{ion}(v)$

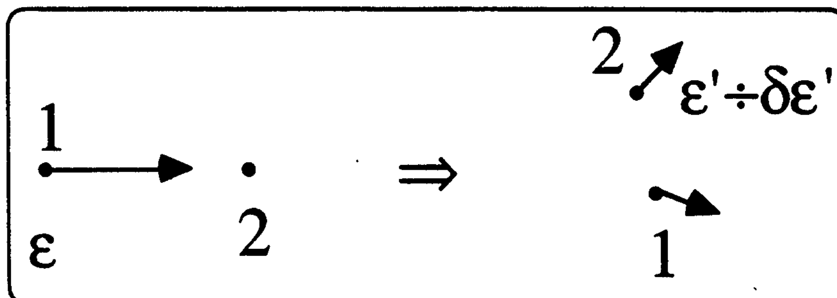

$$F = (e/r)^2, \ \upsilon' \approx F t_r/m, \ t_r \approx r/\upsilon, \ r \approx e^2/(\upsilon' \upsilon m)$$

$$\sigma(\varepsilon') \propto r^2 \propto 1/\varepsilon\varepsilon' \ \Rightarrow \ \delta\sigma(\varepsilon') = \frac{\pi e^4}{\varepsilon} \frac{\delta\varepsilon'}{(\varepsilon')^2},$$

$$\sigma_{ion}(\varepsilon) = \int_I^\varepsilon \delta\sigma(\varepsilon') = \frac{\pi e^4}{\varepsilon} \int_I^\varepsilon \frac{d\varepsilon'}{(\varepsilon')^2} = \frac{\pi e^4}{\varepsilon}\left(\frac{1}{I} - \frac{1}{\varepsilon}\right)$$

- Dimensionless analysis:

  i) there are only four dimensional parameters which are characterizing the problem of neutral ionization

  ii) these parameters are: electron charge, e, and mass, m, ionization potential, I, and incident electron energy, ε

  iii) there is only one combination of these parameters which has a cross-section dimension [cm^2], e^4/I^2

  iv) therefore, ionization cross-section can be written as follows

$$\sigma_{ion}(\varepsilon) = \left(e^4/I^2\right) f(\varepsilon/I),$$

where function $f(x)$ must be determined from additional arguments

- From experimental data was found that

$$f(x) = \frac{10(x-1)}{x(x+8)}$$

fits experimental data very well

- Notice that $\sigma_{ion} \approx 10^{-16}\ cm^2 << \sigma_{el} \approx 10^{-15}\ cm^2$

электрона, I — потенциал ионизации атома — энергия связи валентного электрона. Из этих параметров мы можем составить следующее выражение с размерностью сечения: $\frac{e^4}{I^2}\left(\frac{\varepsilon}{I}\right)^k$, причем степень k может быть произвольной. Поэтому наиболее общее выражение с размерностью сечения, которое может быть получено на основе данных параметров, можно представить в виде

$$\sigma_{\text{ион}} = \frac{e^4}{I^2} f\left(\frac{\varepsilon}{I}\right),$$

где $f(x)$ — некоторая функция безразмерного параметра. Отсюда сечение ионизации атома равно

$$\sigma_{\text{ион}} = \sum_i n_i \frac{e^4}{I_i^2} f\left(\frac{\varepsilon}{I_i}\right), \tag{1.34}$$

где n_i — число валентных электронов в данной оболочке, I_i — энергия связи электрона, находящегося в данной оболочке. На рис. 1

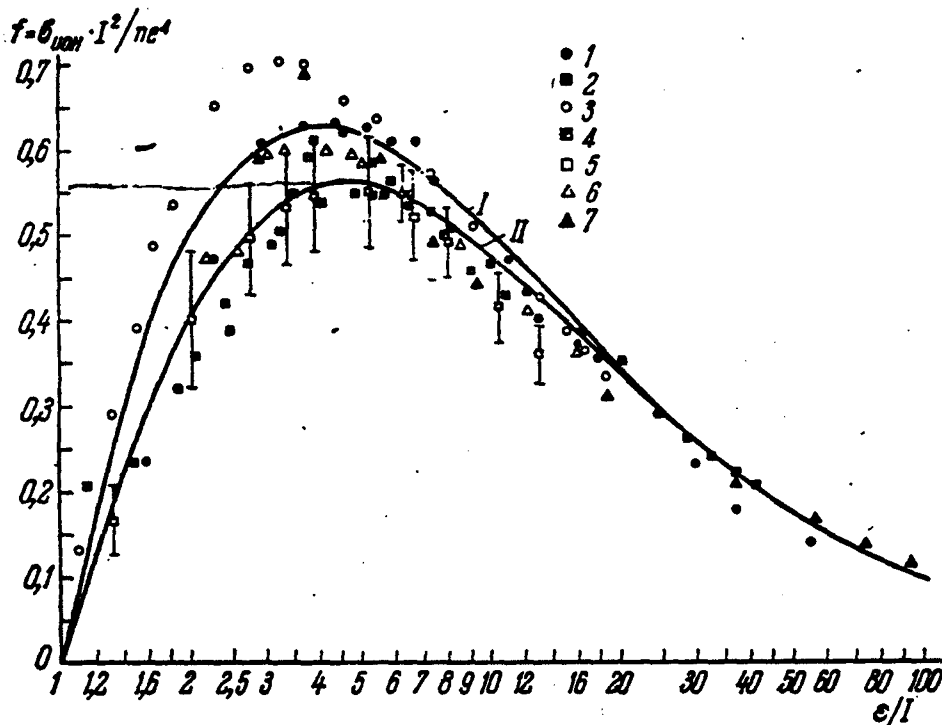

Рис. 1. Ионизация атомов электронным ударом. Эксперимент: 1 — H [12], 2 — He [13], 3 — He+ [14], 4 — Li+ [15], 5 — Li+ [16], 6 — H_2 [17], 7 — Li [18];

$$I - f(x) = \frac{10(x-1)}{x(x+8)}, \quad II - f(x) = \frac{10(x-1)}{(x+0{,}5)(x+8)}.$$

Experimental data on electron impact ionization.

приводятся значения функции $f(x)$, восстановленные на основании формулы (1.34) при сравнении этой формулы с экспериментально измеренными значениями сечений ионизации атомов и ионов электронным ударом. При этом использованы данные для

13

ionization of molecules by electrons has been done with commercial mass spectrometers. Lampe, Franklin, and Field,[27] for example, used a Consolidated Electrodynamics Corporation Model 21-620 mass spectrometer, which employs crossed electric and magnetic fields and cycloidal ion

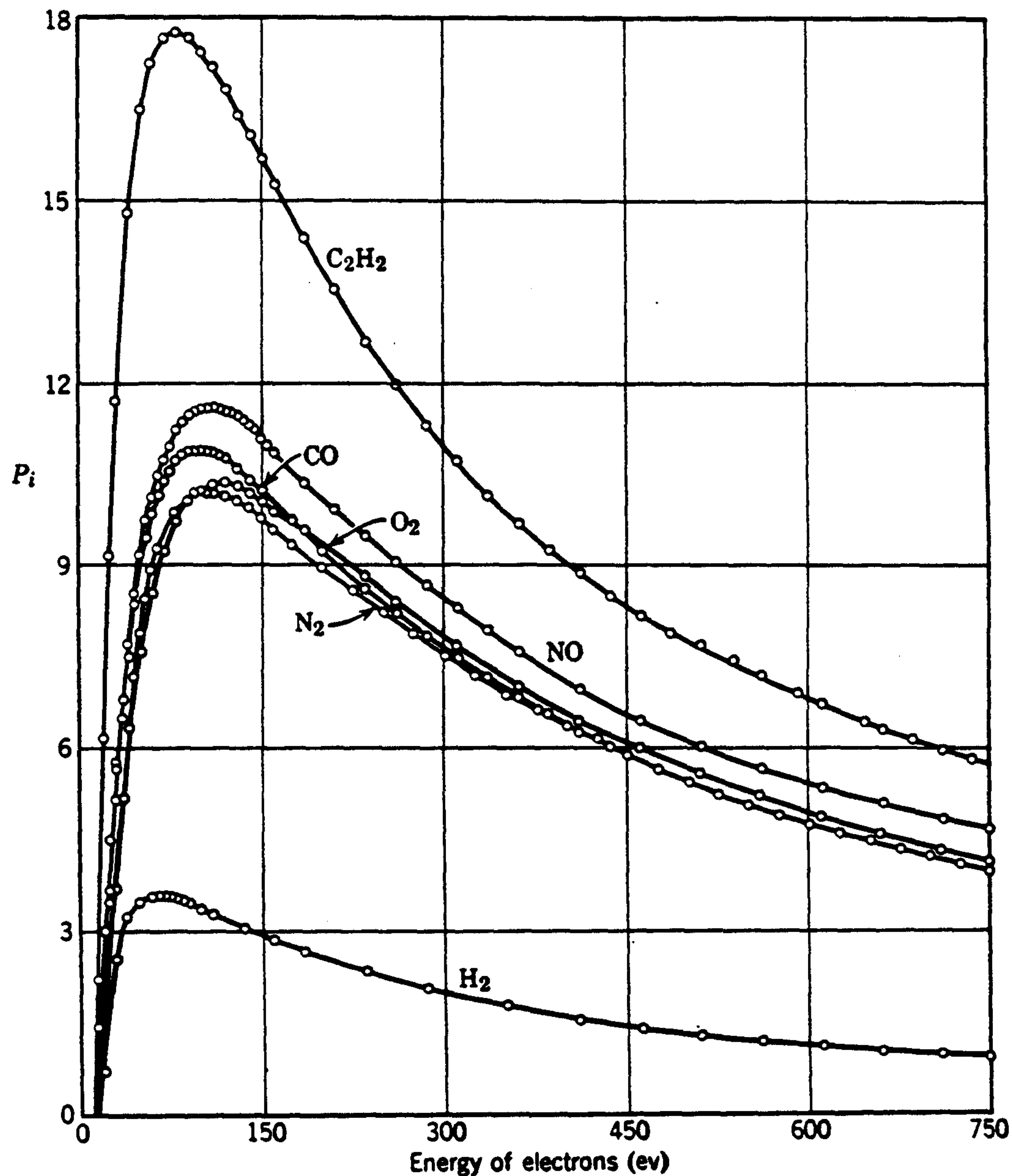

FIG. 5-3-11. The probability of ionization of N_2, CO, O_2, NO, H_2 and C_2H_2. The ordinate represents the number of positive charges per electron per cm path at 1 mm Hg pressure and 0°C. J. T. Tate and P. T. Smith, *Phys. Rev.* **39**, 270 (1932).

orbits. They obtained relative values for the cross sections at a fixed electron energy (75 ev) for a large number of gases, including argon, and converted the results to absolute data by comparison of their argon data

Ionization potentials (eV)

3. ПОТЕНЦИАЛЫ ИОНИЗАЦИИ АТОМОВ И ИХ ИОНОВ (*эв*)

$^{1,008}_{1}\mathrm{H}$ 13,595

$^{4,003}_{2}\mathrm{He}$ 24,59; 54,38

$^{6,94}_{3}\mathrm{Li}$ 5,39; 75,6; 122,4

$^{9,013}_{4}\mathrm{Be}$ 9,32; 18,2; 153,8

$^{10,82}_{5}\mathrm{B}$ 8,30; 25,2; 37,9

$^{12,01}_{6}\mathrm{C}$ 11,26; 24,4; 47,9

$^{14,01}_{7}\mathrm{N}$ 14,53; 29,6; 47,4

$^{16,00}_{8}\mathrm{O}$ 13,61; 35,2; 54,9

$^{19,00}_{9}\mathrm{F}$ 17,42; 35,0; 62,6

$^{20,19}_{10}\mathrm{Ne}$ 21,56; 41,1; 64,0

$^{22,99}_{11}\mathrm{Na}$ 5,14; 47,3; 71,6

$^{24,32}_{12}\mathrm{Mg}$ 7,64; 15,0; 80,1

$^{26,98}_{13}\mathrm{Al}$ 5,98; 18,8; 28,4

$^{28,09}_{14}\mathrm{Si}$ 8,15; 16,3; 33,4

$^{30,98}_{15}\mathrm{P}$ 10,48; 19,6; 30,2

$^{32,07}_{16}\mathrm{S}$ 10,36; 23,4; 35,0

$^{35,46}_{17}\mathrm{Cl}$ 13,01; 23,8; 39,9

$^{39,94}_{18}\mathrm{Ar}$ 15,76; 27,7; 40,9

$^{39,10}_{19}\mathrm{K}$ 4,34; 31,8; 46,0

$^{40,08}_{20}\mathrm{Ca}$ 6,11; 11,9; 5,12

$^{44,96}_{21}\mathrm{Sc}$ 6,54; 12,8; 24,75

$^{47,90}_{22}\mathrm{Ti}$ 6,82; 13,6; 27,5

$^{50,95}_{23}\mathrm{V}$ 6,74; 14,65; 29,3

$^{52,01}_{24}\mathrm{Cr}$ 6,76; 16,5; 30,95

$^{54,94}_{25}\mathrm{Mn}$ 7,43; 15,6; 33,7

$^{55,85}_{26}\mathrm{Fe}$ 7,90; 16,2; 30,6

$^{58,94}_{27}\mathrm{Co}$ 7,86; 17,05; 33,5

$^{58,69}_{28}\mathrm{Ni}$ 7,63; 18,15; 35,2

$^{63,54}_{29}\mathrm{Cu}$ 7,72; 20,3; 36,8

$^{65,38}_{30}\mathrm{Zn}$ 9,39; 18,0; 39,7

$^{69,72}_{31}\mathrm{Ga}$ 6,00; 20,4; 30,6

$^{72,60}_{32}\mathrm{Ge}$ 7,88; 15,9; 34,1

$^{74,91}_{33}\mathrm{As}$ 9,81; 20,1; 28,0

$^{78,96}_{34}\mathrm{Se}$ 9,75; 21,3; 33,9

$^{79,92}_{35}\mathrm{Br}$ 11,84; 19,1; 25,7

$^{83,80}_{36}\mathrm{Kr}$ 14,00; 26,4; 36,8

$^{85,48}_{37}\mathrm{Rb}$ 4,19; 23,0; 36,0

$^{87,63}_{38}\mathrm{Sr}$ 5,69; 10,38

$^{88,92}_{39}\mathrm{Y}$ 6,38; 12,2; 20,5

$^{91,22}_{40}\mathrm{Zr}$ 6,84; 13,1; 23,0

$^{92,91}_{41}\mathrm{Nb}$ 6,88; 14,3; 25,0

$^{95,95}_{42}\mathrm{Mo}$ 7,1; 16,15; 27,1

$^{99,0}_{43}\mathrm{Tc}$ 7,28; 15,3

$^{101,1}_{44}\mathrm{Ru}$ 7,36; 16,8; 28,5

$^{102,9}_{45}\mathrm{Rh}$ 7,46; 18,1; 31,05

$^{106,7}_{46}\mathrm{Pd}$ 8,33; 19,4; 32,9

$^{107,9}_{47}\mathrm{Ag}$ 7,57; 21,5; 34,8

$^{112,4}_{48}\mathrm{Cd}$ 8,99; 16,9; 37,5

15

Продолжение

${}^{114,8}_{49}\mathrm{In}$ 5,78; 18,8; 27,9

${}^{118,7}_{50}\mathrm{Sn}$ 7,34; 14,5; 30,5

${}^{121,8}_{51}\mathrm{Sb}$ 8,64; 18,0; 24,7

${}^{127,6}_{52}\mathrm{Te}$ 9,01; 18,6; 30,5

${}^{126,9}_{53}\mathrm{I}$ 10,45; 19,4

${}^{131,3}_{54}\mathrm{Xe}$ 12,13; 21,1; 32,0

${}^{132,9}_{55}\mathrm{Cs}$ 3,89; 23,4; 35,0

${}^{137,4}_{56}\mathrm{Ba}$ 5,21; 10,0; 56,0

${}^{138,9}_{57}\mathrm{La}$ 5,61; 11,1; 20,4

${}^{140,1}_{58}\mathrm{Ce}$ 6,91; 14,8; 15,8

${}^{140,9}_{59}\mathrm{Pr}$ 5,76

${}^{144,3}_{60}\mathrm{Nd}$ 6,31

${}^{145,0}_{61}\mathrm{Pm}$ 6,3

${}^{150,4}_{62}\mathrm{Sm}$ 5,1; 11,4

${}^{152,0}_{63}\mathrm{Eu}$ 5,67; 11,4

${}^{156,9}_{64}\mathrm{Gd}$ 11,4

${}^{158,9}_{65}\mathrm{Tb}$ 6,74

${}^{162,5}_{66}\mathrm{Dy}$ 6,82

${}^{164,9}_{67}\mathrm{Ho}$ 6,9

${}^{167,2}_{68}\mathrm{Er}$ 6,9

${}^{168,9}_{69}\mathrm{Tu}$ 6,9

${}^{173,0}_{70}\mathrm{Yb}$ 6,2

${}^{175,0}_{71}\mathrm{Lu}$ 5,0

${}^{178,6}_{72}\mathrm{Hf}$ 7,0; 14,9

${}^{181,0}_{73}\mathrm{Ta}$ 7,88; 16,2

${}^{183,9}_{74}\mathrm{W}$ 7,98; 17,7

${}^{186,3}_{75}\mathrm{Re}$ 7,87; 16,6

${}^{190,2}_{76}\mathrm{Os}$ 8,7; 17,0

${}^{192,2}_{77}\mathrm{Ir}$ 9,0

${}^{195,2}_{78}\mathrm{Pt}$ 9,0; 18,6

${}^{197,0}_{79}\mathrm{Au}$ 9,22; 10,5

${}^{200,6}_{80}\mathrm{Hg}$ 10,44; 18,75; 34,2

${}^{204,4}_{81}\mathrm{Tl}$ 6,11; 20,3; 29,7

${}^{207,2}_{82}\mathrm{Pb}$ 7,42; 15,0; 31,9

${}^{209,0}_{83}\mathrm{Bi}$ 7,29; 16,6; 25,4

${}^{210,0}_{84}\mathrm{Po}$ 8,3

${}^{210,0}_{85}\mathrm{At}$ 9,4

${}^{222,0}_{86}\mathrm{Rn}$ 10,75

${}^{223,0}_{87}\mathrm{Fr}$ 4,0

${}^{226,0}_{88}\mathrm{Ra}$ 5,28; 10,1

${}^{227,0}_{89}\mathrm{Ac}$ 5,5

${}^{232,0}_{90}\mathrm{Th}$ 5,7; 19,4

${}^{231,0}_{91}\mathrm{Pa}$ 5,7

${}^{238,9}_{92}\mathrm{U}$ 4,0

iii. Excitation

a. Excitation of electronic states

- Electronic states in atom

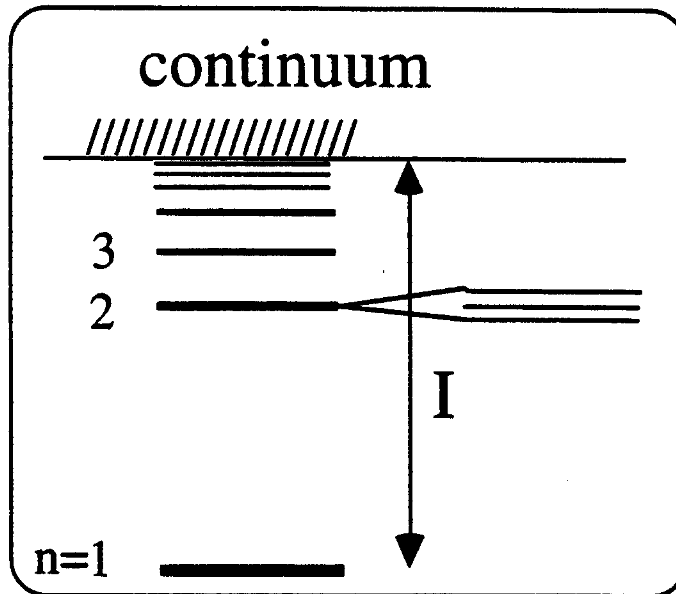

- Electron impact excitation, $\varepsilon > \varepsilon_{th} \Rightarrow$

  $e_{\varepsilon} + A(n) \rightarrow e_{\varepsilon-\varepsilon_{th}} + A(n')$

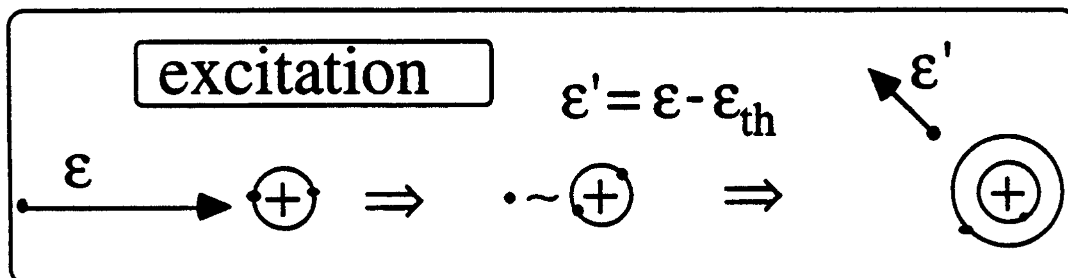

- From balance of direct and reverse processes

$$\sigma_{excit}(\varepsilon) \propto \sqrt{\varepsilon - \varepsilon_{th}}$$

Excitation of N2

Рис. 3.5. Сечения возбуждения различных электронных состояний молекулы $N_2(X^1\Sigma_g^+, v = 0)$ электронами

1 — $a^1\Pi_g$;
2 — $b^1\Pi_u$ ($v_k = 0$—4);
3 — переходы с $\Delta E^{ik} = 12{,}96$ эВ;
4 — $B^3\Pi_g$;
5 — $C^3\Pi_u$;
6 — $a''^1\Sigma_g^+$;
7 — $A^3\Sigma_u^+$;
8 — $E^3\Sigma_g^+$ ($\Delta E^{ik} = 11{,}87$ эВ)

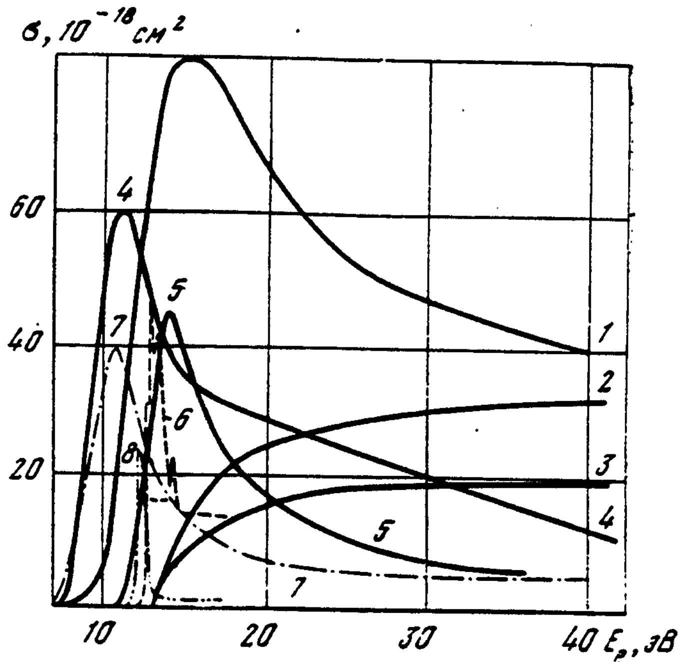

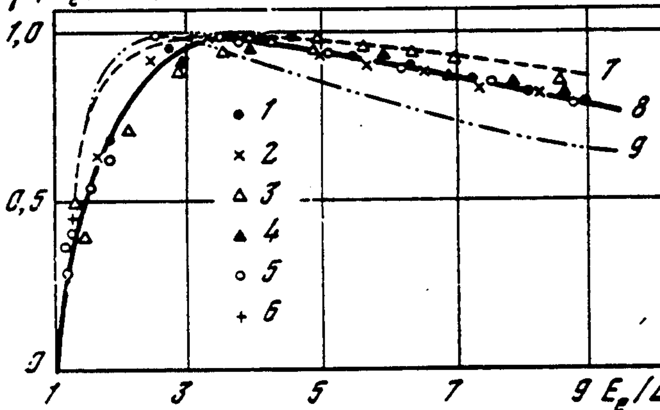

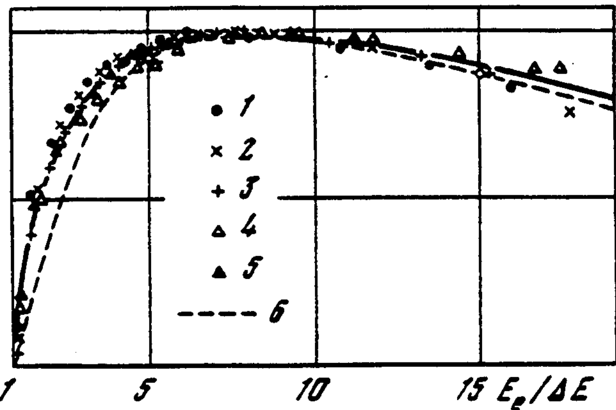

Рис. 3.6. Функция φ(x) для возбуждения оптически разрешенных переходов электронами

1 — H(1S — 2P); 2 — $H_2(X^1\Sigma_g^+ - B^1\Sigma_u^+)$; 3 — $H_2(X^1\Sigma_g^+ - C^1\Pi_u)$; 4 — $H_2(X^1\Sigma_g^+ - D^1\Pi_u)$; 5 — CO ($X^1\Sigma_g^+ - A^1\Pi$); 6 — $N_2(X^1\Sigma_g^+ - b^1\Pi_u$, $v_k = 4)$; 7 — расчет по формуле (3.20); 8 — среднее из кривых 1—6; 9 — расчет по формуле (3.26)

Рис. 3.7. Функция φ(x) для ионизации молекул электронами с образованием иона в определенном электронном состоянии

1 — $N_2(X^1\Sigma_g^+$, $v_i = 0) - N_2^+(B^2\Sigma_u^+$, $v_k = 0)$; 2 — CO($X^1\Sigma_g^+$, $v_i = 0$) — $CO^+(A^2\Pi$, $v_k = 0)$; 3 — CO($X^1\Sigma_g^+$, $v_i = 0$) — $CO^+(B^2\Sigma$, $v_k = 0)$; 4 — $CO_2(X^1\Sigma_g^+$, $v_i = 0) - CO_2^+(\tilde{A}^2\Pi)$; 5 — $CO_2(X^1\Sigma_g^+$, $v_i = 0$) — $-CO_2^+(\tilde{B}^2\Sigma)$; 6 — средняя кривая для полных сечений ионизации

лекуле более существенно (рис. 3.8). Это объясняется тем, что ионизация происходит с образованием ионов в различных электронных состояниях. Кроме того, большой вклад в сечение ионизации может давать автоионизация из сверхвозбужденных (автоионизационных) состояний молекул. Все эти процессы имеют различные пороги возбуждения, вследствие чего трудно ожидать универсальности функции φ (x) для полного сечения ионизации молекулы

18

b. Excitation of molecule vibrational states

- Vibrational states of molecule

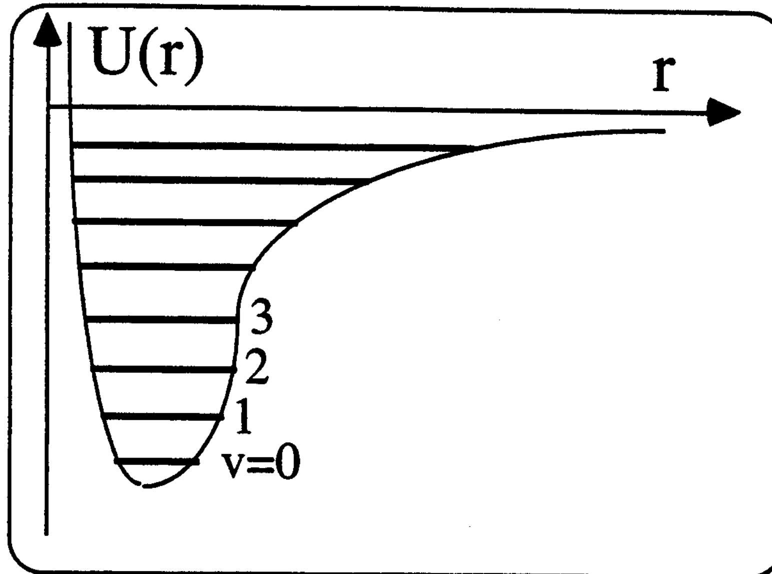

- $E_v = E_0(v + 1/2)(1 - \chi_v(v + 1/2))$

Molecule	H_2	N_2	O_2	CO
E_0, eV	0.54	0.29	0.2	0.27
χ_v, 10^{-3}	27	6.1	7.6	6
v_{max}	14	~ 40	~ 20	~ 40

- Classical mechanism of vibrational excitation of molecule by electron impact is ineffective:

$$\delta\varepsilon \approx (m/M)\varepsilon_T \sim 10^{-3} \div 10^{-4}\,eV << E_0 \sim 0.2 \div 0.5\,eV$$

- In a low temperature plasmas vibrational excitation of molecule by electron impact occurs through the formation of a metastable negative molecular ion

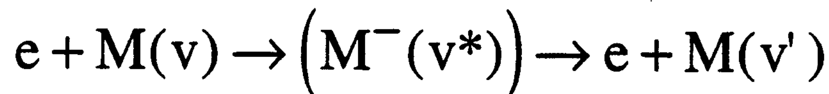

$$e + M(v) \rightarrow \left(M^{-}(v^*)\right) \rightarrow e + M(v')$$

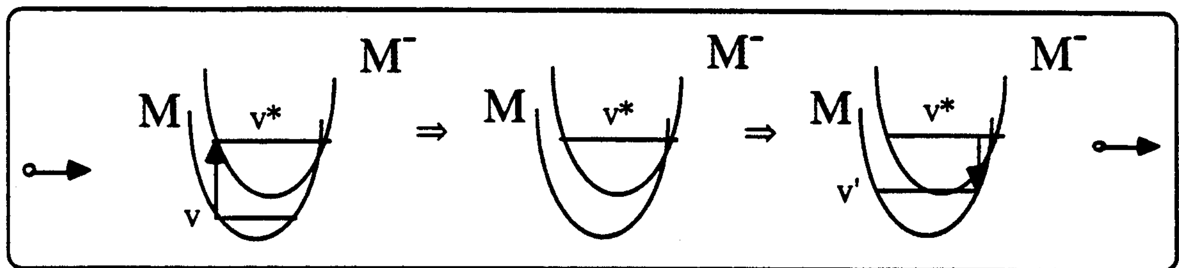

- Formation of a metastable negative molecular ion occurs due to restructure of electron states (orbits) and corresponds to electron-electron like collisions
- Therefore it is very effective mechanism of vibrational excitation, $\delta\varepsilon \approx \varepsilon_T$
- As a result $\sigma_{ev}(v) \sim 10^{-15}\,\mathrm{cm}^2$ and even higher

14. ПОТЕНЦИАЛЬНЫЕ КРИВЫЕ ДВУХАТОМНЫХ МОЛЕКУЛ

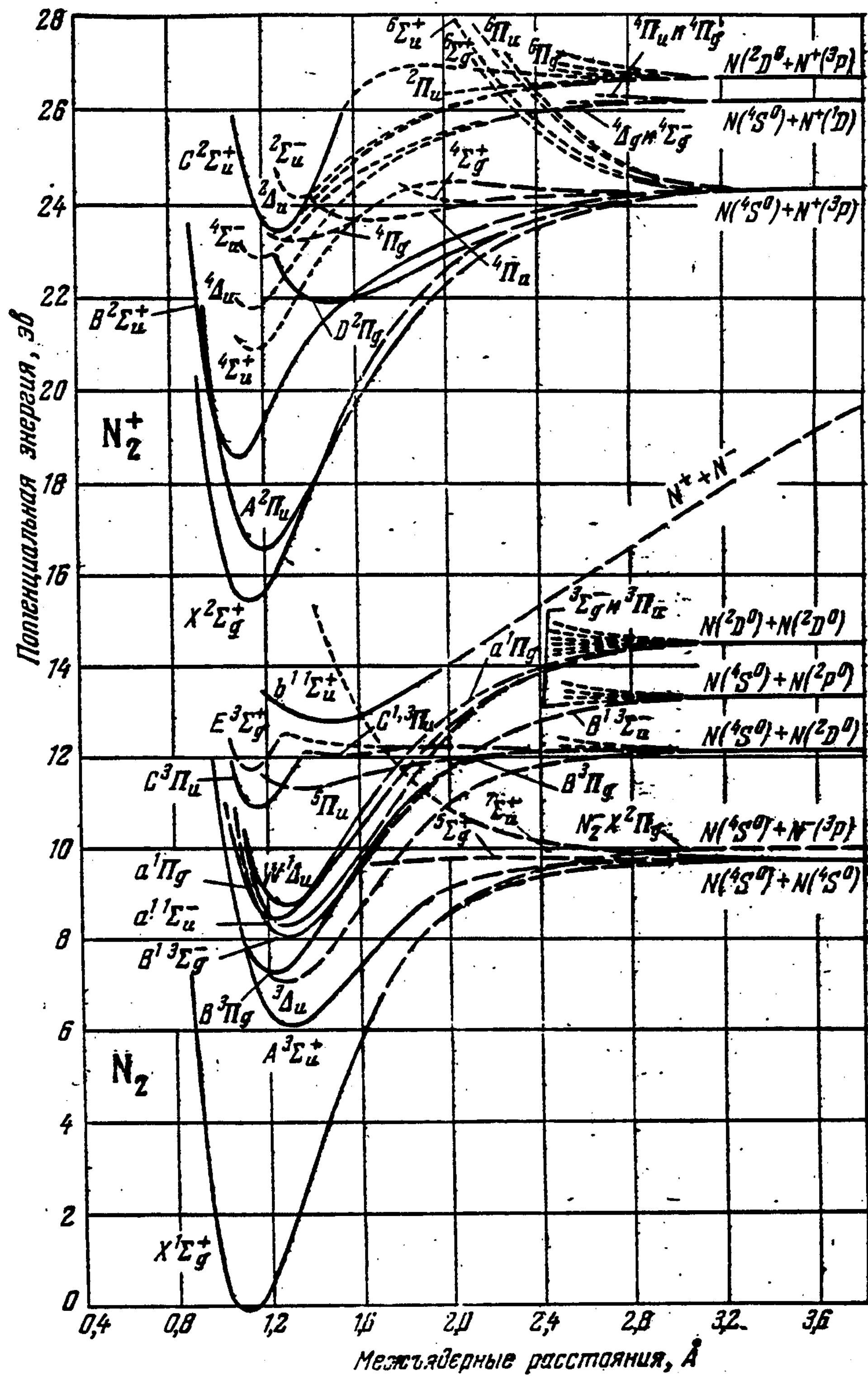

Рис. 11. Потенциальные кривые молекулы азота.

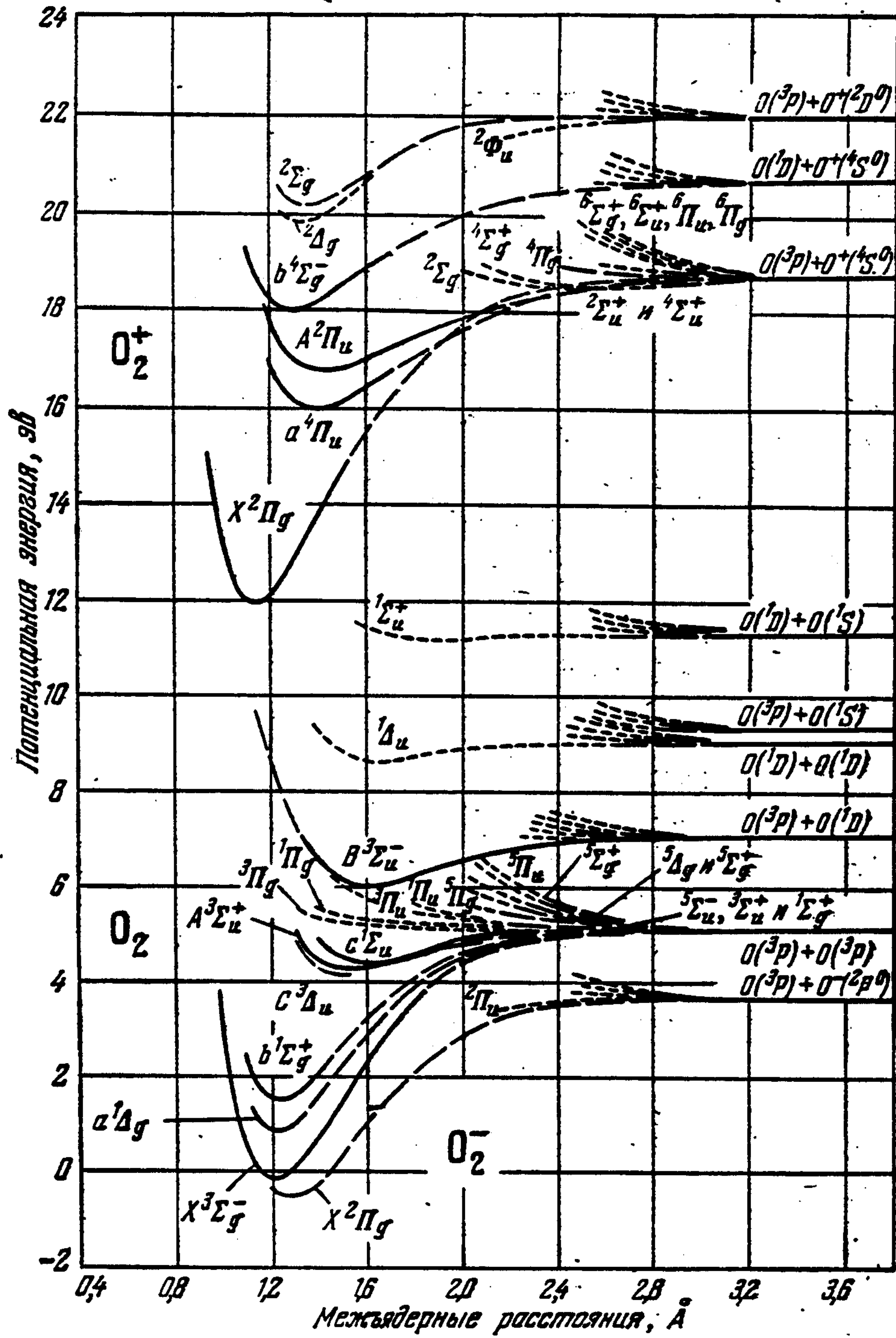

Рис. 13. Потенциальные кривые молекулы окиси азота.

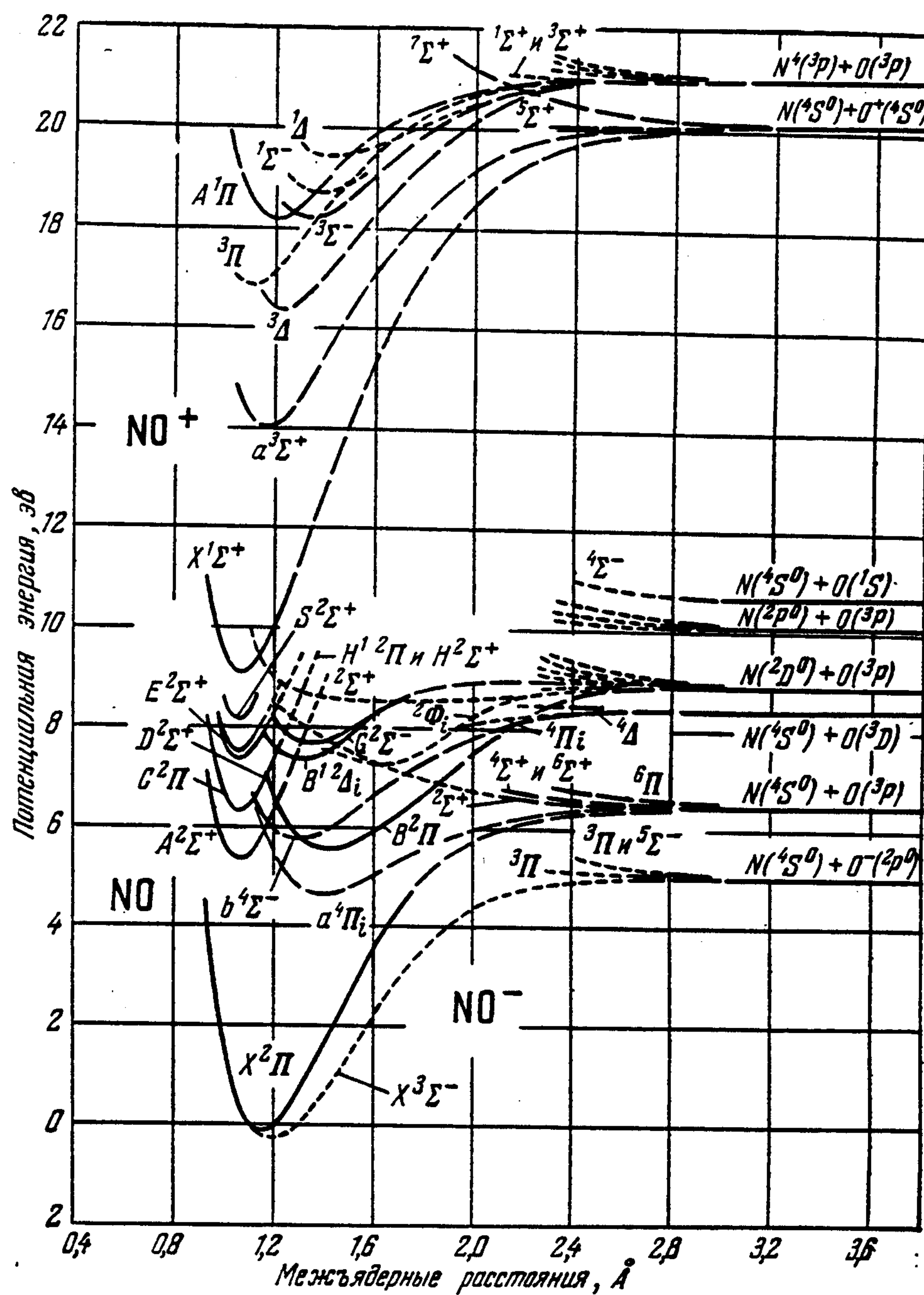

Рис. 12. Потенциальные кривые молекулы кислорода.

vibrational excitation.

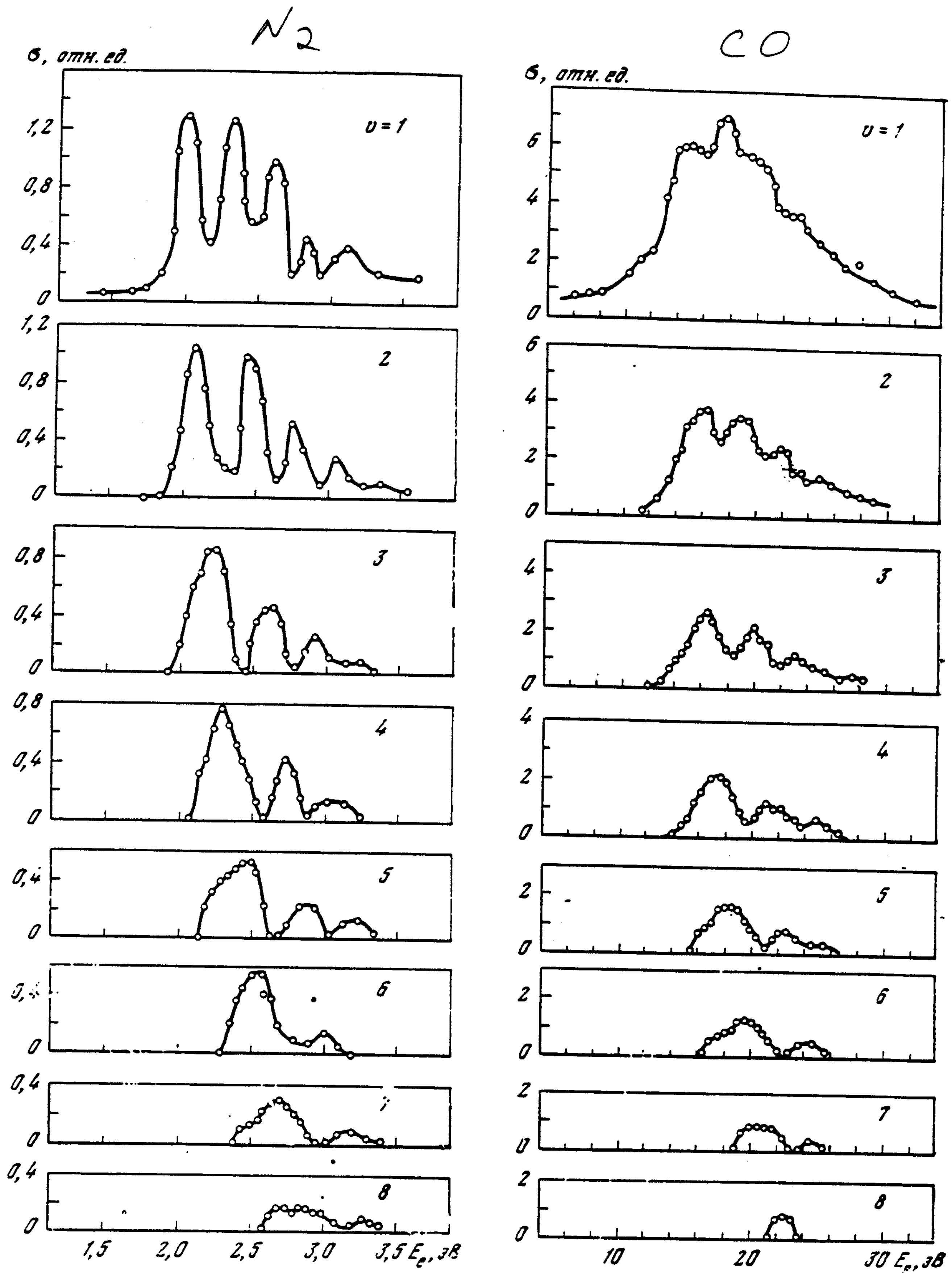

Рис. 3.1. Сечения возбуждения колебательных уровней $v_i = 1—8$ при столкновении молекулы $N_2(X^1\Sigma_g^+)$ с электронами [35]

При E_e = 2,3 эВ сумма сечений равна $5 \cdot 10^{-16}$ см² [28]

iv. Dissociation

- Electron impact dissociation occurs through excitation of repulsive state and its decay

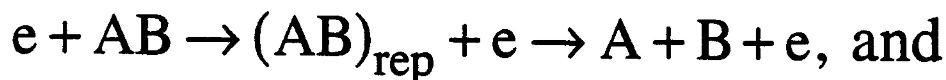

$$e + AB \rightarrow (AB)_{rep} + e \rightarrow A + B + e, \text{ and}$$

$$e + AB \rightarrow (AB)^{-}_{rep} \rightarrow A^{-} + B$$

(dissociative attachment, if A^{-} is stable)

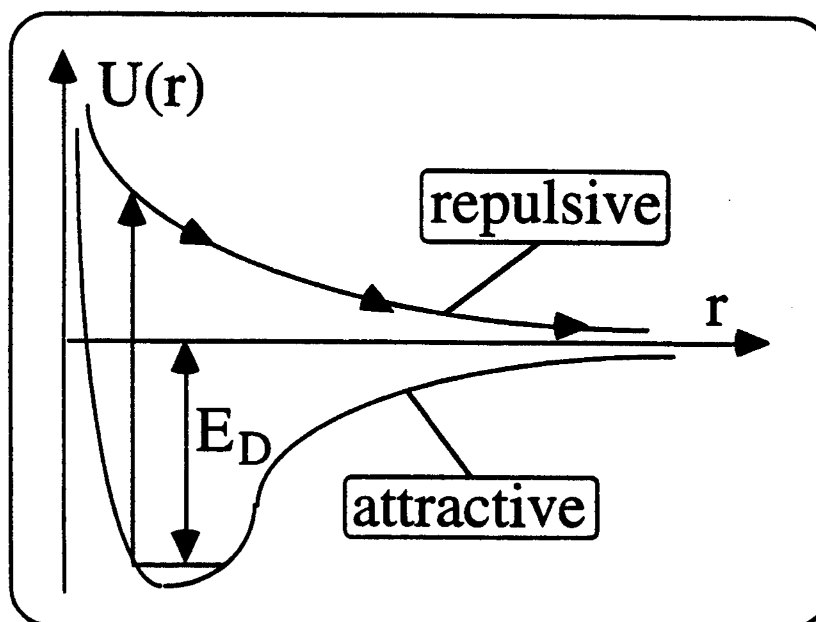

- As a result $E_{th} > E_D$, and the products of dissociation have a significant kinetic energy ~ 1 eV

- Usually $\sigma_{dis}(v) \sim 10^{-16}\,\text{cm}^2$ for $v_{ibr}=0$, however it strongly depend on vibrational excitation of a molecule

Electron impact dissociation

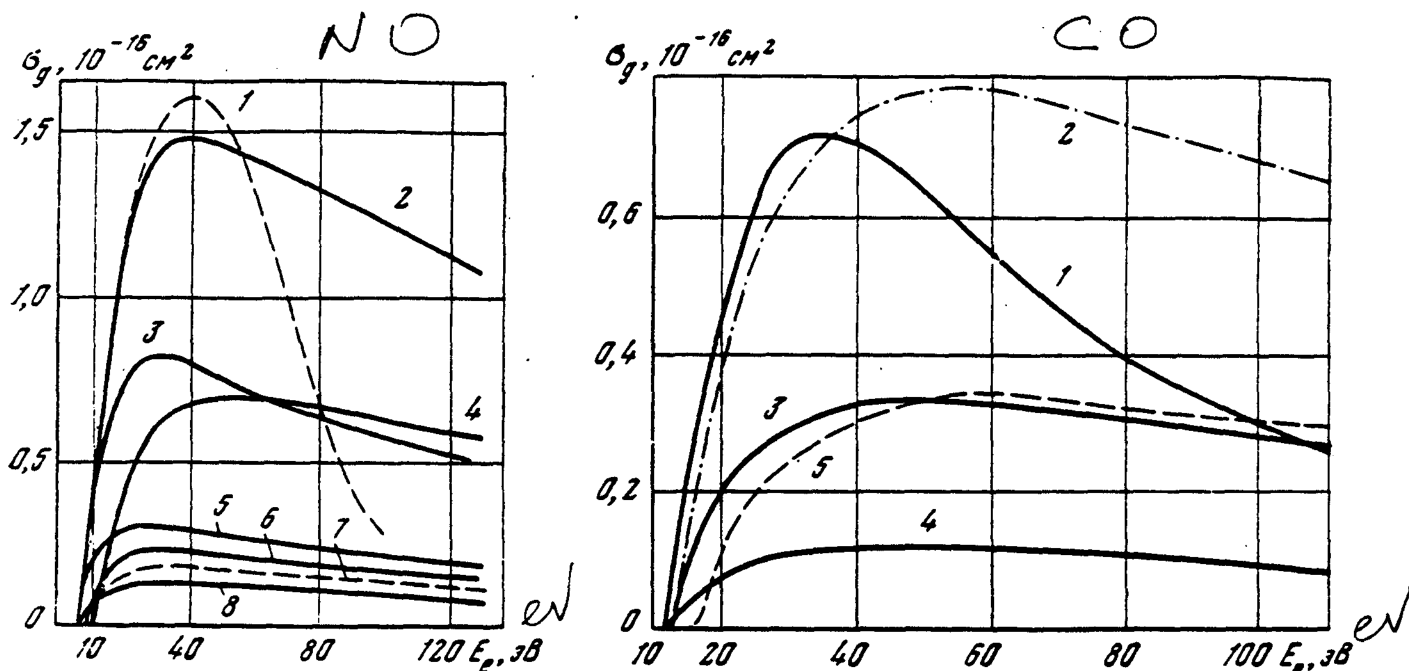

Рис. 3.15. Сечение диссоциации электронным ударом через электронно-возбужденные состояния молекулы $NO(X^2\Pi,\ v=0)$

1 — полное сечение по [142]; *2* — сумма парциальных сечений; *3* — через $\Delta E^{ik} = 6{,}93$—$9{,}2$ *эВ*; *4* — то же, 9,2—17,3; *5* — 6,93—7,3; *6* — 8,5—9,2; *7* — 8,0—8,5; *8* — 7,6—8,0

Рис. 3.16. Сечение диссоциации электронным ударом через электронно-возбужденные состояния молекулы $CO(X^1\Sigma_g^+,\ v=0)$

1 — полное сечение по [142]; *2* — сумма парциальных сечений; *3* — через $\Delta E^{ik} = 13$—14 *эВ*; *4*—12,5—13; *5* — $\Delta E > 14{,}01$

решенными. Полное сечение диссоциации через электронно-возбужденные состояния получалось суммированием парциальных сечений (рис. 3.15). На этом же рисунке изображено сечение диссоциации окиси азота, полученное по данным [142] путем вычитания из них сечения диссоциативной ионизации. Удовлетворительное согласие кривых *1* и *2* наблюдается при $E_e < 40$ *эВ*, что свидетельствует о надежности данных в этой области энергий. Однако сильное различие кривых при увеличении энергии электронов приводит к выводу, что в результатах [142] возможна большая систематическая погрешность, повышающаяся по мере увеличения энергии электронов. В противном случае пришлось бы предположить необычную зависимость сечений возбуждения разрешенных переходов $\varphi(x)$ от энергии налетающих электронов.

Из данных рис. 3.15 видно, что в полное сечение диссоциации молекулы окиси азота дает вклад большое число электронно-колебательных уровней, расположенных более или менее равномерно между первым потенциалом диссоциации и $\Delta E^{ik} \simeq 18$ *эВ*. Вблизи порога диссоциации основной вклад дает предиссоциация состояний $A^2\Sigma^+$, $B^2\Pi$ и $D^2\Sigma^+$.

Окись углерода. В спектре излучения полос окиси углерода наблюдается предиссоциация с уровней $B^1\Sigma^+$ ($v_k = 0,\ j \geqslant 38$; $v_k = 1,\ j > 18$) (обрыв полос), а уровни $v_k > 2$ $B^1\Sigma^+$, $C^1\Sigma^+$ ($v_k \geqslant 1$), $E^1\Sigma^+$ ($v_k \geqslant 1$) вообще не наблюдаются в излучении, так же как и все уровни с потенциалами возбуждения выше 12,5 *эВ*. В поглощении света и при электронном ударе переходы на эти уровни наблюдаются [143—148]. Обрыв полос с уровня $B^1\Sigma^+$ неполный, а ин-

26

Electron impact dissociation

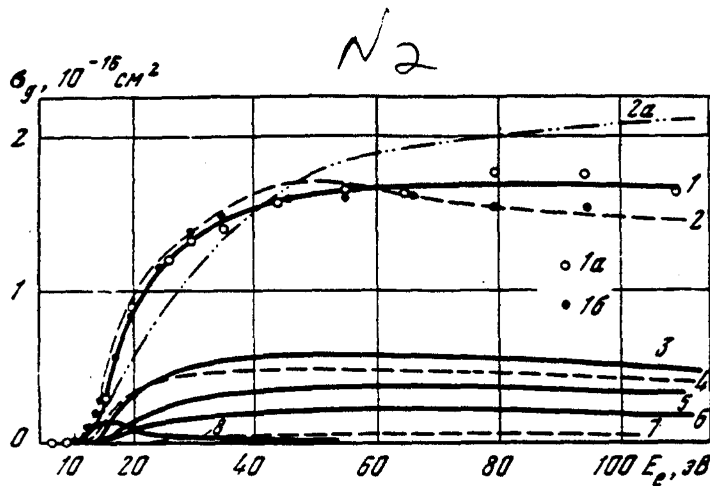

Рис. 3.13. Сечения диссоциации электронным ударом через электронные состояния молекулы $N_2(X^1\Sigma_g^+, v = 0)$

1 — полное, *1а* — то же [130], *1б* — [131, 130]; *2* — сумма парциальных сечений (*3*—*8*) по [64]; *2а* — [129]; *3* — через состояния с ΔE^{ik} = 13,8—14,4 *эВ*; *4* — то же, 12,4—13,05; *5* — 14,41—17,70; *6* — 13,06—13,80; *7* — > 20; *8* — $a^1\Pi_g$

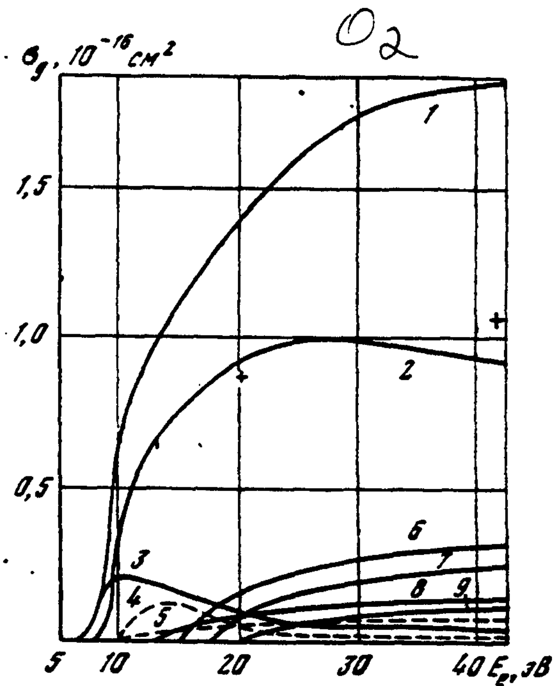

Рис. 3.14. Сечение диссоциации электронным ударом через электронно-возбужденные состояния молекулы $O_2(X^3\Sigma_g^-, v = 0)$

1 — полное сечение (сумма *2*—*9*); *2* — через $B^3\Sigma_u^-$; + — [134]; *3* — ΔE^{ik} = 6,1 *эВ*; *4* — 10,29; *5* — 9,9; *6* — 15,3; *7* — 16,8; *8* — 12,9; *9* — 19,7

спонтанной предиссоциации и радиационных переходов для уровней $b^1\Pi_u$ и всех, лежащих выше 12,4 *эВ*, были сделаны на основании сил осцилляторов, измеренных в поглощении в работе [122], а также данных [123—128] по уширению полос и наблюдению излучения при возбуждении этих состояний. Если линия не наблюдалась в излучении, но уширение не было зарегистрировано, полагалось, что для таких уровней справедливо соотношение (3.59). Относительные вероятности диссоциации для этих групп уровней приведены ниже.

ΔE^{ik}, *эВ*	12,4—13,05	13,06—13,30	13,31—13,80	13,81—15,58	>15,58
$Y^{д}(k, v_к)$	0,63	0,33	0,55	1	0,4

Для автоионизационных уровней (ΔE^{ik} > 15,58 *эВ*) вероятность диссоциации определялась по данным работы [126].

Сечение диссоциации молекулы азота с уровня $v_i = 0$ основного состояния, рассчитанное по формуле (3.60), а также парциальные сечения диссоциации через ряд электронных состояний приведены на рис. 3.13. Использовались сечения возбуждения уровней по данным [64] (кривая *2*) и по [129] — кривая *2а*. Полное сечение диссоциации путем возбуждения нейтральной молекулы азота, рассчитанное из данных [130] и относительных данных [131], нормированных по [130] при E_e = 45 *эВ*, изображено на рис. 3.13 в виде точек и кривой *1*. При построении кривых *2* и *2а* было также учтено сечение диссоциации с образованием возбужденных атомов азота [132], половина ко-

Dissociation potentials (eV)

12. ЭНЕРГИЯ ДИССОЦИАЦИИ ДВУХАТОМНЫХ МОЛЕКУЛ *)

Молекула	Энергия диссоциации (эв)	Молекула	Энергия диссоциации (эв)	Молекула	Энергия диссоциации (эв)	Молекула	Энергия диссоциации (эв)
BaBr	2,8	CsF	5,0	ICl	2,15	NaF	5,0
BaCl	2,7	CsH	1,9	IF	2,9	NaH	2,1
BaF	3,8	CsI	3,6	IO	1,9	NaI	3,1
BaH	1,8	Cu_2	0,2	K_2	0,51	NaK	0,61
BaO	4,7	CuBr	3,4	KBr	3,95	O_2	5,1
BaS	2,4	CuCl	3,7	KCl	4,4	OH	4,4
Br_2	1,97	CuF	3,0	KF	5,1	Rb_2	0,48
BrCl	2,23	CuH	2,9	KH	1,86	RbBr	4,0
BrF	2,4	CuI	3,0	KI	3,33	RbCl	4,4
BrO	2,4	CuO	4,8	Li_2	1,1	RbF	5,4
C_2	6,2	F_2	1,6	LiBr	4,4	RbH	1,8
CCl	2,8	H_2	4,48	LiCl	4,8	RbI	3,3
CF	4,7	HD	4,51	LiF	6,0	S_2	4,3
CH	3,47	D_2	4,55	LiH	2,4	SH	3,5
CN	8,4	HT	4,52	LiI	3,6	SO	5,3
CO	11,1	T_2	4,59	LiO	3,4	TlBr	3,4
CaBr	2,9	HBr	3,75	MgBr	3,2	TlCl	3,8
CaCl	2,8	HCl	4,43	MgCl	3,9	TlF	4,7
CaF	3,1	HF	5,9	MgF	5,0	TlH	2,0
CaH	1,7	HI	3,05	MgH	2,2	TlI	2,8
CaI	2,8	Hg_2	0,06	MgO	3,4	ZnCl	2,6
CaO	5,0	HgBr	0,7	N_2	9,76	ZnH	0,85
CaS	3,0	HgCl	1,0	NBr	2,9	ZnI	1,4
Cl_2	2,48	HgF	1,8	NH	3,6		
ClF	2,6	HgH	0,38	NO	6,5		
ClO	2,8	HgI	0,36	NS	5,0		
Cs_2	0,45	HgS	2,8	Na_2	0,73		
CsBr	4,3	I_2	1,54	NaBr	3,8		
CsCl	4,4	IBr	1,82	NaCl	4,2		

*) В. И. Веденеев, Л. В. Гурвич, В. Н. Кондратьев, В. А. Медведев, Е. Л. Франкевич, Справочник, Изд-во АН СССР, М., 1962.

13. ЭНЕРГИИ ДИССОЦИАЦИИ МОЛЕКУЛЯРНЫХ ИОНОВ

Молекулярный ион	Энергия диссоциации (эв)	Молекулярный ион	Энергия диссоциации (эв)	Молекулярный ион	Энергия диссоциации (эв)	Молекулярный ион	Энергия диссоциации (эв)
Ar_2^+	1,1	Cs_2^+	0,7	I_2^+	2,8	Na_2^+	1,0
ArH^+	2,3	F_2^+	3,3	IBr^+	2,0	Ne_2^+	1,4
Br_2^+	3,3	H_2^+	2,65	ICl^+	2,2	NeH^+	2,2
C_2^+	5,5	HBr^+	4,0	K_2^+	0,75	O_2^+	6,7
CH^+	3,6	HCl^+	4,7	Kr_2^+	1,1	O_2^-	4,1
CO^+	8,35	HF^+	3,7	KrH^+	3,7	OH^+	4,9
CN^+	4,6	HI^+	3,1	Li_2^+	1,4	OH^-	4,7
CS^+	7,3	He_2^+	2,24	N_2^+	8,7	Rb_2^+	0,7
Cl_2^+	4,2	HeH^+	1,78	NO^+	10,9	Xe_2^+	1,0
ClO^+	5,3	HgH^+	2,3				

Rate constants

- In what follows we will use both cross section and the rate constant, $K_{(...)} = \langle \sigma_{(...)}(v)v \rangle$, of atomic processes (...)
- The reasons for that are

  a) lack of detailed information about $\sigma_{(...)}(v)$
  b) in many cases the details are not important
  c) rate constant enters in the balance equations

- As an example consider electron density balance equation

$$\frac{\partial n_e}{\partial t} + \nabla \cdot \vec{j}_e = S_e^{(+)} - S_e^{(-)}$$

where $\vec{j}_e$ is the electron flux, $S_e^{(+)}$ and $S_e^{(-)}$ are the electron volumetric sources and sinks

- If electron source is due to electron impact ionization of neutrals then

$$S_e^{(+)} = n_e N \langle \sigma_{ion}(v) v \rangle \equiv n_e N K_{ion}$$

where $K_{ion}\left[\mathrm{cm}^3/\mathrm{s}\right]$ is the ionization rate constant

- If electron sink is due to electron dissociative attachment (DA) then

$$S_e^{(-)} = n_e N_{AB} \langle \sigma_{DA}(v) v \rangle \equiv n_e N_{AB} K_{DA}$$

where $K_{DA}\left[\mathrm{cm}^3/\mathrm{s}\right]$ is the DA rate constant

- However, in many cases electron sink is due to a three-body processes, e. g. three-body electron attachment (3bA)

$$e + A + B \rightarrow A^- + B$$

- In this case electron sink can be written as

$$S_e^{(-)} = n_e N_A N_B K_{3bA}$$

where $K_{3bA}\left[\mathrm{cm}^6/\mathrm{s}\right]$ is the 3bA rate constant

- Notice that the rate constants usually depend on ε_T, gas temperature, vibr. excitation, etc.

v. Electron attachment

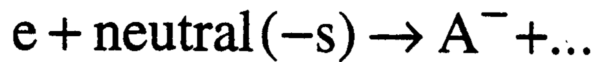

$$e + \text{neutral}(-s) \rightarrow A^- + \ldots$$

- This process (-es) is important, since it reduces a number of electrons in a discharge by converting them into negative ions (sink of electrons!), and can significantly affect both breakdown of gas and plasma parameters
- Tree main channels of electron attachment

  a) dissociative attachment (DA)

$$e + AB \rightarrow A^- + B$$

  b) radiative attachment (RA)

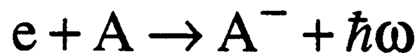

$$e + A \rightarrow A^- + \hbar\omega$$

  c) three body attachment (3bA)

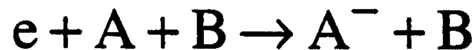

$$e + A + B \rightarrow A^- + B$$

- Notice that electron kinetic energy is transferred here to either neutrals or photon
- However, in the presence of rather complex molecules (e. g. SF_6) electron kinetic energy can also be transferred to internal degrees of freedom $e + M \rightarrow (M^*)^-$ (CMA)

Electron attachment cross-sect. and rate const.

- DA: "normally" $\max(\sigma_{DA}) \sim 10^{-18}\text{cm}^2$ however it is strongly depend on vibrational excitation of a molecule (as well as electron impact dissociation)

- However, for some gases (e. g. $e + HJ \rightarrow J^- + H$) $\max(\sigma_{DA}) \sim 10^{-14}\text{cm}^2$

- RA: K_{RA} can be as high as $10^{-15\div16}\,\text{cm}^3/\text{s}$, but strongly depends on the binding energy of A^-

- 3bA: K_{3bA} can roughly be estimated assuming that during electron-neutral collision, the second neutral particle (B) stays close to the first one (A) to be able to take electron kinetic energy out

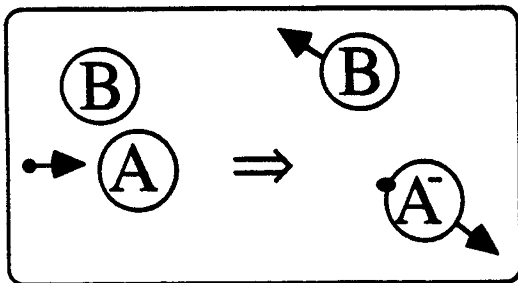

$$K_{3bA}N_B \sim K_{el} \times \left(\pi r_b^3 N_B\right)$$
$$K_{3bA} \sim 10^{-30}\,\text{cm}^6/\text{s}$$

- CMA: for SF_6 and electron energy <0.2 eV, $\sigma_{CMA} \sim 10^{-15}\,\text{cm}^2$

Binding energy of negative ions (eV)

6. ЭНЕРГИЯ СВЯЗИ ЭЛЕКТРОНА В ОТРИЦАТЕЛЬНОМ ИОНЕ *)

Отрицательный ион	Энергия связи электрона (эв)	Отрицательный ион	Энергия связи электрона (эв)	Отрицательный ион	Энергия связи электрона (эв)
$H^-(^1S)$	0,754	$K^-(^1S)$	0,30	$Zr^-(^4F)$	1,0
$He^-(^4P)$	0,08	Ca^-	Не существует	$Nb^-(^5D)$	1,3
$Li^-(^1S)$	0,6	$Ti^-(^4F)$	0,4	$Mo^-(^6S)$	1,3
Be^-	Не существует	$V^-(^5D)$	0,6	$Tc^-(^5D)$	1,0
$B^-(^3P)$	0,3	$Cr^-(^6S)$	1,0	$Ru^-(^4F)$	1,4
$C^-(^4S)$	1,2	Mn^-	Не существует	$Rh^-(^3F)$	1,3
$O^-(^2P)$	1,46	$Fe^-(^4F)$	0,6	$Pd^-(^2D)$	1,4
$F^-(^1S)$	3,40	$Co^-(^3F)$	0,9	$Ag^-(^1S)$	1,9
Ne^-	Не существует	$Ni^-(^2D)$	1,3	Sb^-	1,5
$Na^-(^1S)$	0,35	$Cu^-(^1S)$	1,8	Te^-	2,0
Mg^-	Не существует	As^-	2,0	$J^-(^1S)$	3,08
$Al^-(^3P)$	0,5	Se^-	2,0	$Cs^-(^1S)$	0,23
$Si^-(^4S)$	1,4	$Br^-(^1S)$	3,37	$Au^-(^1S)$	2,8
$P^-(^3P)$	0,8	$Rb^-(^1S)$	0,27	Pb^-	1,6
$S^-(^2P)$	2,1	Sr^-	Не существует	Tl^-	2,1
$Cl^-(^1S)$	3,62	Y^-	0,3	Bi^-	1,8
Ar^-	Не существует				

*) Б. М. Смирнов, Атомные столкновения и элементарные процессы в плазме, Атомиздат, М. 1968.

7. ДЛИНА РАССЕЯНИЯ ЭЛЕКТРОНА НА АТОМАХ ИНЕРТНЫХ ГАЗОВ [1]

Атом	He	Ne	Ar	Kr	Xe
Длина рассеяния (a_0)	1,14	0,2	−1,6	−3,2	−5,8

ДЛИНА РАССЕЯНИЯ ЭЛЕКТРОНА НА АТОМАХ ЩЕЛОЧНЫХ МЕТАЛЛОВ И АТОМЕ ВОДОРОДА [2]

Атом	H	Li	Na	K	Cs
Синглетная длина рассеяния (a_0)	5,8	3,6	4,2	0,4	−4,0
Триплетная длина рассеяния (a_0)	1,88	−5,7	−5,9	−15	−25

1. Б. М. Смирнов, Атомные столкновения и элементарные процессы в плазме, Атомиздат, 1968.
2. Э. М. Каруле, В сб. статей «Атомные столкновения», «Зинатне», Рига, 1965, т. 3, стр. 33.

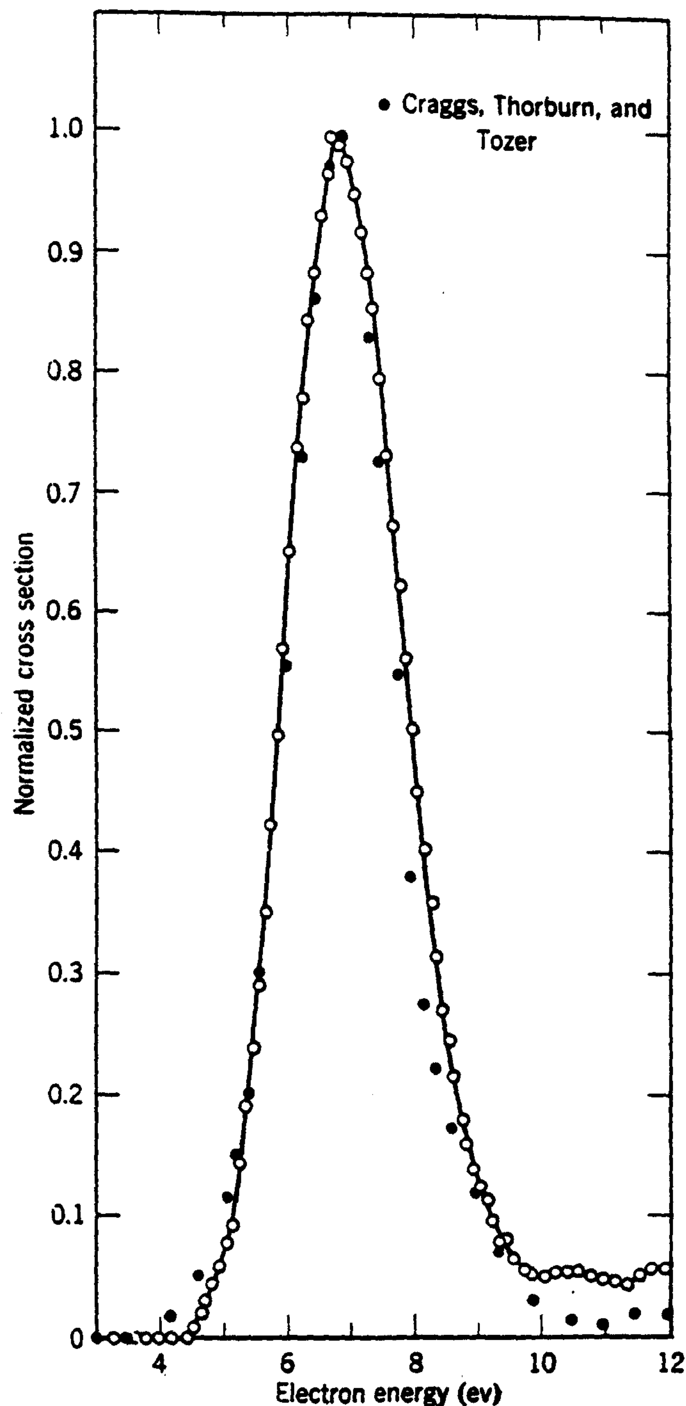

FIG. 8-7-6. The normalized cross section for formation of O^- ions by electron impac on O_2 molecules. The open circles represent the data of Schulz[56]; the black dots, th results of Craggs, Thorburn, and Tozer.[49] Electron-beam techniques were used in eac case. Schulz's cross section has a peak value of 1.25×10^{-18} cm^2 at 6.7 ev. The curv obtained by Craggs et al. has a shape similar to that of Schulz, but its peak value i almost twice as high. Additional data on electron attachment and ionization in oxyge have been recently reported by R. K. Asundi, J. D. Craggs, and M. V. Kurepa, *Pro Phys. Soc.* (*London*) **82**, 967 (1963)

MIT PLASMA FUSIO

For plotting, the detachment frequency ν_d is divided by N, the number density of the gas, with which the ions are essentially in thermal equilibrium. Also shown for comparison is the thermal electron three-body attachment frequency ν_a, divided by N^2. The collisional detachment results of Pack and Phelps are of particular interest in connection with ionospheric studies, for they show that the frequency of electron detachment collisions between O_2^- ions and a thermal distribution of oxygen or nitrogen molecules in the lower ionosphere is at least two orders of magnitude smaller

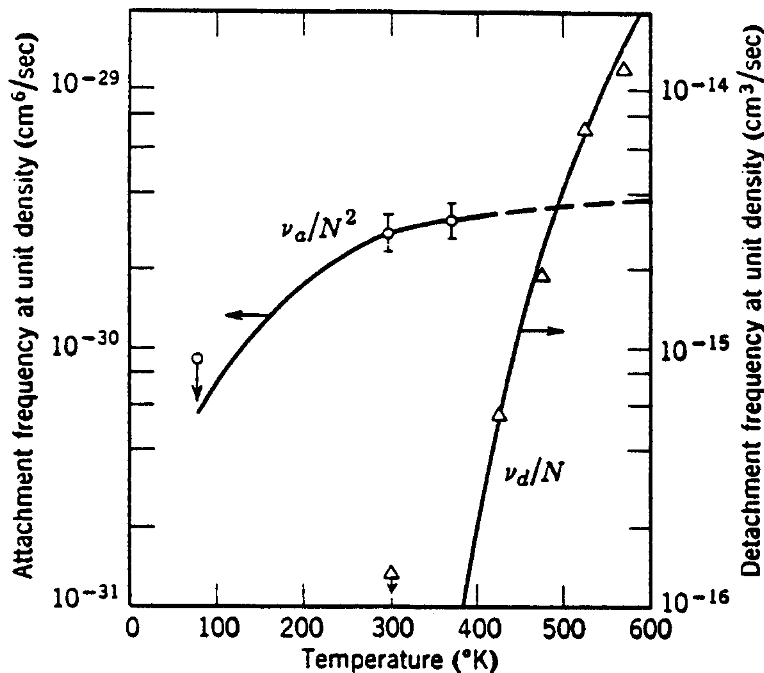

FIG. 8-7-7. Thermal attachment and detachment coefficients in molecular oxygen as a function of the gas temperature. The reactions are $e + 2O_2 \rightleftharpoons O_2^- + O_2$.

than the previously accepted values. (More recent work by Pack and Phelps[81] indicates, however, that the detachment frequencies are really about 30% higher than those plotted in Fig. 8-7-7.) Another important result of this study was the determination of the electron affinity of O_2, which was obtained by equating the rates of attachment and detachment and using the law of mass action. The value thus determined by Pack and Phelps[69] was 0.46 ± 0.02 ev (later revised to 0.44 ev[39]).

We have already mentioned (Section 8-6-C) the work done at the National Bureau of Standards on photodetachment of electrons from atomic and molecular negative ions of oxygen. The photodetachment cross sections for O_2^-, derived from measurements by Burch, Smith, and Branscomb,[78] are displayed in Fig. 8-7-8. Also shown are results for O^- obtained by Branscomb, Burch, Smith, and Geltman,[73] whose measurements are particularly important because they furnish the most accurate

shown in Fig. 8-7-11. Three illustrative curves are also shown for molecular oxygen for various assumed values of the vertical detachment energy E_0. These curves are correct only if the experimental photodetachment spectrum from which they were calculated refers to single initial and final vibrational states. Curves of the radiative attachment cross sections for H and O are also given in Branscomb's review.[10]

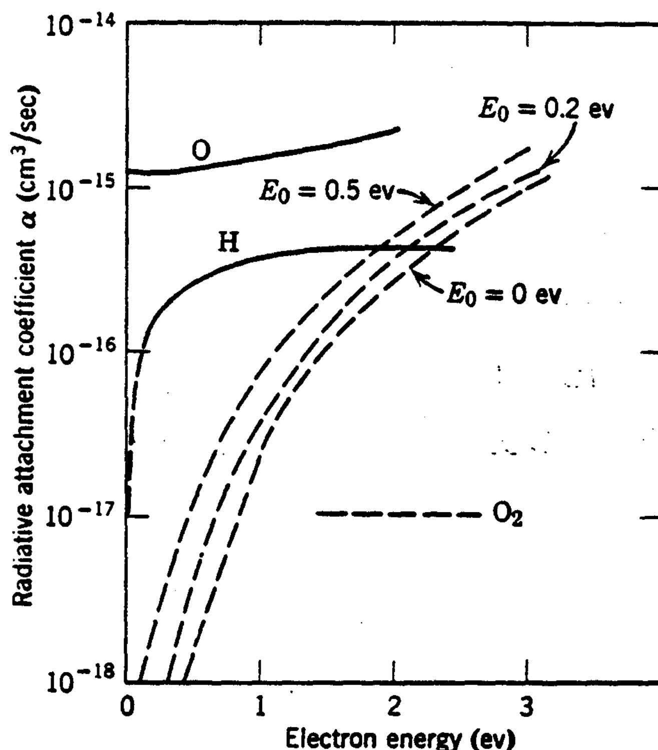

FIG. 8-7-11. Radiative attachment coefficients for atomic hydrogen and oxygen and illustrative curves for molecular oxygen.

C. CARBON. Electron attachment to carbon atoms has never been studied experimentally in the laboratory, but Seman and Branscomb[75] have investigated the structure and photodetachment spectrum of the C^- negative ion. The C^- photodetachment spectrum was measured in the visible region of the spectrum relative to the O^- spectrum, and the O^- data of Smith[73] were used to obtain absolute values for the C^- photodetachment cross section shown in Fig. 8-7-12. The circles (whose diameters indicate the magnitude of the statistical experimental errors) and the circles with error bars represent the experimental cross section data. The solid line represents the best fit to the C^- ground-state threshold data. The lower dashed line indicates absorption by an excited metastable (^2D) state of the C^- ion. Since the relative populations of the metastable ^2D and the ground ^4S states of the C^- in this experiment were unknown, it is impossible to calculate the cross section for photodetachment from the excited state.

36

vi. Plasma recombination

- Electron-ion recombination include

a) radiative recombination (RR)

$$e + A^+ \rightarrow A + \hbar\omega$$

$K_{RR} \propto (\varepsilon_T)^{-1/2}$, $K_{RR} \sim 10^{-12}\,\text{cm}^3/\text{s}$ for $\varepsilon_T \approx 1$ eV

b) three-body recombination (3bR)

$$e + A^+ + B \rightarrow A + B$$

rough estimate $K_{3bR} N_B \sim K_{ei}(\varepsilon_T) \times (\pi r_b^3 N_B)$,

gives $K_{3bR} \sim 10^{-28}\,\text{cm}^6/\text{s}$ for $\varepsilon_T \approx 1$ eV

- Dissociative recombination (DR)

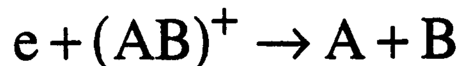

$$e + (AB)^+ \rightarrow A + B$$

very fast, $K_{DR} \sim 10^{-7}\,\text{cm}^3/\text{s}$ for $\varepsilon_T \approx 1$ eV, and strongly increase with decreasing ε_T

- Charge-exchange recombination (CXR)

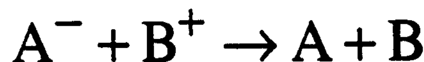

$$A^- + B^+ \rightarrow A + B$$

can be very fast, $K_{CXR} \sim 10^{-6}\,\text{cm}^3/\text{s}$ for $H^- + H^+ \rightarrow 2H$ and $T_N \approx 1000$ K, and strongly increase with decreasing T_N

vii. Interactions between heavy particles

- Ion-neutral elastic and charge-exchange collisions

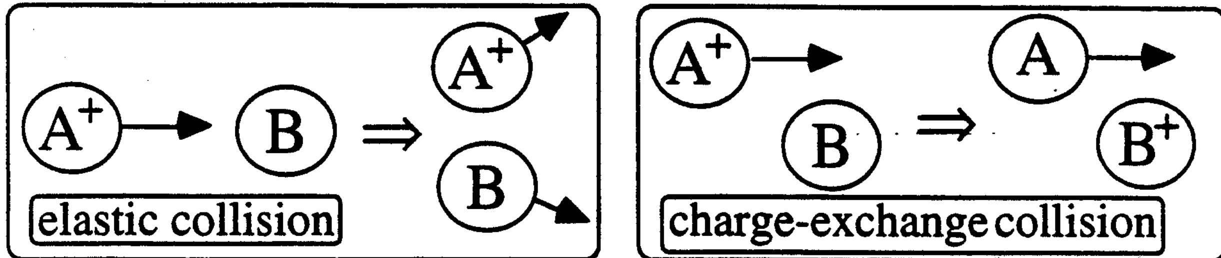

- These processes are very important since they determine ion transport (mobility and diffusion) in a gas discharge
- Typically $K_{iN}^{(el)} \approx 10^{-9} cm^3/s$.
- In case of resonance charge-exchange $(A^+ + A \rightarrow A + A^+)$ $K_{iN}^{(CX)} \approx 10^{-8} cm^3/s$

- "Penning ionization" (PI):
  $A^* + B \rightarrow A + B^+ + e$, where A^* is the neutral particle in excited metastable state and $E_A^* > I_B$

$$K_{PI} \sim 10^{-9} cm^3/s$$

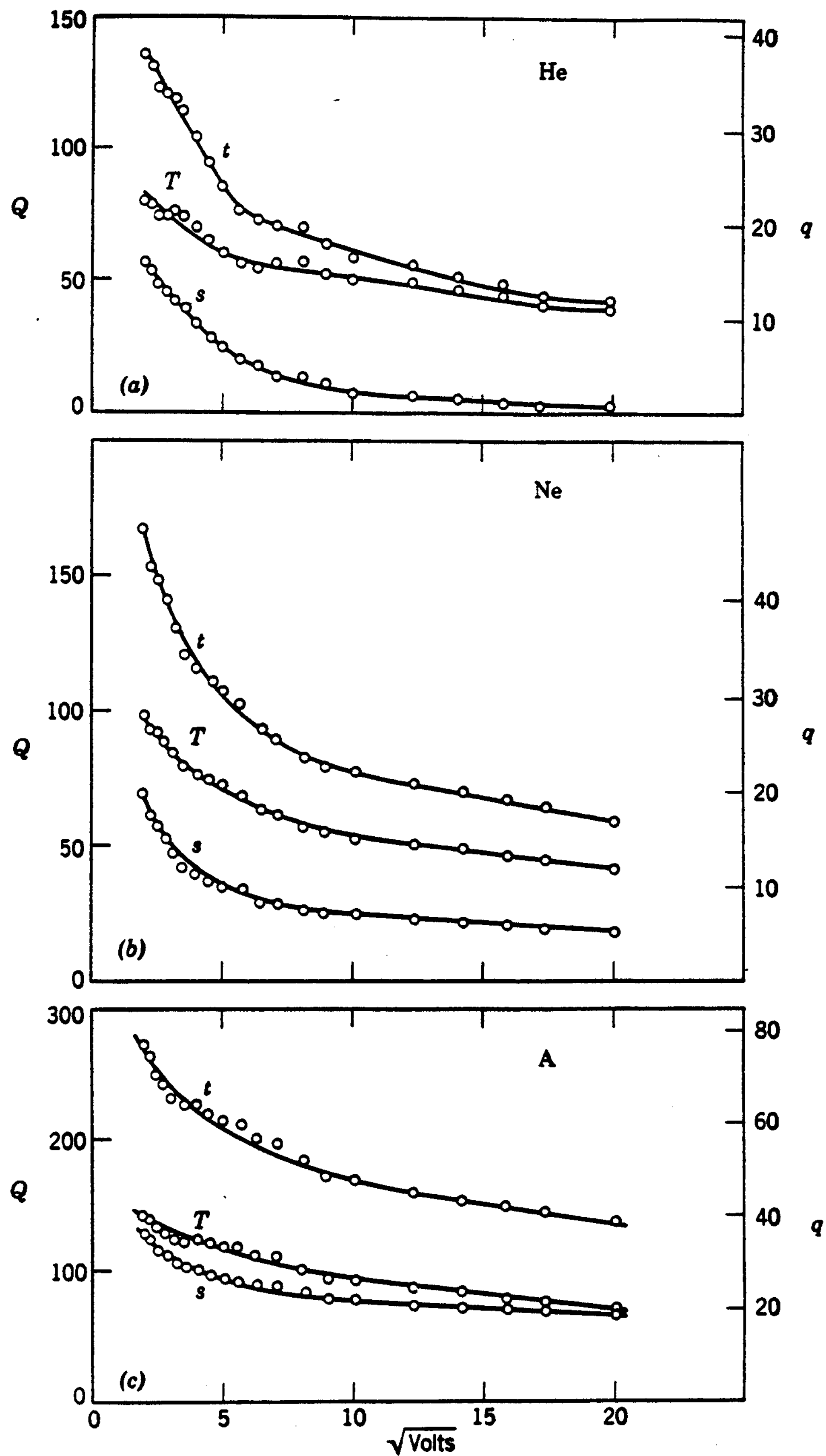

FIG. 4-9-1. Experimental values for scattering cross sections of ions in He, Ne, and A. The macroscopic cross sections Q are expressed in units of cm^{-1} and the microscopic cross sections q in units of 10^{-16} cm^2. The symbol s refers to elastic scattering, T to charge transfer, and t to the sum of s and T. (*a*) He^+ on He, W. H. Cramer and J. H. Simons, *J. Chem. Phys.* **26**, 1272 (1957); (*b*) Ne^+ on Ne, W. H. Cramer, *J. Chem. Phys.* **28**, 688 (1958); (*c*) A^+ on A, W. H. Cramer, *J. Chem. Phys.* **30**, 641 (1959).

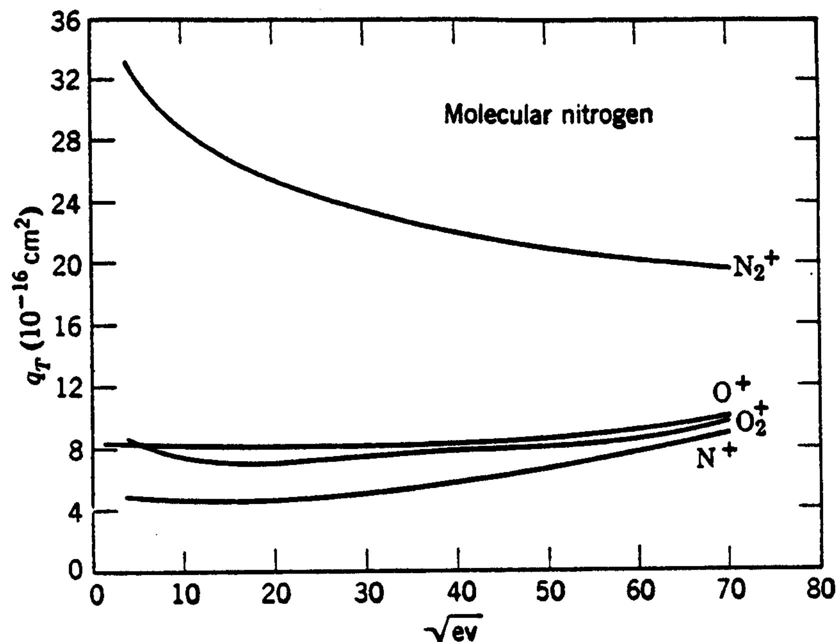

FIG. 6-2-13. Cross sections for charge transfer of various ions in molecular nitrogen. The data are normalized to the results of Stier and Barnett for charge transfer between protons and nitrogen at high energy. At 5000 ev, q_T is taken to be 11.6×10^{-16} cm² for H^+–N_2 (Stebbings, Turner, and Smith[27]). As explained in the text, the curves for O_2^+–N_2 and N_2^+–N_2 in this figure probably pertain to incident ions in excited states.

ions had high energy, about 100 ev. Amme and Utterback,[28] on the other hand, worked with ion source electrons whose energy could be varied between 16 and 24 ev. The latter investigators observed a resonance shape for the O_2^+–N_2 cross section when electron energies above 22 ev were used, but a strongly non-resonance behavior when the electron energy was reduced below 18 ev. The resonant N_2^+–N_2 cross section observed by Amme and Utterback varied as a function of ion energy in the manner generally reported by other investigators, but its value decreased by about 15 per cent when the source electron energy was increased from 17 to 23 ev. The ion impact energy range covered by Amme and Utterback extended from 40 to 1000 ev.

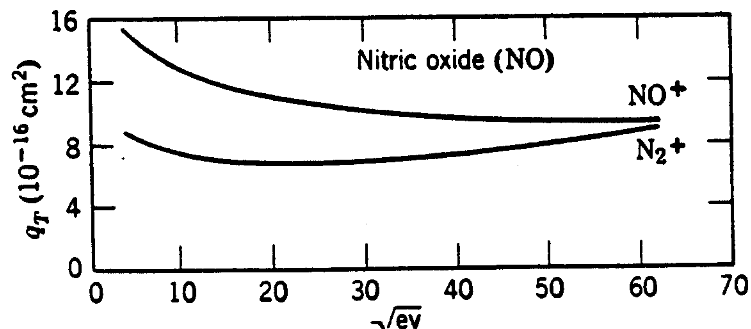

FIG. 6-2-14. Charge transfer cross sections for NO^+ and N_2^+ ions in nitric oxide (Stebbings, Turner, and Smith[27]).

40

vii. Electron emission from material surface

- Electron emission from the surface due to ion bombardment

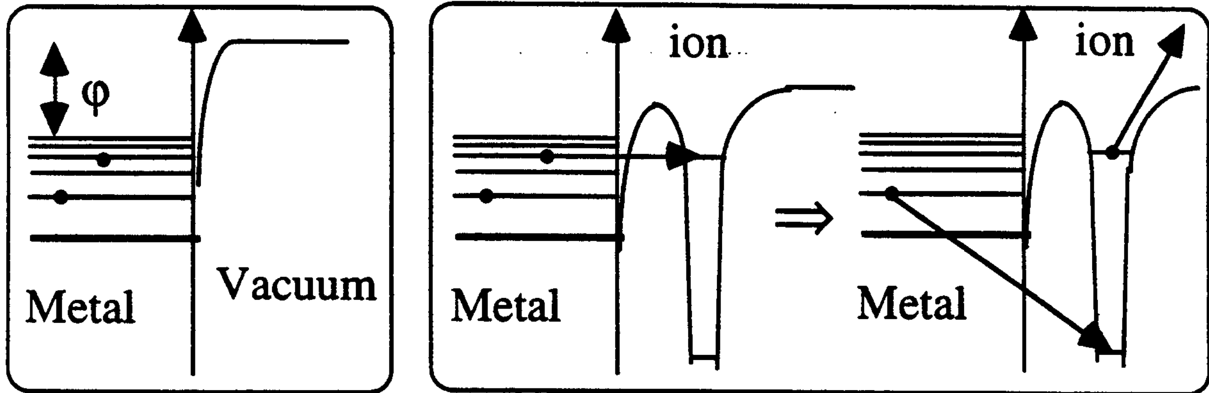

- Electron yield, γ_i, (electron per ion ratio) strongly depends on a surface purity, in practice $\gamma_i \approx 10^{-1 \div 4} << 1$
- Secondary electron emission

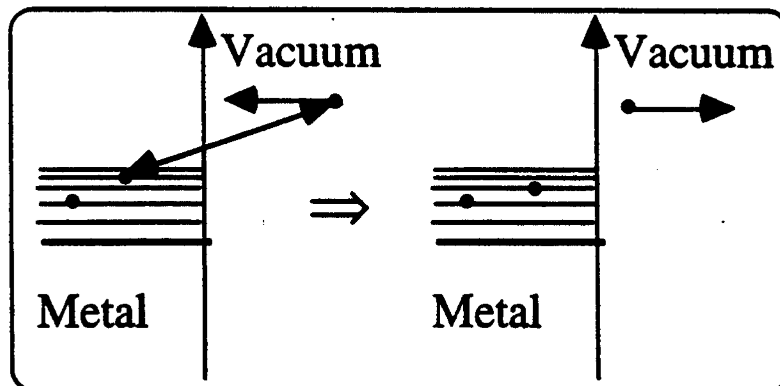

- Secondary electron emission yield, δ, (electron per electron ratio) strongly depends on surface material and primary electron energy, usually $\delta << 1$

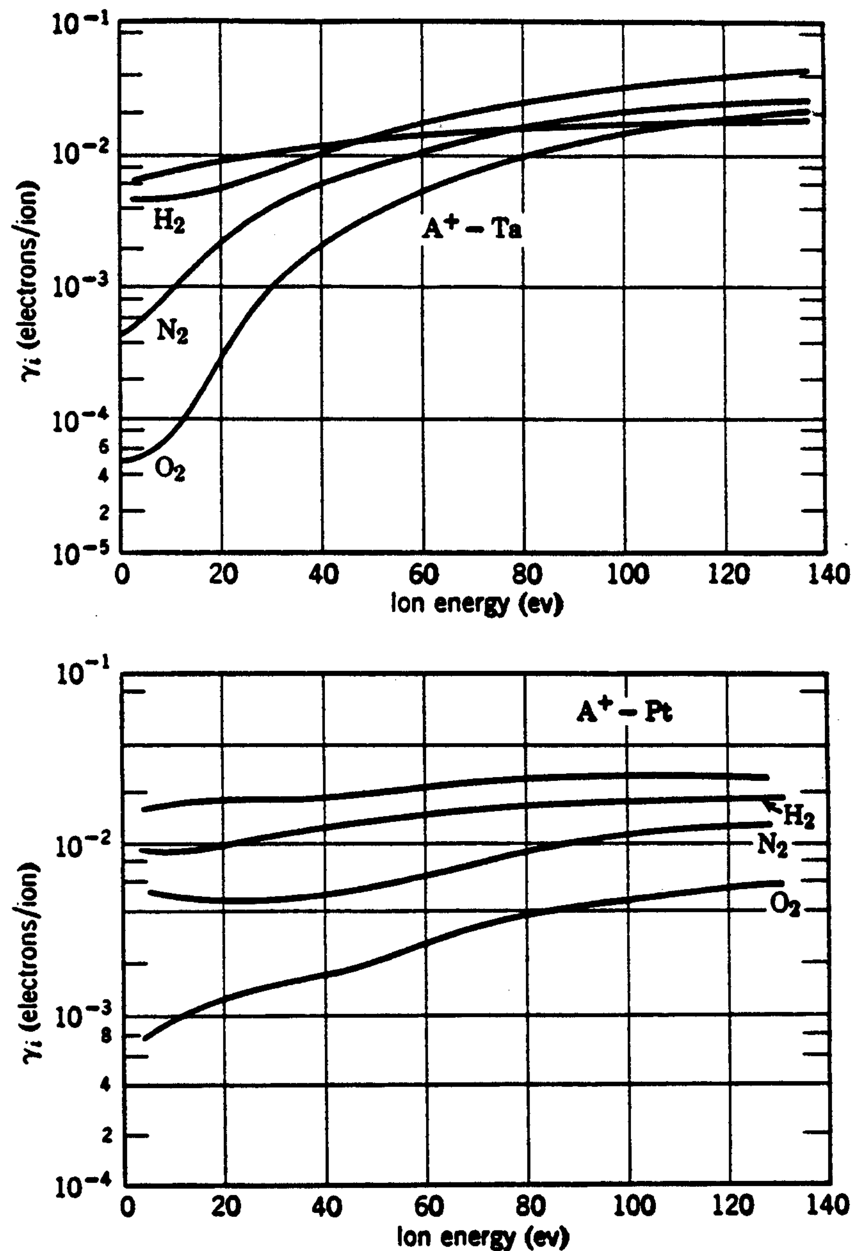

FIG. 13-2-11. Electron yields for A^+ ions on outgased tantalum and platinum and on these metals after treatment with hydrogen, nitrogen, and oxygen. J. H. Parker, *Phys. Rev.* **93**, 1148 (1954).

projectiles, the observed yields must be due entirely to kinetic ejection. Kinetic ejection is also the dominant mechanism at very high ion energies. Data for such energies are displayed in Figures 13-2-16 and 13-2-17.

Oliphant[18] and Allen[19] have investigated the dependence of γ_i on the angle of incidence of the bombarding ions. Figure 13-2-18 shows the behavior observed by Oliphant for 1000 ev He^+ ions on nickel. The angle made by the ions with the normal to the surface is denoted by θ. Allen employed ions in the energy range 48 to 212 kev and observed a yield

maximum predicted for each ion by theory. The agreement is quite good in every case except that of neon. These data are interpreted as meani that He^+, A^+, Kr^+, and Xe^+ ions are neutralized in the process of dire Auger neutralization but that some 10% of the Ne^+ ions are resonanc neutralized near the surface and form excited atoms that go to the grou state by Auger de-excitation. This two-stage process can produce fast electrons and has a higher yield per ion than the direct process.

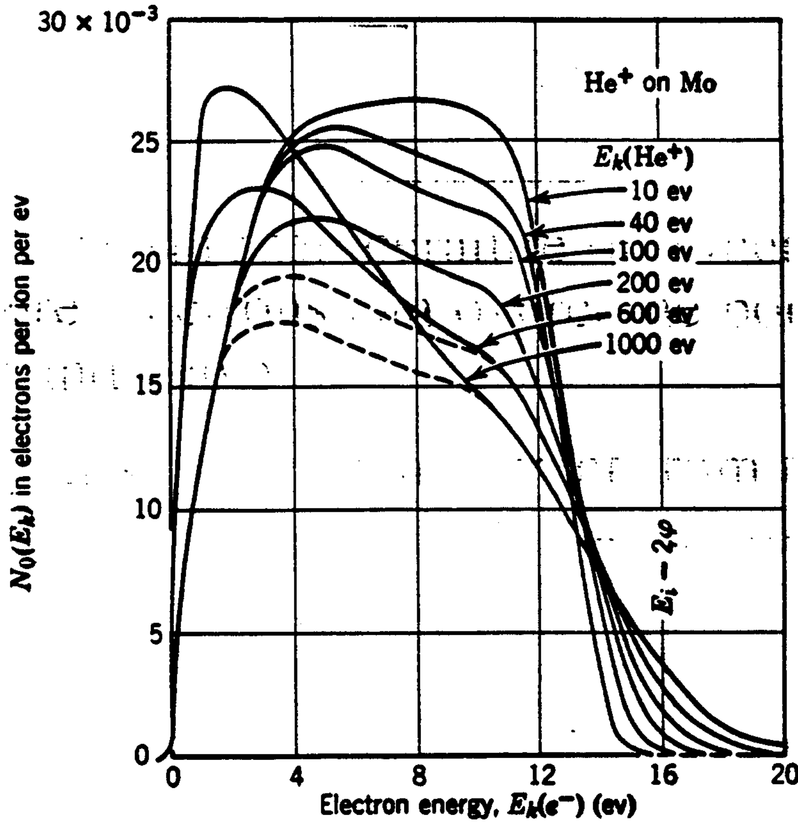

FIG. 13-2-20. Energy distributions of secondary electrons ejected from Mo by He^+ ions of various energies. H. D. Hagstrum, *Phys. Rev.* **104**, 672 (1956).

Hagstrum's lowest energy, 10 ev, the maximum observed electron energy was $E_i - 2\varphi$ for Ne^+ as well as for the other ions.

Figure 13-2-20 illustrates the energy distributions of secondary electrons ejected from atomically clean molybdenum by helium ions as a function of ion kinetic energy. The energy distributions in the ion energy range 10 to 200 ev are explained in terms of Auger neutralization. The low-energy peaks for the 600-ev and 1000-ev ions must come from another process. The dashed portions of these curves describe the behavior expected if only an Auger process were operative. These "excess" low-energy secondaries are probably the result of kinetic ejection.

Kronenberg et al.[20] have recently established the presence of high energy

are produced deep within the target and lose so much energy in collisions with other electrons before they reach the surface that they too cannot escape. We let E_{p0} denote the energy at which the yield reaches its maximum value δ_{max}; E_{p+} and E_{p-} are the primary electron energies at which the yield curve crosses the line $\delta = 1$ with positive and negative slopes, respectively.

Values of δ_{max}, E_{p0}, E_{p+}, and E_{p-} for 31 different metals are listed in Table 13-3-1. Note that δ_{max} varies only from 0.5 to 1.7 in this table, whereas other properties of these metals, such as density and electrical conductivity, vary over a much wider range.

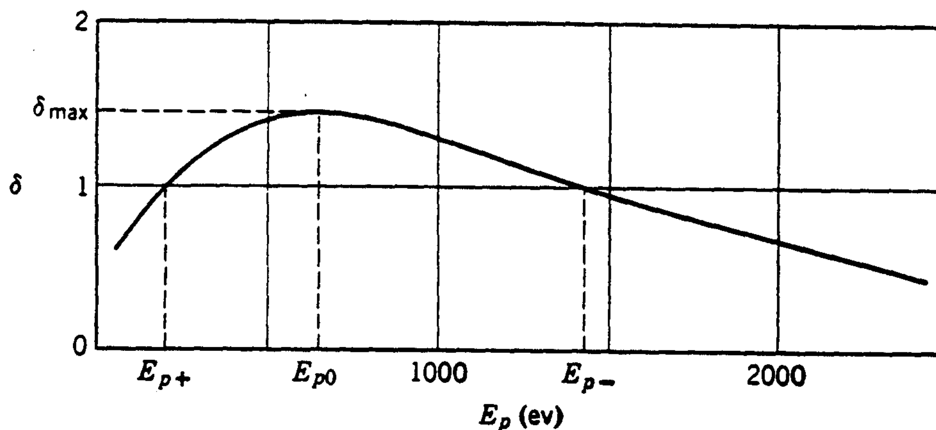

FIG. 13-3-2. A typical plot of secondary electron yield δ as a function of the energy of the primary electrons E_p. The numerical values of the yield shown here are representative of pure metals and many semiconductors, although intermetallic compounds and insulators may have considerably higher yields (see Table 13-3-2).

The secondary electron yield is sensitive to surface contamination and roughness, and values of δ_{max} obtained for metals by various investigators may differ by 10%. Determination of yields for insulators is more difficult than for metals, and discrepancies in the data are considerably wider. The principal difficulty in making measurements on an insulator arises because its low conductivity permits the bombarded surface to acquire a net electrical charge. Thus, if $E_p < E_{p+}$, the surface will charge negatively until it approaches the primary electron accelerating potential and no more primary electrons can strike it. If $E_{p+} < E_p < E_{p-}$, the surface will charge positively to a potential near that of the secondary electron collector, and space charge effects will reduce the effective yield to unity. If $E_p > E_{p-}$, the surface will charge negatively until the yield is increased to unity.

In order to avoid the charging effects experienced with insulators, it is necessary to determine the yield by a pulsed beam technique,[60] in which the surface is allowed to recover completely between pulses of electron

44

collisions within the target. These electrons are the "rediffused primaries" just referred to. Separation of the rediffused primaries and true secondaries is not possible, and the boundary between regions II and III is arbitrary. It is usually taken at 50 ev.

The *total secondary electron yield* δ is defined as the average number of external electrons produced per incident electron. The *true secondary electron yield* δ_{true} is the average number of external electrons in the energy range 0 to 50 ev produced per primary electron. The *backscattering*

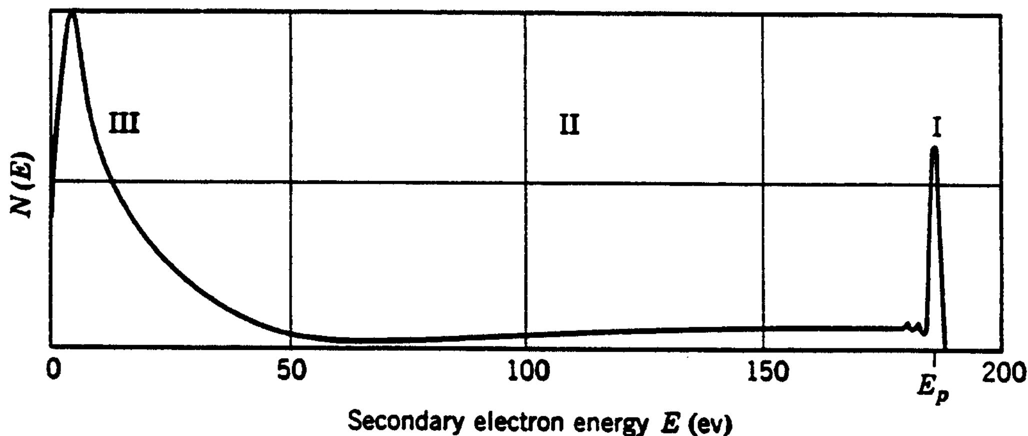

FIG. 13-3-1. A typical energy distribution for secondary electrons; E_p denotes the energy of the primary electrons which produce the secondary emission.

coefficient η is defined as the average number of external electrons with energies greater than 50 ev per incident electron. From these definitions it follows that

$$\delta = \delta_{true} + \eta \tag{13-3-1}$$

Although η may be small in some cases, it certainly is not always small in relation to δ. In spite of this fact, the terms "secondaries" and "true secondaries" are frequently used interchangeably, and most data on secondary emission are expressed in terms of δ rather than δ_{true}.*

1. *Dependence of δ on the energy of the primary electrons.* The secondary yield δ varies with the energy of the primary electrons E_p in approximately the same manner for *all* target materials. Figure 13-3-2 shows the shape of a typical yield curve. At very low and very high energies few secondaries are ejected, but the yield is substantial at intermediate energies and may exceed unity there. At low primary energies the energy of many of the secondaries at the surface is less than the work function of the target, and they cannot escape. At high energies most of the secondaries

* Some Russian authors have attempted to remove this ambiguity by using different letter symbols for the total and true yields. They denote the total yield by σ and the true yield by δ. The relation involving these symbols which is equivalent to (13-3-1) is $\sigma = \delta + \eta$.

45

TABLE 13-3-1. Values of the peak secondary electron yields δ_{max} and the primary electron energies E_{p0} at which they occur for different metals. The electron energies E_{p+} and E_{p-} for which the yields equal unity are also indicated. This table is taken from the review by Hachenberg and Brauer.[57]

Atomic Number	Chemical Symbol	δ_{max}	E_{p0}	E_{p+}	E_{p-}
3	Li	0.5	85	–	–
4	Be	0.5	200	–	–
11	Na	0.82	300	–	–
12	Mg	0.95	300	–	–
13	Al	0.95	300	–	–
19	K	0.7	200	–	–
22	Ti	0.9	280	–	–
26	Fe	1.3	(400)	120	1400
27	Co	1.2	(500)	200	–
28	Ni	1.35	550	150	1750
29	Cu	1.3	600	200	1500
37	Rb	0.9	350	–	–
40	Zr	1.1	350	175	(600)
41	Cb	1.2	375	175	1100
42	Mo	1.25	375	150	1300
46	Pd	>1.3	>250	120	–
47	Ag	1.47	800	150	>2000
48	Cd	1.14	450	300	700
50	Sn	1.35	500	–	–
51	Sb	1.3	600	250	2000
55	Cs	0.72	400	–	–
56	Ba	0.82	400	–	–
73	Ta	1.3	600	250	>2000
74	W	1.35	650	250	1500
78	Pt	1.5	750	350	3000
79	Au	1.45	800	150	>2000
80	Hg	1.3	600	350	>1200
81	Tl	1.7	650	70	>1500
82	Pb	1.1	500	250	1000
83	Bi	1.5	900	80	>2000
90	Ta	1.1	800	–	–

bombardment. Even so, the yield of insulators is so sensitive to surface conditions and method of preparation that results may be quite misleading. The yield of MgO, for example, varies from 2.4 to 25, depending on the method of target preparation, surface treatment, and even the past history of the sample. Table 13-3-2, prepared from data compiled by Hachenberg

46

TABLE 13-3-2. Maximum secondary electron yields from semiconductors and insulators under electron bombardment. These data are taken from the review by Hachenberg and Brauer.[57]

Group	Substance	δ_{max}	E_{p0}
Semiconductive elements	Ge (single crystal)	1.2–1.4	400
	Si (single crystal)	1.1	250
	Se (amorphous)	1.3	400
	Se (crystal)	1.35–1.40	400
	C (diamond)	2.8	750
	C (graphite)	1	250
	B	1.2	150
Semiconductive compounds	Cu_2O	1.19–1.25	400
	PbS	1.2	500
	MoS_2	1.10	
	MoO_2	1.09–1.33	
	Ag_2O	0.98–1.18	
	ZnS	1.8	350
Intermetallic compounds	$SbCs_3$	5–6.4	700
	SbCs	1.9	550
	$BiCs_3$	6–7	1000
	Bi_2Cs	1.9	1000
	GeCs	7	700
Insulators	LiF (evaporated layer)	5.6	
	NaF (layer)	5.7	
	NaCl (layer)	6–6.8	600
	NaCl (single crystal)	14	1200
	NaBr (layer)	6.2–6.5	
	NaBr (single crystal)	24	1800
	NaI (layer)	5.5	
	KCl (layer)	7.5	1200
	KCl (single crystal)	12	
	KI (layer)	5.5	
	KI (single crystal)	10.5	1600
	RbCl (layer)	5.8	
	KBr (single crystal)	12–14.7	1800
	BeO	3.4	2000
	MgO (layer)	4	400
	MgO (single crystal)	23	1200
	BaO (layer)	4.8	400
	BaO—SrO (layer)	5–12	1400
	Al_2O_3 (layer)	1.5–9	350–1300
	SiO_2 (quartz)	2.4	400
	Mica	2.4	300–384
Glasses	Technical glasses	2–3	300–420
	Pyrex	2.3	340–400
	Quartz-glass	2.9	420

- Thermionic electron emission

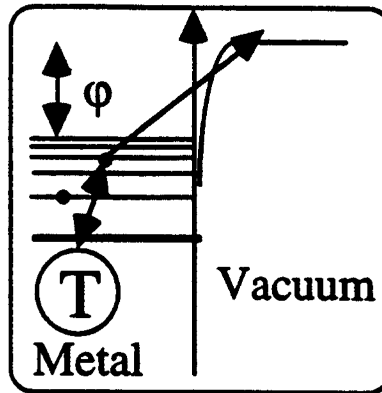

- With increasing temperature of a metal more and more electrons can overcome potential barrier and leave
- This results in electron current from the surface, $j_e^{(Surf)}$, which is described by the Richardson's equation

$$j_e^{(Surf)} = AT^2 \exp(-\varphi/T)$$

$$\text{where } A = me/\left(2\pi^2\hbar^3\right)$$

Lectures outline

L1. Introduction and atomic processes in weakly ionized plasmas

<u>L2. Electric breakdown of a gas and steady state gas discharges</u>

L3. Electron and vibrational kinetics in non-equilibrium plasmas

L4. Waves and instabilities in gas discharge plasmas

L5. Plasma-chemical processes in non-equilibrium weakly ionized plasmas

A. Electric breakdown of a gas

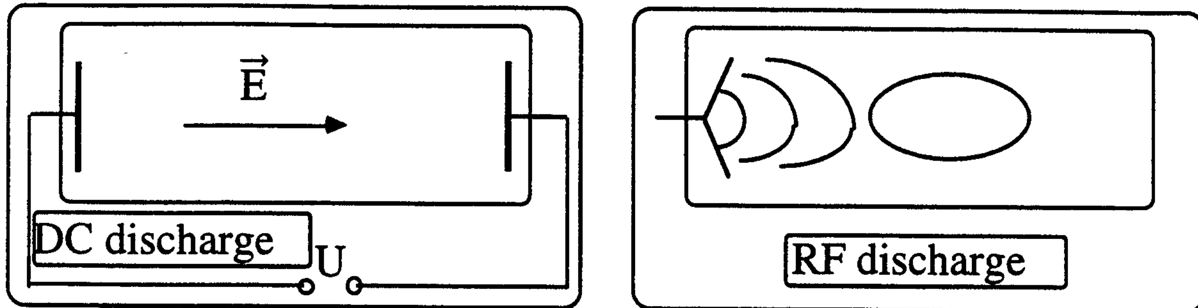

- Evolution of electron and ion densities is described by continuity equations

$$\frac{\partial n_e}{\partial t} + \nabla \cdot \vec{j}_e = S_{(+)} - S_{(-)}, \quad \frac{\partial n_i}{\partial t} + \nabla \cdot \vec{j}_i = S_{(+)} - S_{(-)}$$

where $\vec{j}_e$ and $\vec{j}_i$ are the electron and ion fluxes; $S_{(+)}$, and $S_{(-)}$ are the electron and ion volumetric sources and sinks (we assume no negative ions)

- Before we apply strong DC electric field or RF the electron and ion densities are usually very small ($n_0 \sim 10^3 cm^{-3}$)

- This is not a plasma yet! Electrons and ions are not coupled through ambipolar electric field, E_{amb}, which occurs due to electron and ion separation
- Estimation of ambipolar potential, φ_{amb}, which can be caused by electron and ion separation in a chamber with a scale L can be found from Poisson equation

$$\nabla \cdot (\nabla \varphi) = 4\pi e (n_e - n_i)$$

$$e\varphi^{(0)}_{amb} / \varepsilon_T \lesssim 4\pi e^2 n_0 L^2 / \varepsilon_T \equiv (L/\lambda_D)^2$$

where λ_D is the Debye length and ε_T is electron averaged energy

- For $n_0 \sim 10^3 \mathrm{cm}^{-3}$, $\varepsilon_T \sim 0.1$ eV, we find $\lambda_D \sim$ 100 cm and, therefore, for L ~ 10 cm we have

$$e\varphi^{(0)}_{amb} / \varepsilon_T \lesssim 10^{-2} \text{ and } E^{(0)}_{amb} \lesssim 10^{-4} \text{ V/cm}$$

which are negligibly small

- Notice that for electric breakdown of the gas at the pressure of 1 torr we need an external electric field

$$E_{ext} > 100 \text{ V/cm}$$

- To determine electron and ion fluxes ($\vec{j}_e$ and $\vec{j}_i$) we consider electron and ion momentum balance equations

$$\frac{\partial m n_e \vec{V}_e}{\partial t} + m n_e \left(\vec{V}_e \cdot \nabla\right)\vec{V}_e$$
$$= -e\vec{E}n_e - \nabla\left(n_e \varepsilon_T\right) - m n_e N K_{eN} \vec{V}_e$$

$$\frac{\partial M n_i \vec{V}_i}{\partial t} + M n_i \left(\vec{V}_i \cdot \nabla\right)\vec{V}_i$$
$$= e\vec{E}n_i - \nabla\left(n_i T\right) - M n_i N K_{iN} \vec{V}_i$$

where $\vec{E}$ is the electric field ($\vec{E} = \vec{E}_{ext} + \vec{E}_{amb}$); $\vec{V}_e$ and $\vec{V}_i$ are the electron and ion flow velocities ($\vec{j}_e = n_e\vec{V}_e$, $\vec{j}_i = n_i\vec{V}_i$); m and M are the electron and ion masses; K_{eN} and K_{iN} are the rate constants of elastic electron-neutral and ion-neutrals collisions; T is the neutral/ion temperature and ε_T is the electron "effective" temperature (averaged energy) which can be much higher than T

- Recall that usually $K_{eN} \sim 10^{-7} cm^3/s$ and $K_{iN} \sim 10^{-9} cm^3/s$

- We are interested in a slow processes $\partial_t << \nu_{eN} \equiv NK_{eN}, \nu_{iN} \equiv NK_{iN}$ where left hand sides of momentum balance equations can be ignored and we have

$$\vec{j}_e = -\frac{en_e}{m\nu_{eN}}\vec{E} - \frac{\varepsilon_T}{m\nu_{eN}}\nabla(n_e) \equiv -n_e\mu_e\vec{E} - D_e\nabla(n_e)$$

$$\vec{j}_i = \frac{en_e}{M\nu_{iN}}\vec{E} - \frac{T}{M\nu_{iN}}\nabla(n_i) \equiv n_i\mu_i\vec{E} - D_i\nabla(n_i)$$

where $\mu_e = e/m\nu_{eN}$ and $\mu_i = e/M\nu_{iN}$ are the electron and ion mobilities; $D_e = \varepsilon_T/m\nu_{eN}$ and $D_i = T/M\nu_{iN}$ are the electron and ion diffusion coefficients

- Notice that since $mK_{eN} << MK_{iN}$ we have $\mu_e >> \mu_i$ and $D_e >> D_i$ (a rough estimate gives $mK_{eN}/MK_{iN} \sim \mu_i/\mu_e \sim D_i/D_e \sim \sqrt{m/M}$)
- Since we are considering a conditions for a breakdown of gas we can assume that the electron and ion densities are small and

$$\vec{E} \approx \vec{E}_{ext} >> \vec{E}_{amb}$$

- At low plasma density we also can ignore recombination processes assuming that electrons and ions only are disappear at the surfaces of the chamber (we assume no negative ions!)

- As a result, the electron and ion continuity equations can be written as

$$\frac{\partial n_e}{\partial t} = \nabla \cdot \left(n_e \mu_e \vec{E}_{ext}\right) + \nabla \cdot \left(D_e \nabla (n_e)\right) + n_e \nu_{ion}(\varepsilon_T) + S_0$$

$$\frac{\partial n_i}{\partial t} = -\nabla \cdot \left(n_i \mu_i \vec{E}_{ext}\right) + \nabla \cdot \left(D_i \nabla (n_i)\right) + n_e \nu_{ion}(\varepsilon_T) + S_0$$

where $\nu_{ion}(\varepsilon_T) = NK_{ion}(\varepsilon_T)$, and S_0 is a source of primary electrons and ions (e. g. cosmic UV)

- Notice that in this approximation ion density evolution is completely determined by the evolution of electron one

- Recall that ε_T is determined from the balance of electron energy gain from the electric field and inelastic energy loss and, therefore, in DC electric field

$$\varepsilon_T \propto \varepsilon_E \propto \left(eE_{ext}/mNK_{eN}\right)^2 \propto \left(E_{ext}/N\right)^2$$

DC discharge

- We assume that the discharge chamber is "short"

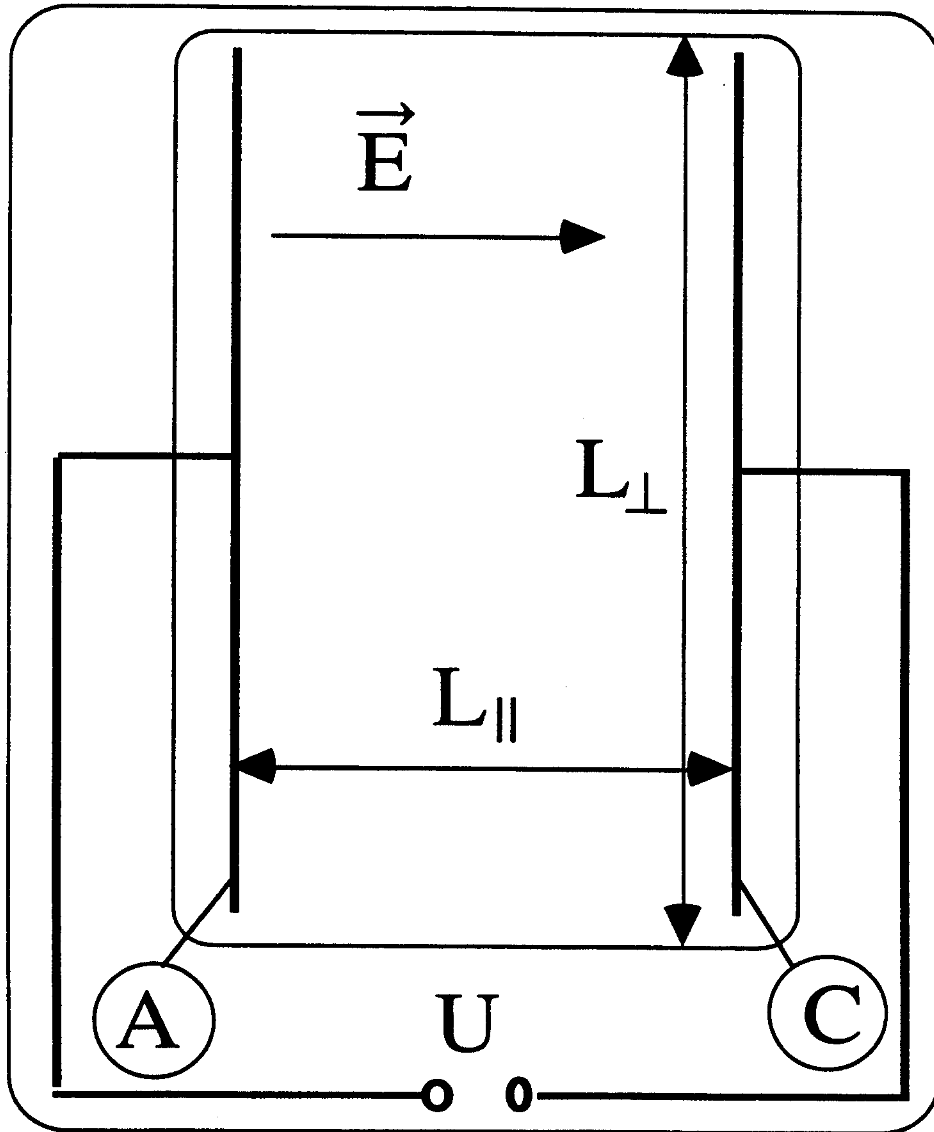

and diffusion loss of charged particles to the sidewalls is small compare to their loss to the electrodes

- Then a steady state solution can be found from equations

$$\frac{d(n_e \mu_e E_{ext})}{dx} + n_e \nu_{ion}(\varepsilon_T) + S_0 = 0$$
$$-\frac{d(n_i \mu_i E_{ext})}{dx} + n_e \nu_{ion}(\varepsilon_T) + S_0 = 0$$

with boundary conditions for the electron, $j_e \equiv -n_e \mu_e E_{ext}$, and ion, $j_i \equiv n_i \mu_i E_{ext}$, fluxes at the electrodes (recall secondary electron emission from the surface due to ion bombardment):

at a cathode: $j_e = -\gamma_i j_i$

at an anode: $j_i = 0$

Notice that E_{ext}, ε_T, μ_i, μ_e, and S_0 do not depend on x-coordinate

- Extracting one of these equations from another and integrating equation for j_e we find that

$$j_i - j_e = j \equiv \text{const.}$$

$$e^{\alpha L_{\parallel}} j_e(\text{Cathode}) - j_e(\text{Anode}) = S_0 \alpha \left(e^{\alpha L_{\parallel}} - 1\right)$$

$\alpha = \nu_{ion} / \mu_e E_{ext}$ is a first Townsend coefficient

- Taking into account boundary conditions at anode and cathode we find

$$j = \frac{S_0 \alpha \left(e^{\alpha L_{\parallel}} - 1 \right)}{1 - \gamma_i e^{\alpha L_{\parallel}} / (1 + \gamma_i)}$$

- Townsend's gas breakdown condition:

$$\alpha L_{\parallel} \equiv L_{\parallel} \nu_{ion} / \mu_e E_{ext} = \ell n \{ (1 + \gamma_i) / \gamma_i \}$$

- Recall that $E_{ext} = U/L_{\parallel}$, $\mu_e = e/mNK_{eN}(\varepsilon_T)$
$\nu_{ion} = NK_{ion}(\varepsilon_T)$, $\varepsilon_T \equiv \varepsilon_T(E_{ext}/N) \equiv \varepsilon_T(U/NL_{\parallel})$
Townsend's criterion can be written as

$$U \left(\frac{NL_{\parallel}}{U} \right)^2 K_{ion} \left(\varepsilon_T \left(\frac{U}{NL_{\parallel}} \right) \right) K_{eN} \left(\varepsilon_T \left(\frac{U}{NL_{\parallel}} \right) \right) \frac{m}{e}$$

$$= \ell n \left\{ \frac{1 + \gamma_i}{\gamma_i} \right\} \quad \Rightarrow$$

$$U \equiv U_{Paschen}(NL_{\parallel})$$

- Ionization rate constant, which has the most crucial dependence on the ratio $NL_{\parallel}/U$ can be approximated as

$$K_{ion}\left(\varepsilon_T\left(U/NL_{\parallel}\right)\right) = A\exp\left(-B\left(NL_{\parallel}/U\right)\right)$$

where A and B are the constant which only depend on a gas properties

- Then Townsend's criterion has the form

$$F\left(NL_{\parallel},U\right) \equiv \frac{\left(NL_{\parallel}\right)^2}{U}\exp\left(-B\frac{NL_{\parallel}}{U}\right) = C$$

where C is some constant

- For given U function $F(NL_{\parallel},U)$ looks like

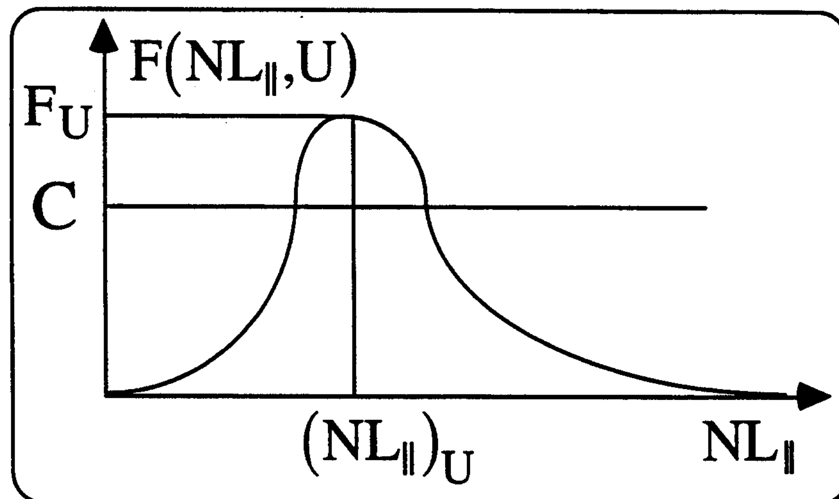

- Where $F_U = 4U/(eB)^2$ and $(NL_{\parallel})_U = 2U/B$

- Therefore:

  a) gas breakdown is only possible for

$$U \geq U_{min} \equiv C(eB)^2/4$$

  b) for given $U > U_{min}$ the breakdown is possible for

$$(NL_{\|})_{min}(U) \leq NL_{\|} \leq (NL_{\|})_{max}(U)$$

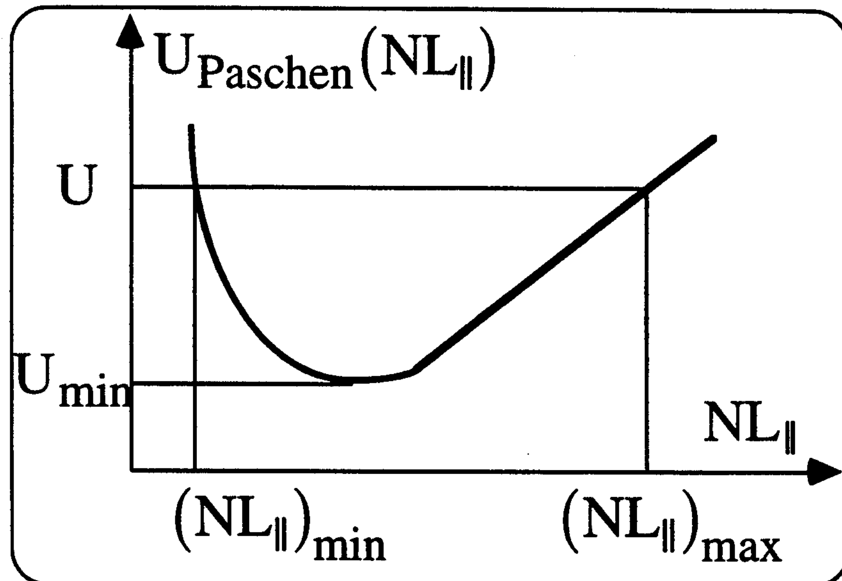

электр... могут исчезать из объема плазмы. Введем понятие частоты прилипания электронов: ν_a — величина, обратно пропорциональная характерному времени, за которое электрон прилипает к какой-либо электроотрицательной молекуле.

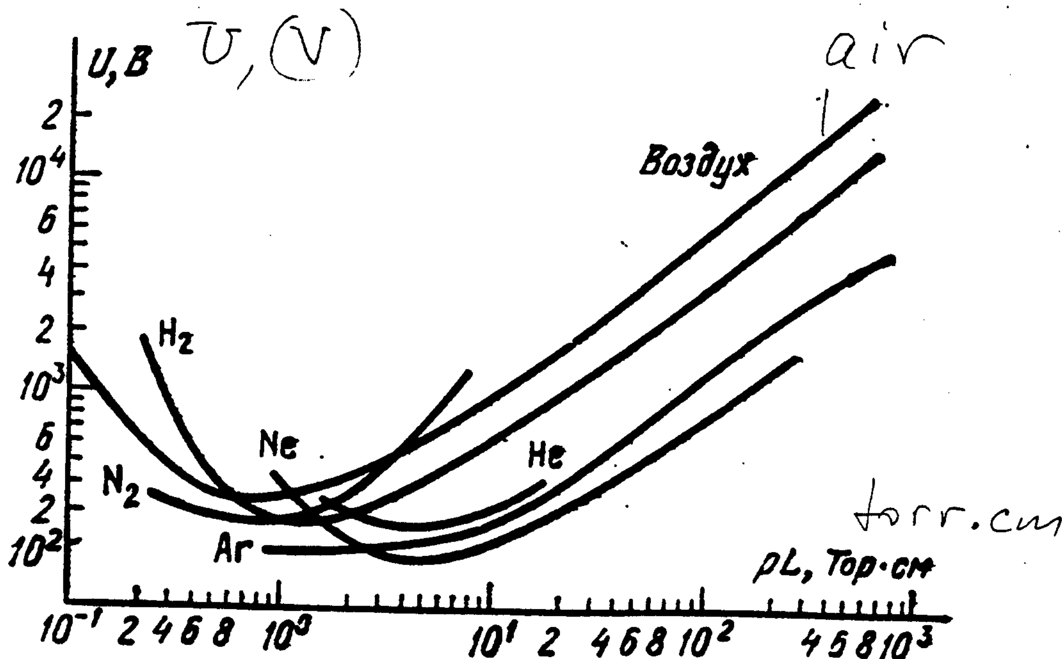

Рис. 1.1. Зависимость напряжения пробоя от параметра pL (кривые Пашена) для различных газов

Тогда условия пробоя таких газов, естественно, изменяются таким образом, что во всех вышеприведенных выражениях величину ν_i необходимо заменить на разность $\nu_i - \nu_a$.

§ 1.2. Пространственно однородный стримерный пробой

Как указывалось выше, критерий пробоя Таунсенда в виде (1.11) и закон подобия Пашена являются очень упрощенными. Основное предположение, допущенное при выводе этих утверждений, заключалось в ограничении плотности вторичных электронов, возникающих на стадии развития пробоя. Естественно, что с ростом параметра pL это условие нарушится (p — давление газа). Опыт показывает, что критерий пробоя в виде (1.11) применим лишь при не слишком высоких значениях $pL < 10^1 - 10^2$ Тор·см.

В случае, когда электрическое поле образующихся

RF discharge

- In RF discharge the energy which electron can gain in electric field depends on RF frequency, ω, and, therefore,

$$\varepsilon_T \propto \varepsilon_E \propto \frac{(eE_{RF}/m)^2}{(NK_{eN})^2 + \omega^2}$$

- Due to oscillation of electric field there is no effect of drift velocity on gas breakdown

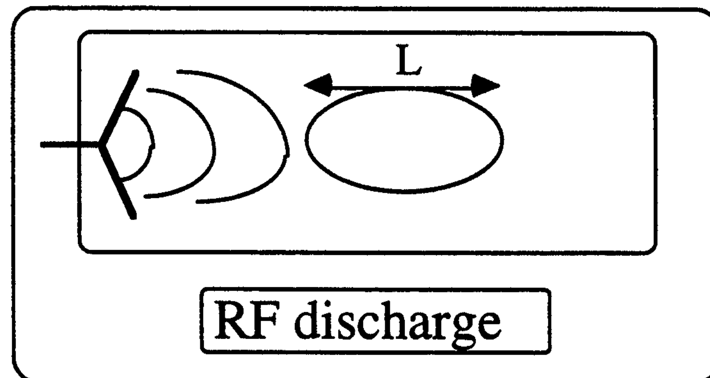

- Then, approximating diffusion loss to the walls in electron continuity equation as $D_e n_e / L^2$ (where L is the scale length the region with high RF wave intensity) we have

$$\frac{\partial n_e}{\partial t} = \left(\nu_{ion}(\varepsilon_T) - D_e/L^2\right) n_e + S_0 \equiv \nu_{RF} n_e + S_0$$

- It gives electron density time evolution

$$n_e(t) = n_0 \exp(\nu_{RF} t) + S_0 (\exp(\nu_{RF} t) - 1) / \nu_{RF}$$

- Exponential growth of electron density corresponds to RF gas breakdown

$$\nu_{RF} \equiv \nu_{ion}(\varepsilon_T) - D_e / L^2 > 0$$

- Recall: $D_e \propto 1/NK_{eN}(\varepsilon_T)$, $\nu_{ion} \propto NK_{ion}(\varepsilon_T)$, and $\varepsilon_T \propto (E_{RF})^2 / \left\{ (NK_{eN})^2 + \omega^2 \right\}$, therefore RF breakdown criterion can be written as

$$N^2 \exp\left\{ -B_{RF} \frac{\sqrt{(NK_{eN})^2 + \omega^2}}{E_{RF}} \right\} \geq C_{RF}$$

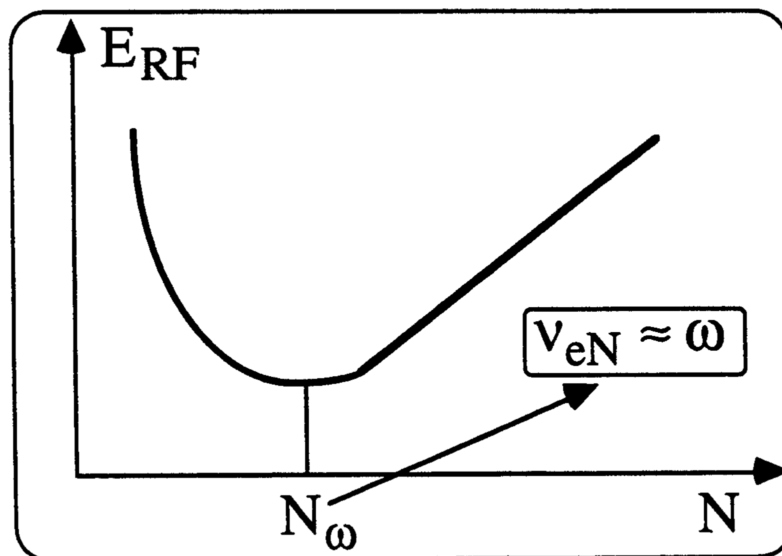

Streamer

- The main simplification we have used to derive Townsend's gas breakdown criterion is that the electric field strength, E, does not vary during gas breakdown and $E \sim E_{ext}$
- However, in many cases this approximation fails (spark, lightning) and electric field can be significantly altered due to electron avalanching

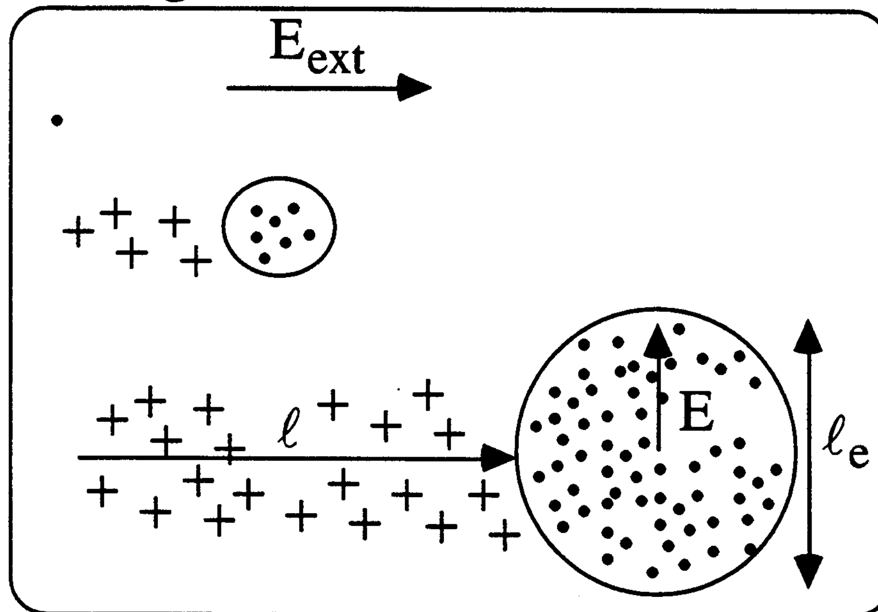

- In this case analysis of a gas breakdown requires to consider both electron transport and electrodynamics equations and becomes very complex
- Here we will just to make some simple estimates to show when it may happen

- Assume that $E_{ext} \gtrsim E$, then

$$\ell(t) \approx \mu_e E_{ext} t \equiv w_e t, \quad \frac{d\ell_e}{dt} \approx \mu_e E, \quad E \approx eN_e/(\ell_e)^2$$

$$N_e \approx \exp(\nu_{ion}\ell/w_e) \equiv e^{\alpha\ell} \quad \Leftarrow \quad \begin{cases} dn_e/dt = \nu_{ion} n_e \\ \\ d\ell/dt = w_e \end{cases}$$

where N_e is the number of electrons in an avalanche

- As a result of avalanching E increases

$$E(t) \approx \left(\sqrt{e}\alpha E_{ext}\right)^{2/3} \exp(\alpha w_e t/3)$$

and $E(t_*) \approx E_{ext}$

- At $t = t_*$ we have

$$N_e \approx E_{ext}/\left(e\alpha^2\right) >> 1 \text{ (applicability limit)}$$

$$\ell(t_*) \approx \ell n\left\{E_{ext}/\left(e\alpha^2\right)\right\}/\alpha >> \ell_e(t_*) \approx 1/\alpha$$

- If different avalanches merge together before $E \sim E_{ext} \Rightarrow$ homogeneous streamer

$$n_0 > \left(\ell_e(t_*)\right)^{-3} \approx \alpha^3 \sim 10^{4\div 6}\,\text{cm}^{-3}$$

B. Steady-state conditions

- After electric gas breakdown electron and ion densities are strongly increased ($\lambda_D << L$) and ambipolar electric field becomes very important to keep ambipolarity $n_e \approx n_i$
- Therefore, electrons can not diffuse freely as before and their life-time can significantly increase
- Consider electron and ion fluxes to the sidewalls in the positive column of DC discharge assuming that $n_e \approx n_i \approx n$

$$\vec{j}_e = -n\mu_e\vec{E} - D_e\nabla n, \qquad \vec{j}_i = n\mu_i\vec{E} - D_i\nabla n$$

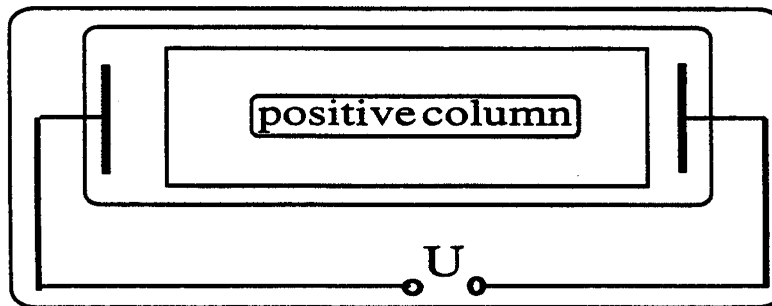

- Since $\vec{j}_e = \vec{j}_i = \vec{j}$ we find electric field $\vec{E}_{amb}$, which maintains ambipolarity, and $\vec{j}$

$$\vec{E}_{amb} = -\frac{(D_e - D_i)}{\mu_e + \mu_i} \nabla \ell n(n)$$

$$\vec{j} = -D_e \frac{\mu_i}{\mu_e} \nabla n \equiv -D_{amb} \nabla n$$

where D_{amb} is the ambipolar diffusion coefficient

$$D_e >> D_{amb} >> D_i$$

- Therefore electron life-time, $\tau_{life} \approx L_\perp^2 / D_{amb}$, becomes much larger than free electron diffusion time, $L_\perp^2 / D_e$,
- As a result, DC electric field, E, in positive column must be significantly lower than it use to be during breakdown and is determined by the balance of neutral ionization and plasma diffusion loss

$$D_{amb}(E) / L_\perp^2 = N K_{ion}(E)$$

$$\frac{\varepsilon_T(E/N)}{K_{iN}(NL_\perp)^2} = K_{ion}(E/N)$$

- In RF discharges reduction of electron loss due to switch from free electron to ambipolar diffusion results in

$$NK_{ion}(E_{RF}) > D_{amb}(E_{RF})/L_{\perp}^{2}$$

- Therefore a steady-state condition can only be reached due to reduction of RF electric field
- Usually it occurs when electrons in the discharge start to alter RF wave propagation
- In simplest case of a planar RF wave it corresponds electron density n

$$\omega_{pe}(n) \equiv \sqrt{4\pi ne^{2}/m} \approx \omega_{RF}$$

- At that conditions RF wave propagation becomes very nonlinear and even anomalous absorption mechanism can appear

Lectures outline

L1. Introduction and atomic processes in weakly ionized plasmas

L2. Electric breakdown of a gas and steady state gas discharges

<u>L3. Electron and vibrational kinetics in non-equilibrium plasmas</u>

L4. Waves and instabilities in gas discharge plasmas

L5. Plasma-chemical processes in non-equilibrium weakly ionized plasmas

A. Electron kinetics in gas discharge plasmas

- In previous lectures we have used some estimates for the rate constants of electron-neutral interactions (K_{eN}, K_{ion}, K_{excit}, ...)
- However, the rate constants of electron-neutral interactions are determined by electron distribution function $f_e(\vec{v},\vec{r},t)$

$$K_{(...)}(\vec{r},t) = \int \sigma_{(...)}(|\vec{v}|)|\vec{v}| f_e(\vec{v},\vec{r},t)d\vec{v}$$

- Where $f_e(\vec{v},\vec{r},t)$ itself is determined by electron heating in applied electric field, $\vec{E}$, and cooling due to elastic and (mainly) inelastic electron-neutral collisions
- Moreover, since ionization degree in gas discharge plasmas is usually small ($< 10^{-4}$), electron-electron collisions (causing Maxwellization of $f_e(\vec{v},\vec{r},t)$) are weak and $f_e(\vec{v},\vec{r},t)$ is far from Maxwellian
- Thus, $f_e(\vec{v},\vec{r},t)$ can only be found from solution of electron kinetic equation

- Kinetic equation for $f_e(\vec{v},\vec{r},t)$

$$\frac{\partial f_e(\vec{v},\vec{r},t)}{\partial t}+\nabla_{\vec{r}}\cdot\left(\vec{v}f_e(\vec{v},\vec{r},t)\right)-\nabla_{\vec{v}}\cdot\left(\frac{e\vec{E}}{m}f_e(\vec{v},\vec{r},t)\right)=$$

$$C_{eN}(f_e)+C_{ee}(f_e,f_e)+C_{ei}(f_e)$$

where $C_{eN}(f_e)$, $C_{ee}(f_e,f_e)$, and $C_{ei}(f_e)$ are the collision terms describing electron-neutral, electron-electron, and electron-ion interactions

- The most important conclusion which can be made from the observation of electron kinetic equation is:

  if electron-neutral collisions dominate than electron kinetics and, hence, all electron-neutral interaction (excitation, dissociation, ionization, elastic collisions, etc.) depend only on the ratio

$$E/N$$

simultaneously, characteristic length and time scale like N^{-1}

- It can be proven by making scaling transformation $t\times N\to t'$ and $\vec{r}\times N\to\vec{r}'$ in general electron kinetic equation

- Recall that if electron energy loss is due to elastic collisions then electron drift velocity, $v_e \approx eE/(mNK_{eN})$, is mach smaller than electron thermal velocity v_T

$$v_e \approx \sqrt{m/M}\, v_T << v_T$$

- In this case electron distribution function is almost spherically symmetric
- This will be true even if electron energy loss is due to inelastic collisions, but $\sigma_{eN}^{elastic} > \sigma_{eN}^{inelastic}$ and symmetrization of $f_e(\vec{v},\vec{r},t)$ in velocity space occurs faster than energy loss
- Fortunately this inequality usually holds and therefore electron kinetic equation can be significantly simplified

- When $f_e(\vec{v},\vec{r},t)$ is almost symmetric in velocity space we can use the expansion of $f_e(\vec{v},\vec{r},t)$ around spherical one

$$f_e(\vec{v},\vec{r},t) = f_0(|\vec{v}|,\vec{r},t) + \cos\vartheta\, f_1(|\vec{v}|,\vec{r},t) + \ldots$$

where $\cos\vartheta = \left(\vec{v}\cdot\vec{E}\right)/(vE)$ and $f_0 >> f_1$

- Consider electron-neutral collision term

$$C_{eN}(f_e)$$
$$= -\int d\vec{v}_1 d\Omega\, q(u,\vartheta)u\left\{f_e(\vec{v})F(\vec{v}_1) - f_e(\vec{v}')F(\vec{v}'_1)\right\}$$

where $F(\vec{v})$ is the neutral distribution function, $u = |\vec{v}-\vec{v}_1|$, $q(u,\vartheta)$ is the differential cross-section, and $\vec{v}'$ and $\vec{v}'_1$ are the particle velocities after collision

- Taking into account that electron velocity is much higher than neutral one and $|\vec{v}| \approx |\vec{v}'|$ in elastic collisions it is possible to show that

$$\left\langle C_{eN}(f_e)\cos\vartheta\right\rangle$$
$$= -N\int d\Omega\, q(v,\vartheta)v(1-\cos\vartheta)f_1(|\vec{v}|,\vec{r},t)$$

and $N\int d\Omega\, q(v,\vartheta)v(1-\cos\vartheta) \equiv NK_{eN}^{(m)}(v) \equiv \nu_{eN}^{(m)}(v)$ is the momentum transfer frequency

- As a result, neglecting f_k (k>1), we have coupled equations for f_0 and f_1

$$\frac{\partial f_0}{\partial t}+\frac{v}{3}\frac{\partial f_1}{\partial x}-\frac{eE}{3mv^2}\frac{\partial\left(v^2 f_1\right)}{\partial v}=C_{eN}\left(f_0\right)$$

$$\frac{\partial f_1}{\partial t}+v\frac{\partial f_0}{\partial x}-\frac{eE}{m}\frac{\partial f_0}{\partial v}=-\nu_{eN}^{(m)}(v)f_1$$

- Considering slow processes, $\partial_t \ll \nu_{eN}^{(m)}$, we find

$$f_1=\frac{eE}{m\nu_{eN}^{(m)}(v)}\frac{\partial f_0}{\partial v}-\frac{v}{\nu_{eN}^{(m)}(v)}\frac{\partial f_0}{\partial x}$$

convection $\Downarrow$ $\Uparrow$ *diffusion* $\Downarrow$ $\Uparrow$

$$\frac{\partial f_0}{\partial t}+\frac{\partial}{\partial x}\left(\frac{eEv}{3m\nu_{eN}^{(m)}(v)}\frac{\partial f_0}{\partial v}\right)=\frac{\partial}{\partial x}\left(\frac{v^2}{3\nu_{eN}^{(m)}(v)}\frac{\partial f_0}{\partial x}\right)$$

$$+\frac{1}{3v^2}\frac{\partial}{\partial v}\left(\frac{(eE/m)^2 v^2}{\nu_{eN}^{(m)}(v)}\frac{\partial f_0}{\partial v}\right)+C_{eN}\left(f_0\right)$$

heating $\Uparrow$ *cooling* $\Uparrow$

- In general case equation for f_0 can only be solved numerically even for a steady-state homogeneous conditions
- However, in some interesting limits it is possible to simplify collision term $C_{eN}(f_0)$ and get analytic solution
- For example, for elastic collisions $C_{eN}(f_0)$ can be written as

$$C_{eN}^{elastic}(f_0) = \frac{m}{M}\frac{1}{\sqrt{\varepsilon}}\frac{\partial}{\partial\varepsilon}\left\{\varepsilon^{3/2}\nu_{eN}(\varepsilon)\left(T_N\frac{\partial f_0}{\partial\varepsilon}+f_0\right)\right\},$$

where $N\int d\Omega q(v,\vartheta)v \equiv NK_{eN}(v) \equiv \nu_{eN}(v)$, and $\varepsilon = mv^2/2$; for excitation process we have

$$C_{eN}^{ext}(f_0) = -\nu_{eN}^{ext}(\varepsilon)f_0(\varepsilon) + \sqrt{\frac{\varepsilon+\varepsilon_{th}}{\varepsilon}}\,\nu_{eN}^{ext}(\varepsilon+\varepsilon_{th})f_0(\varepsilon+\varepsilon_{th})$$

where ε_{th} is a threshold energy, and for $\varepsilon_T >> \varepsilon_{th}$ expression for $C_{eN}^{ext}(f_0)$ can be reduced to

$$C_{eN}^{ext}(f_0) = \frac{\varepsilon_{th}}{\sqrt{\varepsilon}}\frac{\partial}{\partial\varepsilon}\left(\nu_{eN}^{ext}(\varepsilon)\sqrt{\varepsilon}f_0(\varepsilon)\right)$$

- Then electron kinetic equation for these two cases can be written as follows

$$\frac{2}{3\sqrt{\varepsilon}}\frac{\partial}{\partial\varepsilon}\left(\frac{(eE)^2\varepsilon^{3/2}}{m\nu_{eN}^{(m)}(\varepsilon)}\frac{\partial f_0}{\partial\varepsilon}\right) + \frac{m}{M}\frac{1}{\sqrt{\varepsilon}}\frac{\partial}{\partial\varepsilon}\left\{\varepsilon^{3/2}\nu_{eN}(\varepsilon)\left(T_N\frac{\partial f_0}{\partial\varepsilon}+f_0\right)\right\}=0$$

for elastic collisions and

$$\frac{2}{3\sqrt{\varepsilon}}\frac{\partial}{\partial\varepsilon}\left(\frac{(eE)^2\varepsilon^{3/2}}{m\nu_{eN}^{(m)}(\varepsilon)}\frac{\partial f_0}{\partial\varepsilon}\right)+\frac{\varepsilon_{th}}{\sqrt{\varepsilon}}\frac{\partial}{\partial\varepsilon}\left(\nu_{eN}^{ext}(\varepsilon)\sqrt{\varepsilon}f_0(\varepsilon)\right)=0$$

for neutral excitation in the limit $\varepsilon_T >> \varepsilon_{th}$

- Solving these equations we find

$$f_0(\varepsilon)=f_0(0)\exp\left(-\int_0^{\varepsilon}d\varepsilon'/T_{eff}(\varepsilon')\right)$$

where $T_{eff}(\varepsilon)=\frac{2}{3}\frac{(eE/m)^2 M}{\nu_{eN}(\varepsilon)\nu_{eN}^{(m)}(\varepsilon)}+T_N$, and

$$f_0(\varepsilon)\propto\exp\left\{-\int_0^{\varepsilon}d\varepsilon'\,\frac{3\varepsilon_{th}m\,\nu_{eN}^{ext}(\varepsilon')\nu_{eN}^{(m)}(\varepsilon')}{2(eE)^2\varepsilon'}\right\}\ (\varepsilon>\varepsilon_{th})$$

- General trend of $f_0(\varepsilon)$: $f_0(\varepsilon)$ is strongly depleted above excitation threshold. E.g. for $\nu_{eN}^{ext}(\varepsilon) \propto \nu_{eN}^{(m)}(\varepsilon) \propto \sqrt{\varepsilon}$ we have

$$f_0(\varepsilon) \propto \exp\{-\varepsilon/T_{ext}\} \; (\varepsilon > \varepsilon_{th})$$

where $T_{ext} = \left(2(eE)^2\varepsilon\right) \Big/ \left(3\varepsilon_{th} m \, \nu_{eN}^{ext}(\varepsilon)\nu_{eN}^{(m)}(\varepsilon)\right)$ decreases with increasing ν_{eN}^{ext}

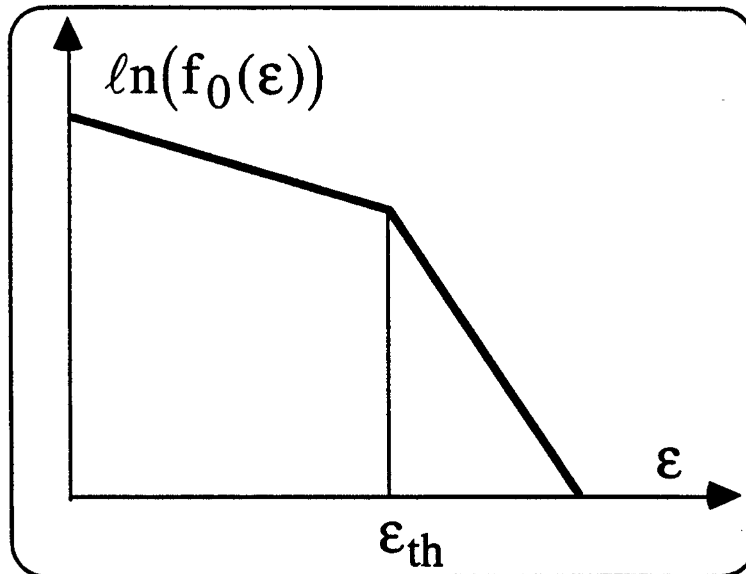

- As a result of $f_0(\varepsilon)$ depletion at $\varepsilon > \varepsilon_{th}$ the excitation rate,

$$S_{ext} = \int_0^\infty d\varepsilon \sqrt{\varepsilon} \, \nu_{eN}^{ext}(\varepsilon) f_0(\varepsilon),$$

saturates with increasing ν_{eN}^{ext}

- Saturated level of excitation rate, $(S_{ext})_{sat}$, can be found by solving kinetic equation for $\varepsilon<\varepsilon_{th}$ and assuming that $f_0(\varepsilon_{th})=0$ (electrons with $\varepsilon>\varepsilon_{th}$ excite instantaneously)
- For $\varepsilon<\varepsilon_{th}$ kinetic equation is simple

$$\frac{\partial(-j_\varepsilon)}{\sqrt{\varepsilon}\,\partial\varepsilon} \equiv \frac{\partial}{\sqrt{\varepsilon}\,\partial\varepsilon}\left(\frac{2(eE)^2\varepsilon^{3/2}}{3m\,\nu_{eN}^{(m)}(\varepsilon)}\frac{\partial f_0}{\partial\varepsilon}\right)=0$$

where j_ε is the particle flux along ε-coordinate into region $\varepsilon>\varepsilon_{th}$ and which is equal to $(S_{ext})_{sat}$

- Therefore, assuming that $f_0(\varepsilon_{th})=0$ we have

$$f_0(\varepsilon)=(S_{ext})_{sat}\int_{\varepsilon}^{\varepsilon_{th}} d\varepsilon'\,\frac{3m\,\nu_{eN}^{(m)}(\varepsilon')}{2(eE)^2\varepsilon'^{3/2}}$$

- Then, taking into account $n_e = \int_0^\infty d\varepsilon\sqrt{\varepsilon}\,f_0(\varepsilon)$,

  we find $(S_{ext})_{sat}$

$$(S_{ext})_{sat}=\frac{n_e}{\int_0^\infty d\varepsilon\sqrt{\varepsilon}\int_{\varepsilon}^{\varepsilon_{th}} d\varepsilon'\,\frac{3m\,\nu_{eN}^{(m)}(\varepsilon')}{2(eE)^2\varepsilon'^{3/2}}}\sim n_e\nu_{eN}^{(m)}\frac{\varepsilon_E}{\varepsilon_{th}}$$

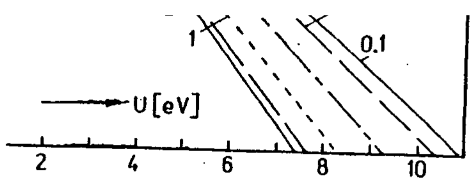

Fig. 10

Fig. 11

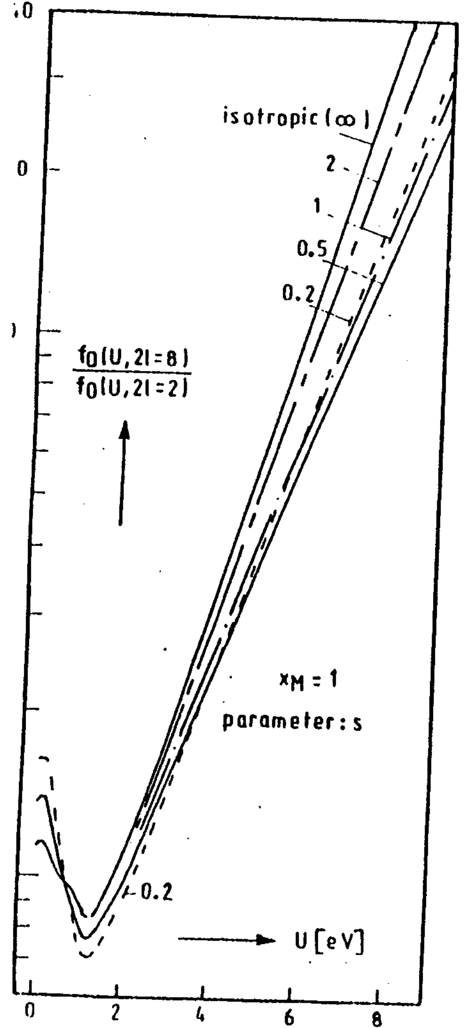

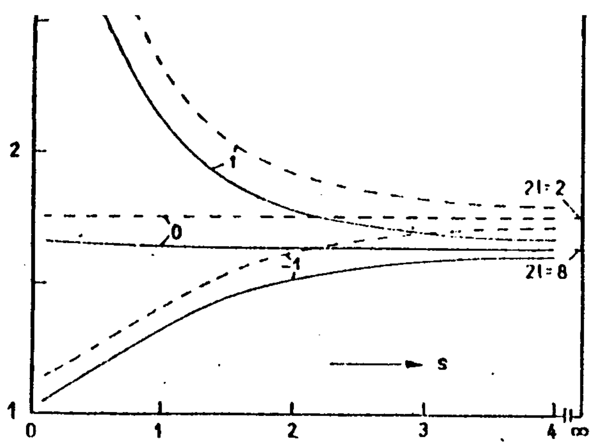

Fig. 12

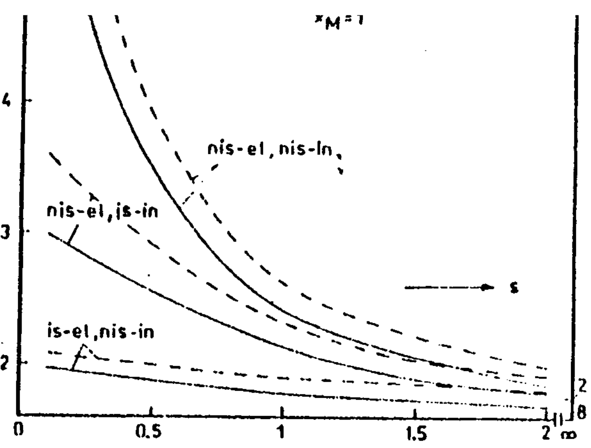

Fig. 13

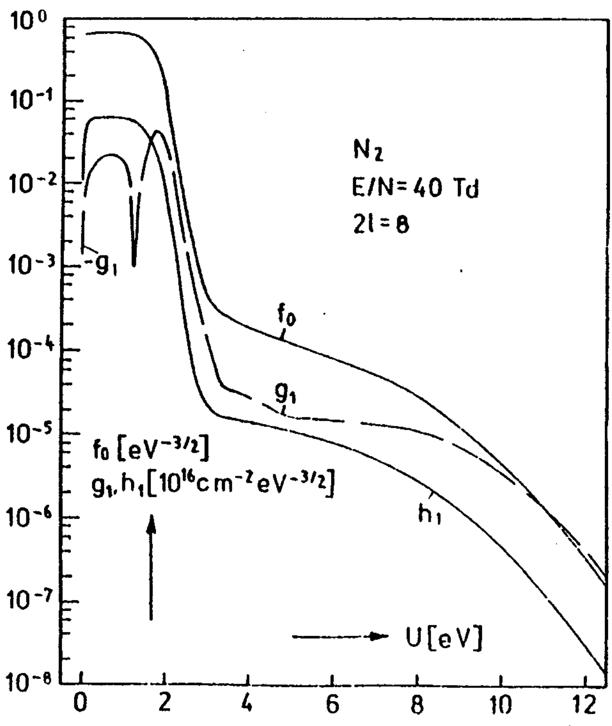

Fig. 14

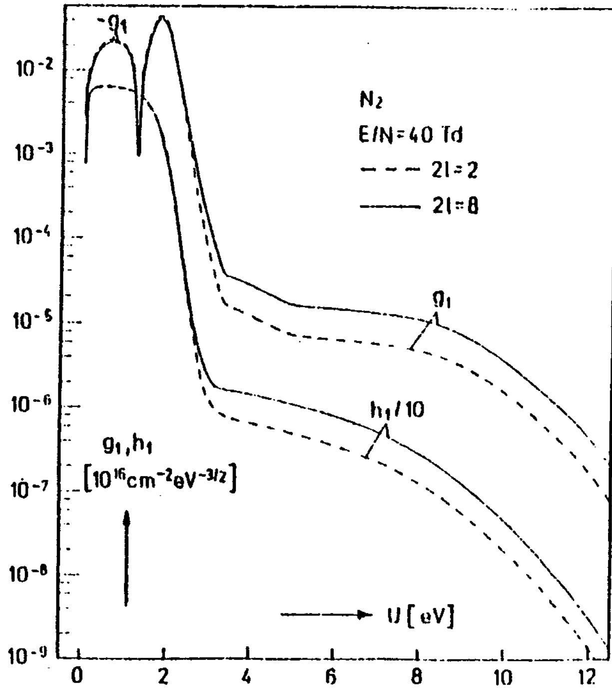

Fig. 15

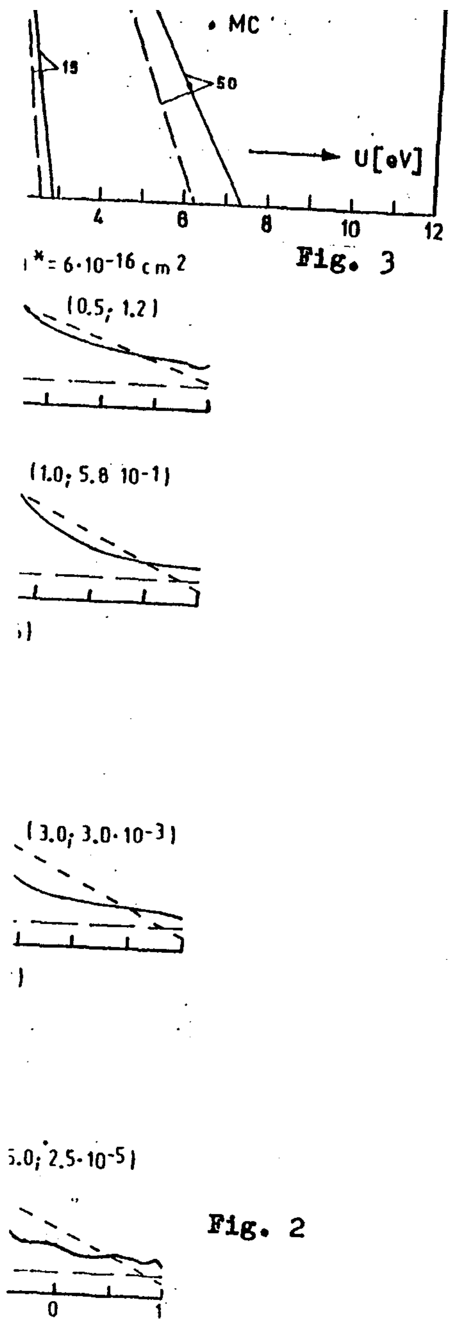

Fig. 3

Fig. 2

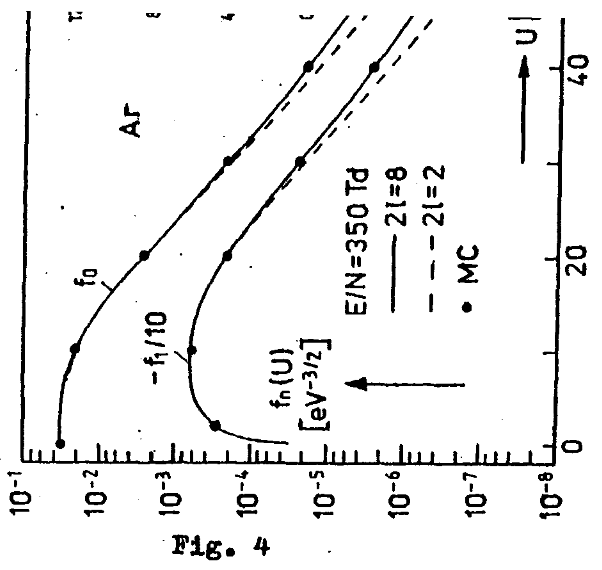

Fig. 4

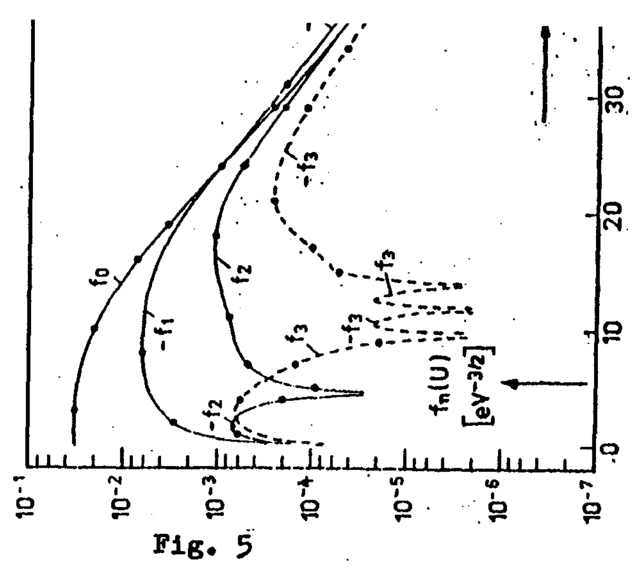

Fig. 5

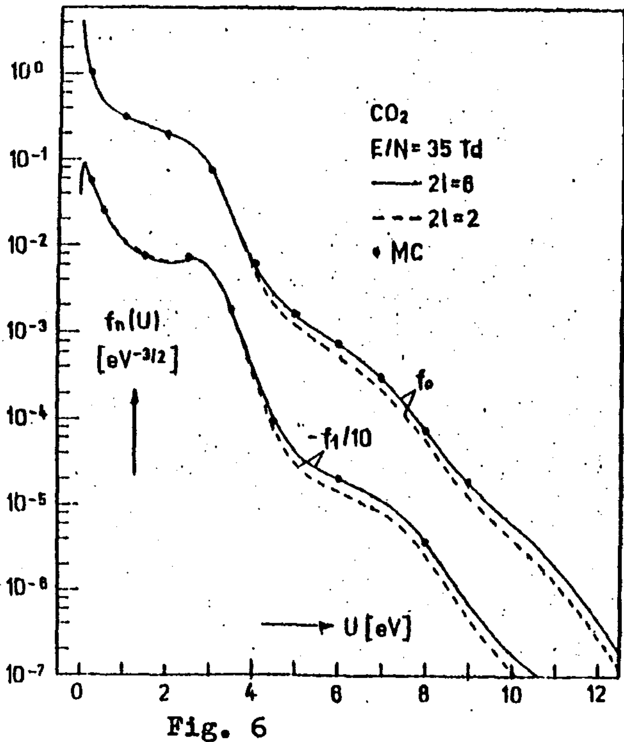

Fig. 6

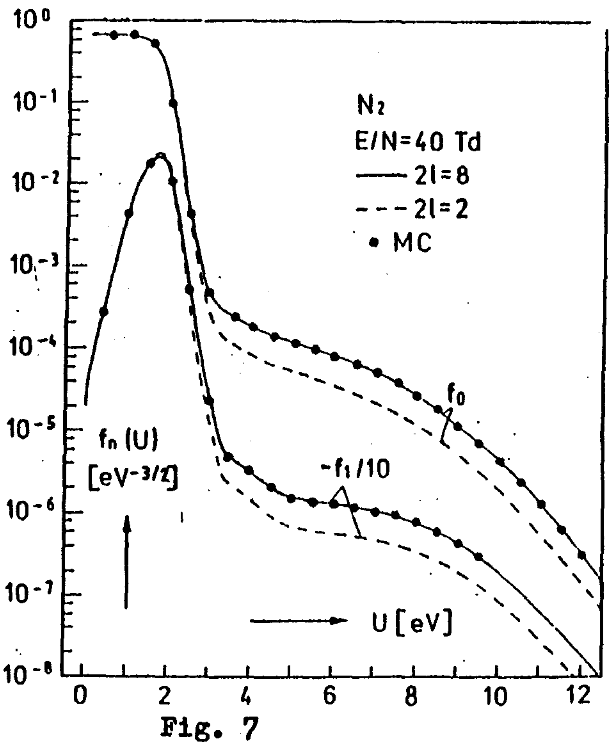

Fig. 7

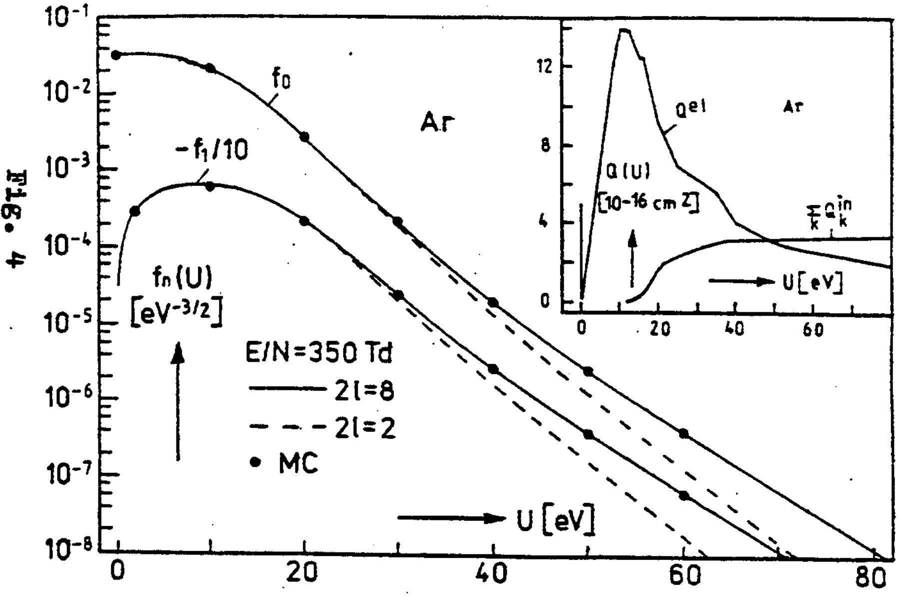

Fig. 4

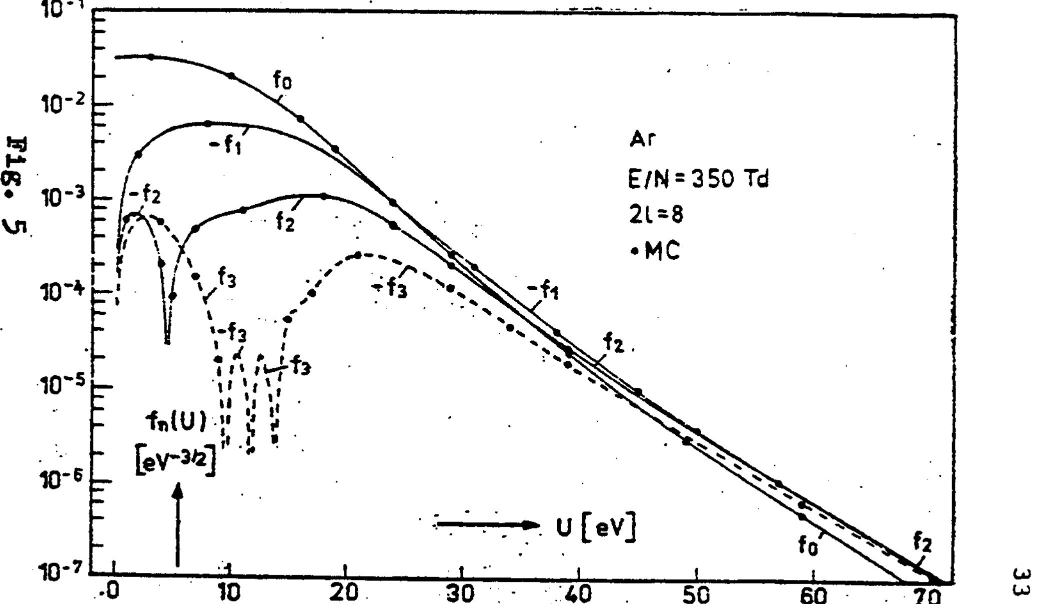

Fig. 5

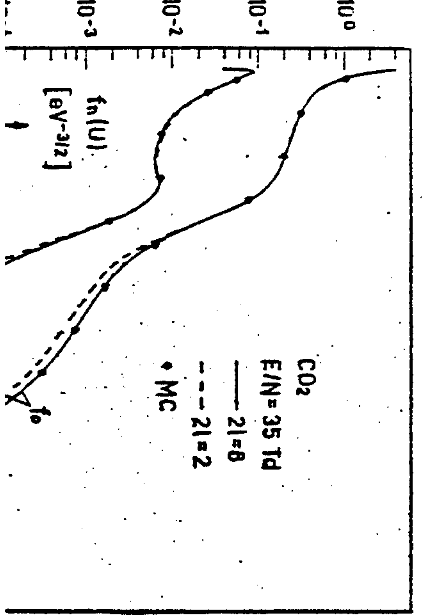

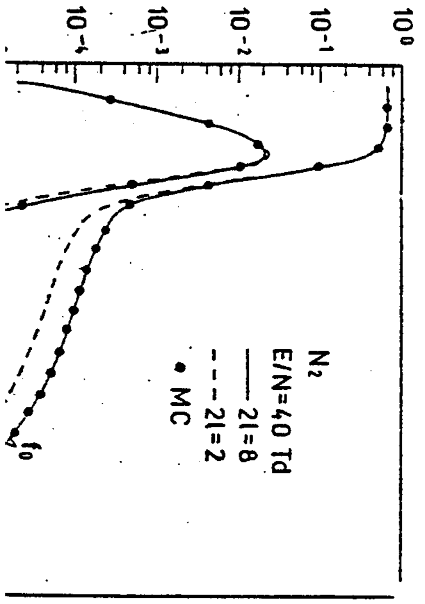

B. Kinetics of vibrationally excited molecules in non-equilibrium plasmas

- Vibrationally excited molecules in gas discharge plasmas play a very important role in:

    a) electron kinetics and energy balance

    b) gas lasers

    c) endothermic chemical reactions (e. g. $AB(v \geq v_{th}) + C \rightarrow A + BC$), since effective vibrational temperature, T_v, can be much higher than gas temperature T_N

- Main mechanisms of vibrational excitation and de-excitation of molecules

    a) *excitation*: by electron impact through the formation and decay of metastable negative molecule (e-v processes)

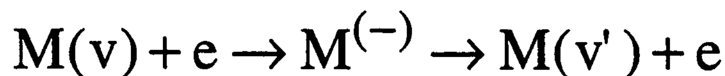

    b) *de-excitation*: by neutral particles (v-T processes)

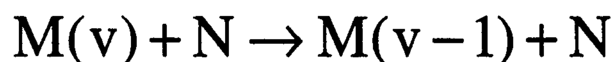

- While e-v processes are very effective, v-T are not and it allows to reach $T_v >> T_N$ in a weakly ionized plasmas
- The reason why v-T processes are not effective is that neutrals are heavy particle and Massey parameter is large

$$Ma \equiv E_0 r_b / \hbar v_T >> 1$$

where E_0 is the energy of vibrational excitation, r_b is the Bohr radius, and v_T is the neutral thermal velocity

- Massey parameter occurs from a quantum mechanic treatment of the probability of vibrational transition, P_{v-T}, due to neutral-molecular interaction $V(\vec{r})$

$$P_{v-T} \propto \int_{-\infty}^{\infty} e^{-i\omega t} V(t) dt \equiv \int_{-\infty}^{\infty} e^{-i(E_0/\hbar)t} V(t) dt$$

where $V(t) \equiv V(\vec{v}_N t)$ varies smoothly at time scale ~ r_b / v_N (e. g. $V(t) \propto 1 / \left\{ 1 + (v_N t / r_b)^2 \right\}$)

- As a result we find

$$P_{v-T} \propto \exp(-E_0 r_b / \hbar v_N)$$

- Averaging P_{v-T} over Maxwellian distribution of neutrals we arrive to Landau-Teller formula for v-T relaxation rate constant K_{v-T}

$$K_{v-T} \approx K_{NN}\, \pi^{-3/2} \times \int \exp\left(-E_0 r_b/\hbar v_N - M v_N^2/2T_N\right) d(\vec{v}_N/v_T)$$

- After some algebra we find

$$K_{v-T} \approx K_{NN}\, 2^{5/6} (Ma)^{2/3} \exp\left\{-3(Ma/2)^{2/3}\right\} \propto \exp\left\{-(E_{Ma}/T_N)^{1/3}\right\}$$

where $E_{Ma} = \frac{27}{8}\left(\frac{E_0 r_b}{\hbar}\right)^2 M_N \equiv E_0 \frac{27}{8}\frac{E_0}{E_b}\frac{M_N}{m}$, in practice $E_{Ma} \sim 100$ eV $>> T_N \lesssim 0.1$ eV $(Ma \sim 30)$

- As a result, e-v excitation can exceed v-T relaxation at a very low ionization degree

$$n_e/N \gtrsim K_{ev}/K_{v-T} \gtrsim 10^{-5\div 7}$$

- While v-T relaxation is slow, an exchange of vibrational quanta (v-v exchange)

$$M(v) + M(v') \rightarrow M(v+1) + M(v'-1)$$

is fast, since it is almost a resonance process (corresponding Massey parameter << 1)

- The kinetic equation for the population of vibrational states of molecules taking into account e-v, v-v, v-T processes and chemical reactions can be written as follows

$$\frac{dN_v}{dt} = C_{e-v} + C_{v-v} + C_{v-T} + C_R$$

where N_v is the density of the molecules on virational level v, C_{e-v}, C_{v-v}, C_{v-T}, and C_R are collisional terms describing vibrational excitation by electron impact, v-v exchange, v-T relaxation, and chemical reactions

- The expressions for C_{e-v}, C_{v-T}, and C_R can be written as

$$C_{e-v} = -n_e \sum_w K_{e-v}(v,w)\left\{N_v - N_{v+w} e^{(E_{v+w}-E_v)/T_e}\right\}$$

$$+n_e \sum_{w>0} K_{e-v}(v-w,w)\left\{N_{v-w} - N_v e^{(E_v-E_{v-w})/T_e}\right\}$$

$$C_{v-T} = -NK_{v-T}(v)\left\{N_v - N_{v-1} e^{(E_{v-1}-E_v)/T_N}\right\}$$

$$C_R = -\nu_R(v)N_v$$

- Consider v-v exchange collisional term

$$C_{v-v} = -\sum_{v',w} K_{v-v}(v',w)\{N_v N_{v'} - N_{v+w} N_{v'-w} \exp(-2E_0\chi_v w(v-v'+w)/T_N)\}$$

where exponential factor, depending on gas temperature, is due to relations between the rate constants of direct and inverse processes

- For the conditions where v-v exchange is a dominant term in vibrational kinetics we find that $C_{v-v}=0$ results in so-called Treanor distribution of vibrationally excited states

$$N_v^{Treanor} \propto \exp\left\{-\frac{E_0(v+1/2)}{T_v} + \frac{E_0\chi_v(v+1/2)^2}{T_N}\right\}$$

where T_v is effective vibr. temperature of v=1

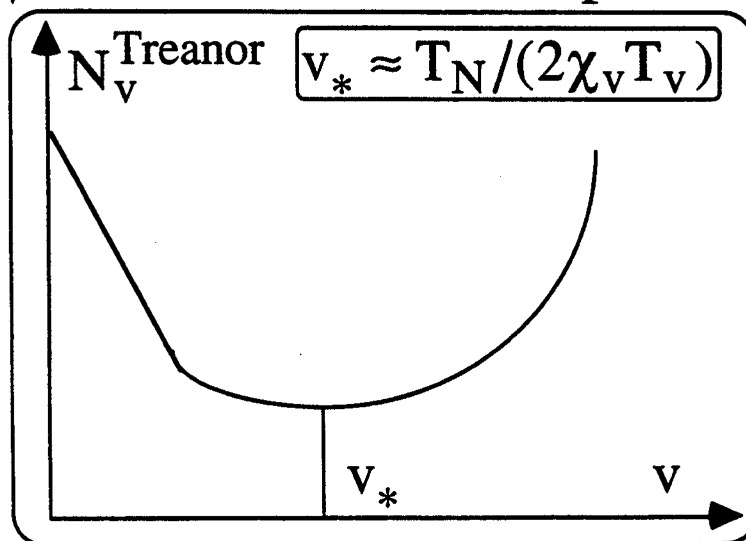

- In practice N_v does not increase as strongly as $N_v^{Treanor}$ does (due to the effects of dissociation boundary and impact of v-T and reaction processes)
- However, N_v usually still has an extended Treanor-like tail with a cut off due to

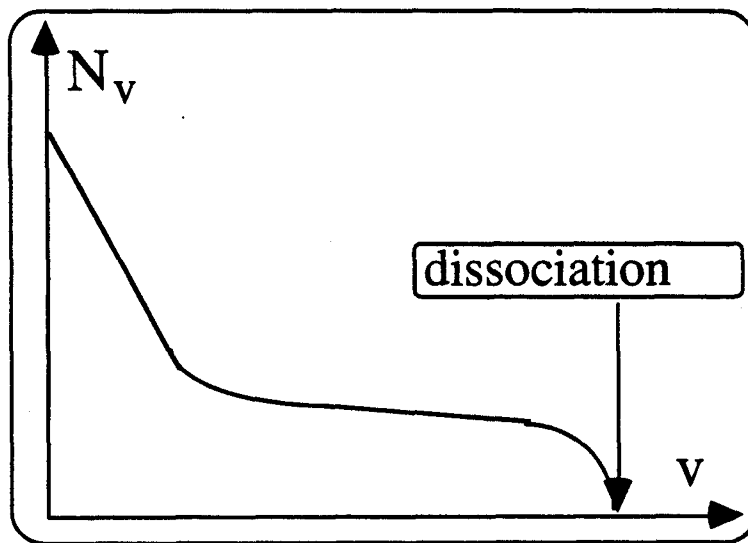

or

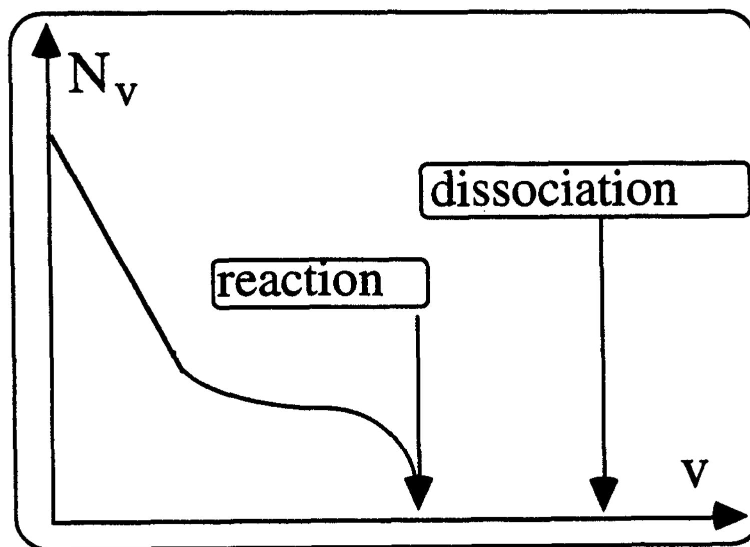

Lectures outline

L1. Introduction and atomic processes in weakly ionized plasmas

L2. Electric breakdown of a gas and steady state gas discharges

L3. Electron and vibrational kinetics in non-equilibrium plasmas

L4. Waves and instabilities in gas discharge plasmas

L5. Plasma-chemical processes in non-equilibrium weakly ionized plasmas

A. Instabilities in gas discharge plasmas

- In many cases in order to provide an efficient process (e. g. population of molecular vibrational states in powerful gaseous lasers, acceleration of plasma-chemical reactions output, increase the power into discharge, etc.) it is necessary to have large product

$$n_e N V$$

where V is the plasma volume

- Therefore it is very desirable to have relatively high ionization degree ($n_e/N \sim 10^{-3}$) of nonequilibrium $T_e >> T_N$ plasmas with relatively high neutral gas density (pressure)
- However, in practice it is very difficult to du due to instabilities of powerful gas discharges
- One of the most universal and the most dangerous instabilities in gas discharge plasmas is a thermal instability
- Thermal instability usually lead to discharge contraction and spoils discharge quality (T_N becomes close to T_e)

- Basic physics of thermal instability can be understood from analysis of positive column of glow discharge

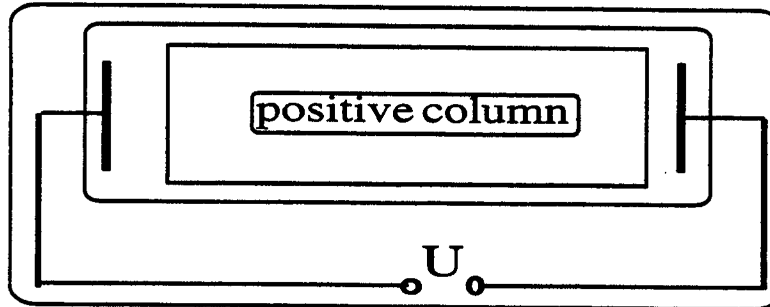

- Recall that all rate constants of electron-neutral interactions (ionization rate constant in particular) depend on the ratio E/N
- Consider relatively high plasma density so that plasma sink is due to recombination

$$(n_e)^2 K_{rec} = n_e \nu_{ion} \equiv n_e N K_{ion} \quad \Rightarrow$$

$$n_e = N K_{ion} / K_{rec}$$

where K_{ion} and K_{rec} are ionization and effective recombination rate constants

- Recombination in atomic gases is usually due to formation of molecular ions

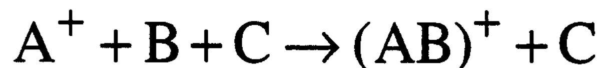

$$A^+ + B + C \rightarrow (AB)^+ + C$$

following by dissociative recombination

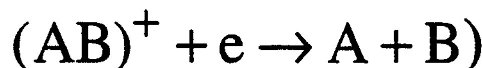

$$(AB)^+ + e \rightarrow A + B)$$

- Radial profiles of the gas temperature, T_N, and density have departure from averaged values T_0 and N_0 due to the gas heating

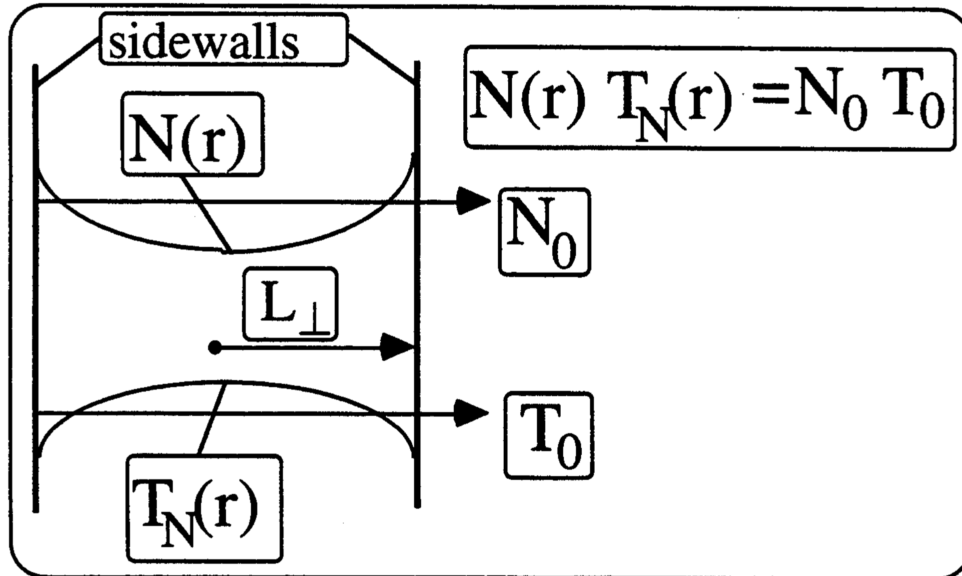

- In atomic gas discharges the gas heating is close to a total energy deposition into discharge (Joule heating)

$$Q_{gh} = ej_e E \equiv en_e \mu_e E^2$$

where $\mu_e \equiv e/(mK_{eN})$ is the electron mobility

- Neutral gas heating supposed to be compensated by the gas cooling due to gas heat conduction, κ_N, to the sidewalls

$$Q_{gc} \approx \frac{\kappa_N (T_N - T_w)}{L_\perp^2} \approx \frac{\kappa_N T_w}{L_\perp^2} \frac{N_0 - N}{N_0}$$

- As a result we find equation describing gas temperature (density) departure ($Q_{gh}=Q_{gc}$)

$$N(eE)^2 \frac{K_{ion}(E/N)}{mK_{eN}K_{rec}} = \frac{\kappa_N T_w}{L_\perp^2} \frac{N_0 - N}{N_0}$$

- Since ionization rate constant has the most strong dependence on the ratio E/N we can neglect all dependencies on neutral gas density in the left hand side of our energy balance equation
- Then, adopting expression

$$K_{ion} = \hat{K}_{ion} \exp\{-B(N/E)\}$$

where $\hat{K}_{ion}$ and B are some constants

we can rewrite energy balance equation as follows

$$\exp\left(\delta\tilde{N}\right) = \delta\tilde{N}/\tilde{Q}$$

where $\tilde{Q} = \left(Q_0 b_0 L_\perp^2\right)/(\kappa_N T_w)$, Q_0 is the energy deposition into discharge at $N = N_0$, $b_0 = B(N_0/E) >> 1$, and $\delta\tilde{N} = b_0\{(N_0 - N)/N_0\} > 0$

- Analyzing energy balance equation we find that solution only exist at $\tilde{Q} < \tilde{Q}_{crit} \equiv e^{-1}$

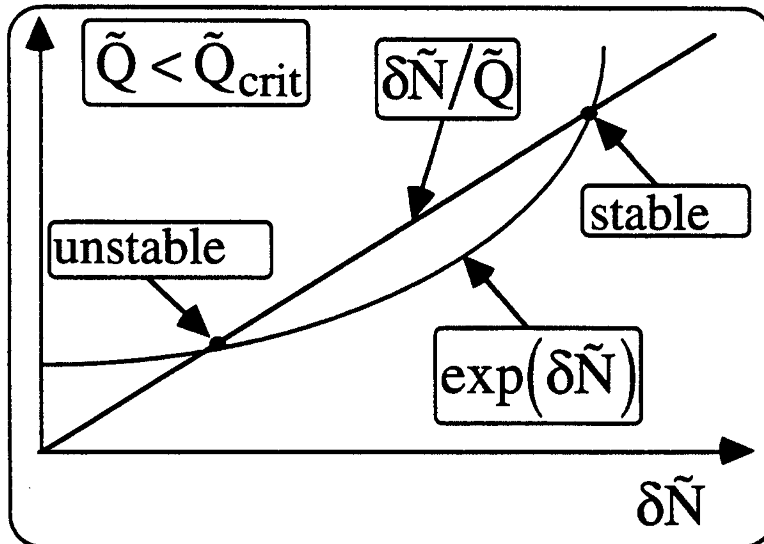

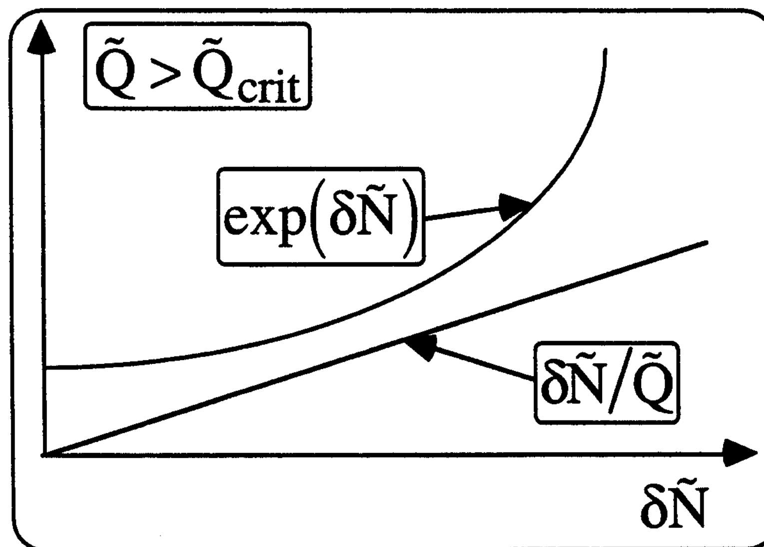

- Thus we find that the power into discharge, Q, is limited by a rather low value Q_{crit}

$$Q < Q_{crit} = (e\kappa_N T_w)/(b_0 L_\perp^2) << (\kappa_N T_w)/L_\perp^2$$

- For higher power ($Q > Q_{crit}$) positive feedback

$$Q\uparrow \Rightarrow T_N(0)\uparrow \Rightarrow N(0)\downarrow \Rightarrow \nu_{ion}(E/N)\uparrow \Rightarrow$$

$$\Rightarrow n_e\uparrow \Rightarrow Q\uparrow \Rightarrow \ ....$$

will cause contraction of the discharge

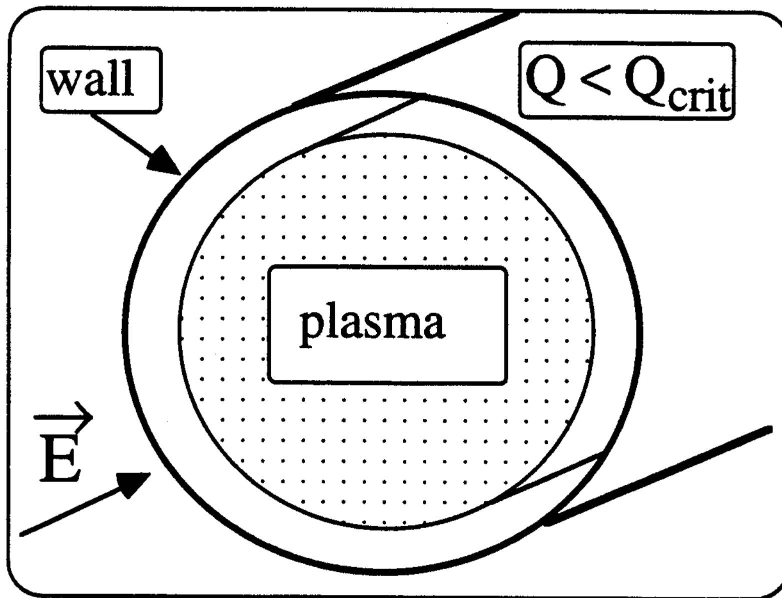

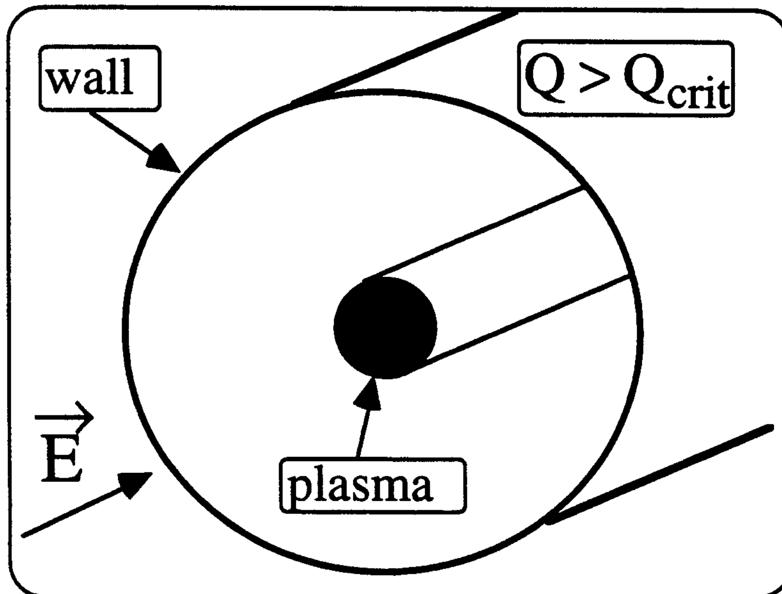

- In RF gas discharge thermal contraction may cause discharge filamentation

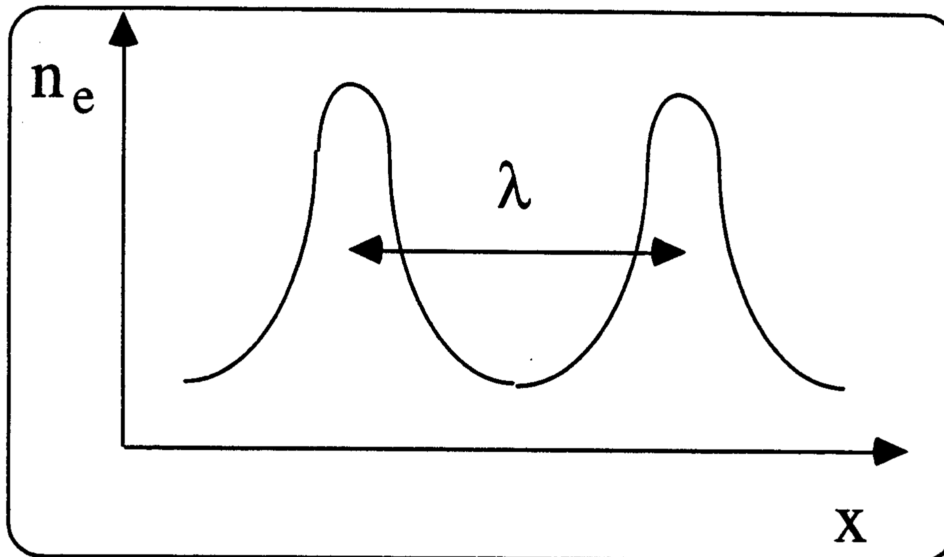

- In dense gas the scale of these filaments, λ, can be about RF wave length λ_{RF}. In some regimes the filamentation of discharge sustained by RF wave starts to exhibit a stochastic properties
- To consider RF discharge filamentation a physical picture we considered for glow discharge must be modified to take into account wave propagation and reflection due to inhomogeneous plasma density
- Such effects are very important for RF wave interaction with atmosphere and ionosphere of the Earth

- There are many varieties of thermal instability of gas discharge plasma which manifest the peculiarities of gas properties
- In noble gases (e. g. argon, krypton) electron-electron collisions can significantly elevate the tail of electron distribution function and, therefore, increase ionization rate constant even in relatively weakly ionized gas with $n_e/N \sim 10^{-6 \div 5}$

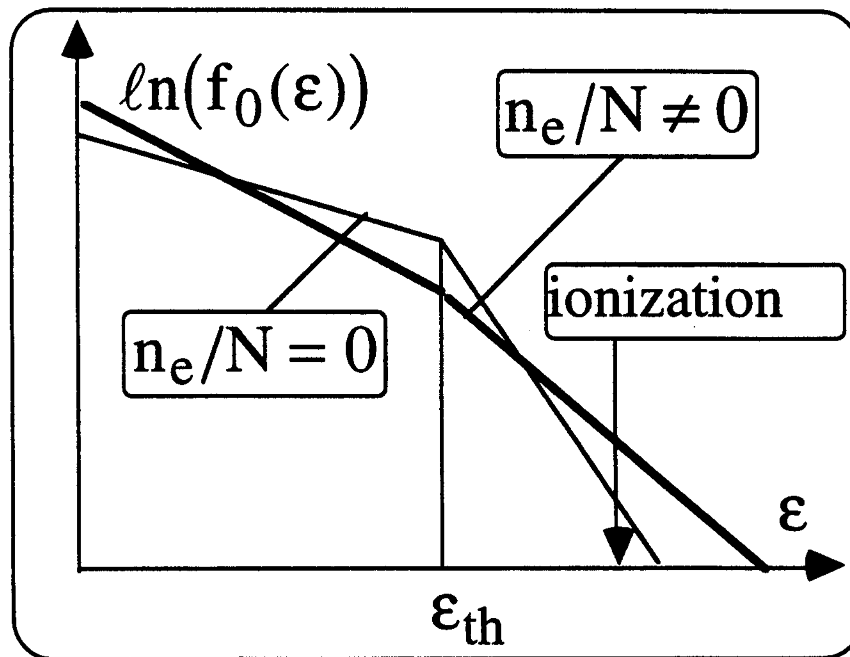

- In this case, a positive feedback occurs not only due to gas heating but also can be caused by dependence of K_{ion} on n_e/N

...ли бы-
...ч иони-
... иллюстрируется рис. 2.2, взятым
й численно рассчитывалась энерге-
ределения электронов в ряде ато-

к только в плазме положительного
нением условия (2.17) появляется
ісимость
яда обо-

м обост-
щего раз-
не проя-
траrиро-
ыполнит-
значении
ов, ког-
для об-
ов, пре-
ации ато-
ведливым
го будет,
ектронов

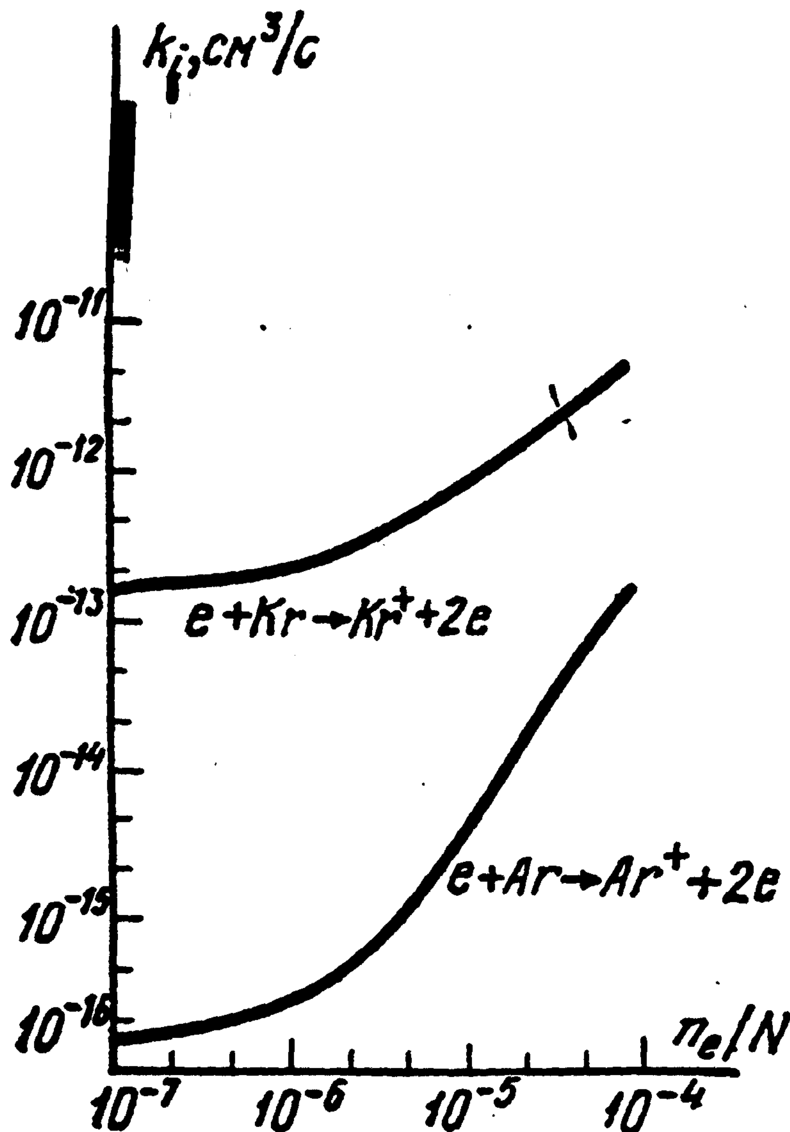

Рис. 2.2. Зависимость коэффициента ионизации k_i от степени ионизации газа n_e/N

- In molecular gases the main part of the power goes into excitation of vibrational levels and not into gas heating
- Gas can be heated due to v-T relaxation of vibrational energy ε_v (energy per molecule)

$$Q_{gh} = \varepsilon_v N \nu_{v-T} \equiv \varepsilon_v N^2 K_{v-T}(T_N)$$

where $K_{v-T}(T_N) \propto \exp\left\{-(E_{Ma}/T_N)^{1/3}\right\}$ is the rate constant of v-T relaxation

- Recall that $E_{Ma} >> T_N$ and, therefore, v-T relaxation processes is very sensitive to neutral gas temperature
- Considering a simple case when vibrational excitation by electron impact is balanced by molecular deactivation at wall we find

$$\varepsilon_v N D_M / L_\perp^2 \approx T_e n_e N K_{e-v} \Rightarrow$$

$$\varepsilon_v \approx T_e n_e K_{e-v} L_\perp^2 / D_M$$

where K_{e-v} is the rate constant of vibrational excitation by electron impact, $T_e >> T_N$ is the electron temperature, and D_M is the diffusion coefficient of the molecules

- Then, taking into account ionization-recombination balance which gives plasma density

$$n_e = NK_{ion}/K_{rec}$$

the expression for the gas heating due to v-T relaxation of vibrational energy can be written as follows

$$Q_{gh} \approx T_e n_e N^2 K_{v-T}(T_N) K_{e-v} L_\perp^2 / D_M$$

$$\approx \frac{T_e N^3 K_{ion}(E/N) K_{v-T}(T_N) K_{e-v} L_\perp^2}{K_{rec} D_M}$$

- Notice, that in addition to strong dependence of K_{ion} on variation of gas temperature (density), in molecular gases we also have sharp dependence of K_{v-T}
- We balance gas heating by heat conduction to the walls

$$Q_{gc} \approx \frac{\kappa_N (T_N - T_w)}{L_\perp^2} \approx \frac{\kappa_N T_w}{L_\perp^2} \frac{N_0 - N}{N_0}$$

- For stability analysis it is enough to consider T_N around T_w and approximate

$$\frac{K_{v-T}(T_N)}{K_{v-T}(T_w)} = \exp\left\{\frac{1}{3}\left(\frac{E_{Ma}}{T_w}\right)^{1/3} \frac{T_N - T_w}{T_w}\right\}$$

$$= \exp\left\{\frac{1}{3}\left(\frac{E_{Ma}}{T_w}\right)^{1/3} \frac{N_0 - N}{N_0}\right\} \equiv \exp\left\{b_v \frac{N_0 - N}{N_0}\right\}$$

- Then, from equilibration $Q_{gh} = Q_{gc}$ we have

$$\exp\{\delta\tilde{N}\} = \delta\tilde{N}/\tilde{Q}_v$$

where $\tilde{Q}_v = (b_v + b_0)\dfrac{Q_v L_\perp^2}{\kappa_N T_w}\dfrac{\nu_{v-T}(T_w) L_\perp^2}{D_M}$, and $Q_v \equiv T_e n_e N K_{e-v}$ is the energy deposition into vibrational levels

- As a result, we find that the discharge is stable if

$$Q_v < (Q_v)_{crit} = \frac{1}{(b_v + b_0)} \frac{\kappa_N T_w}{L_\perp^2} \frac{D_M}{\nu_{v-T} L_\perp^2}$$

- Interesting situation can happen for the case of strong vibrational excitation (ε_v is high)
- Then, v-v exchange processes becomes important and the population of vibrational states, v, trends to form the Treanor function

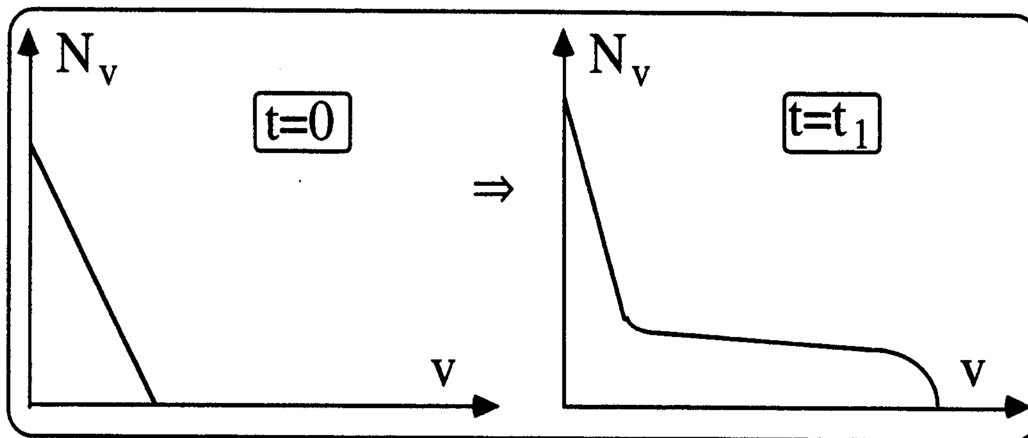

- v-v exchange conserves averaged vibrational quantum number $\langle v \rangle$, but $\langle v^2 \rangle$ increases
- Recall that the energy of vibrational level v is $E_v = E_0(v + 1/2)\{1 - \chi_v(v + 1/2)\}$
- Therefore averaged vibrational energy $\varepsilon_v \approx E_0\langle v \rangle - E_0\chi_v\langle v^2 \rangle$ decreases and T_N increases with increasing $\langle v^2 \rangle$ due to v-v exchange $\Rightarrow$

fast gas heating $\Rightarrow$ thermal contraction

B. Non-linear waves in gas discharge plasmas (domains, strats)

- In Section A we considered instabilities leading to plasma perturbations which are homogeneous along electric field ($\vec{k} \cdot \vec{E} = 0$)

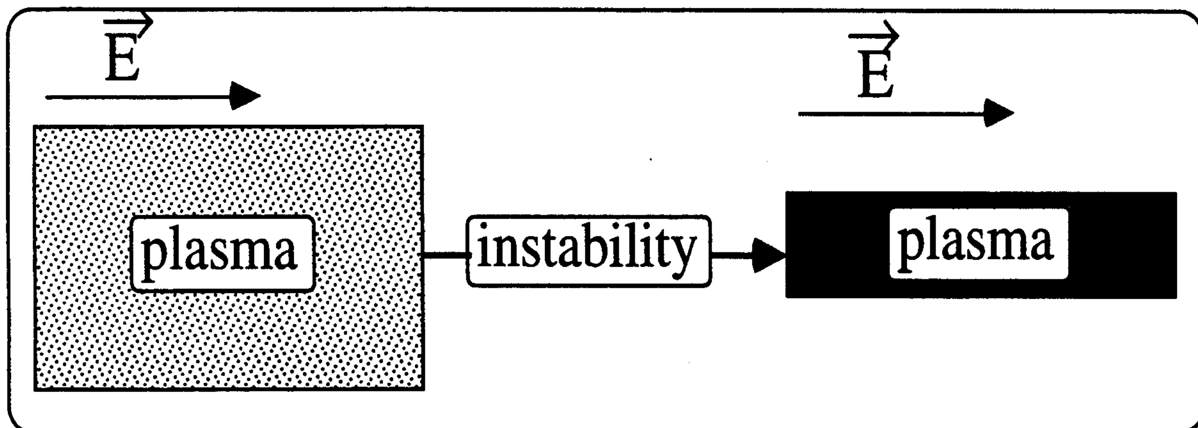

- Here we consider instabilities leading to perturbations along electric field ($\vec{k} \cdot \vec{E} \neq 0$)

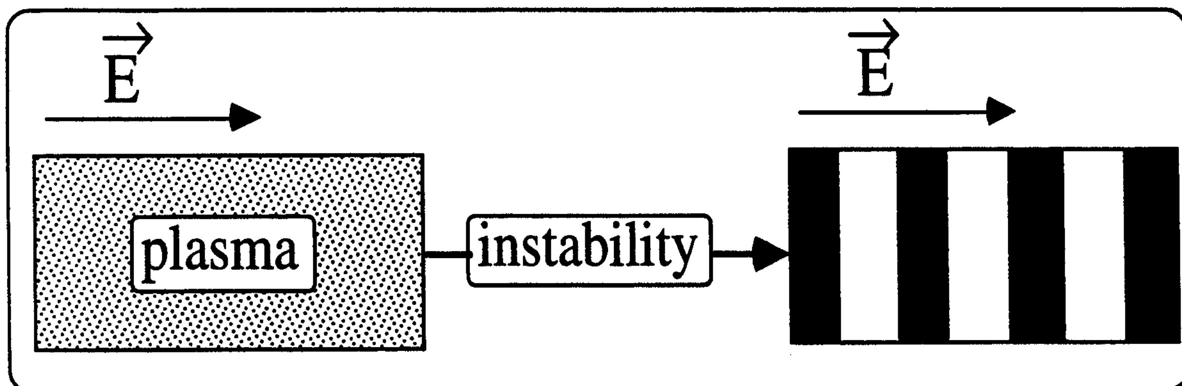

- Nonlinear waves emerging as a result of instabilities with $\vec{k} \cdot \vec{E} \neq 0$ are called domains or strats

- Domains due to electron attachment can be formed in discharges in electro-negative gas (e. g. oxygen)
- Electron density in this type of discharges can be sustained by external ionization source, S_{ext}, (e. g. electron beam) and controlled by: dissociative attachment $e + AB \rightarrow A^{-} + B$, de-attachment $A^{-} + B \rightarrow e + A + B$, and charge exchange recombination $A^{-} + B^{+} \rightarrow A + B$

$$\frac{dn_e}{dt} = S_{ext} - \nu_a n_e + \nu_d n_i^{(-)}$$

$$\frac{dn_i^{(+)}}{dt} = S_{ext} - K_r n_i^{(-)} n_i^{(+)}$$

$$n_e + n_i^{(-)} = n_i^{(+)}$$

where $n_i^{(-)}$ and $n_i^{(+)}$ are the density of negative and positive ions; $\nu_a(T_e)$ and ν_d are attachment and de-attachment frequencies, and K_r is the recombination rate constant

(we assume here that ionization by impact of thermal electron is negligible)

- Solving particle balance equation we find

$$n_e = F(T_e) \equiv \frac{1}{2}\frac{S_{ext}(\nu_d + 2\nu_a)}{(\nu_d + \nu_a)\nu_a} \pm \sqrt{\left\{\frac{1}{2}\frac{S_{ext}(\nu_d + 2\nu_a)}{(\nu_d + \nu_a)\nu_a}\right\}^2 + \frac{S_{ext}\nu_d^2/K_r - S_{ext}^2}{(\nu_d + \nu_a)\nu_a}}$$

- Notice that for $S_{ext} > \nu_d^2/K_r$ there are two solutions for electron density
- Electron temperature T_e is determined by electric field E (gas density we assume constant) and increases with increasing E
- Therefore

$$F(T_e) \equiv F(T_e(E))$$

- For the case when perturbations are along $\vec{E}$, electric current (electron flux) must be conserved $j = n_e \mu_e E = const.$
- As a result, we arrive to the equation for electric field

$$j/(\mu_e E) = F(T_e(E))$$

- Recall that dissociative attachment cross-section has energy threshold so that

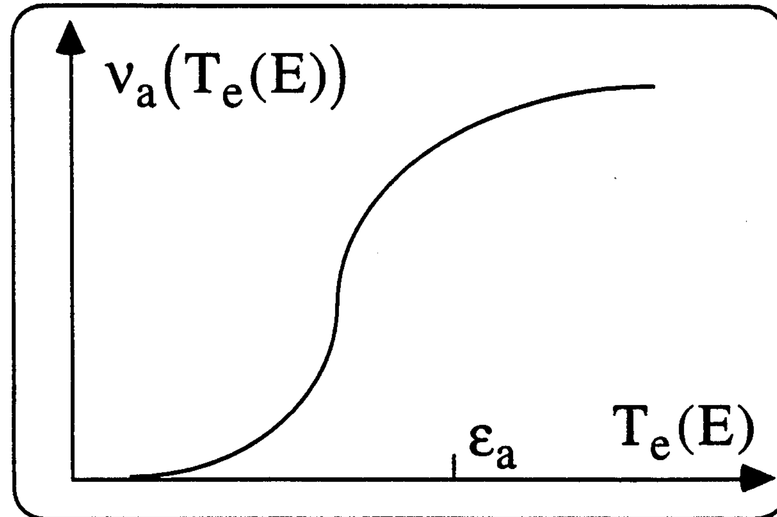

- Meanwhile, ν_d and K_r do not depend on electron energy and, hence, on E

- Therefore, for $S_{ext} > \nu_d^2/K_r$ we find following asymptotic behavior of $n_e(E) \equiv F(E)$

a) for $E \to 0$ ($\nu_a \to 0$)

$$n_e^{(+)} \approx 2S_{ext}/\nu_a \to \infty, \; n_e^{(-)} \approx S_{ext}/\nu_d - \nu_d/K_r$$

b) for $E \to \infty$ ($\nu_a \to$ const.)

$$n_e^{(+)} \approx n_e^{(+)}(\infty) > n_e^{(-)} \approx n_e^{(-)}(\infty)$$

- As a result, schematic dependencies of LHS and RHS of equation for electric field can be shown as follows

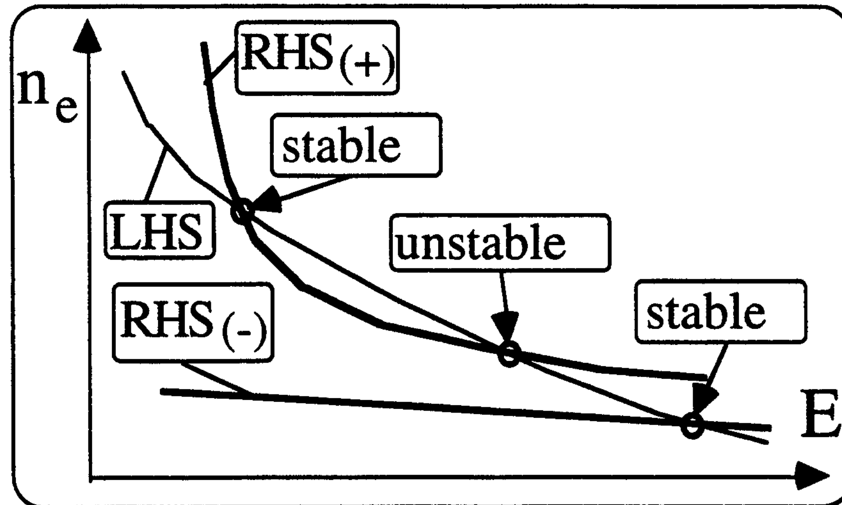

- Domains of low (high) and high (low) electric field (electron density) can co-exsit and as a result

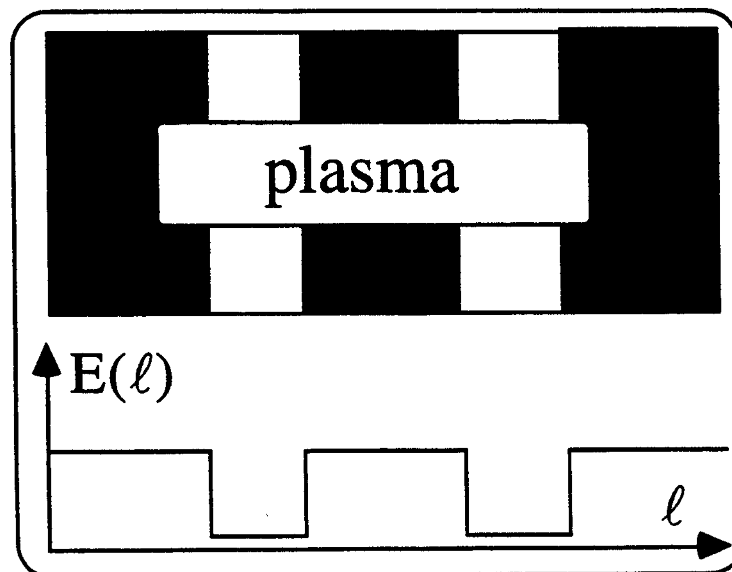

- Similar effect can occurs due to negative differential mobility observed in the mixtures of molecular and noble (argon, xenon) gases

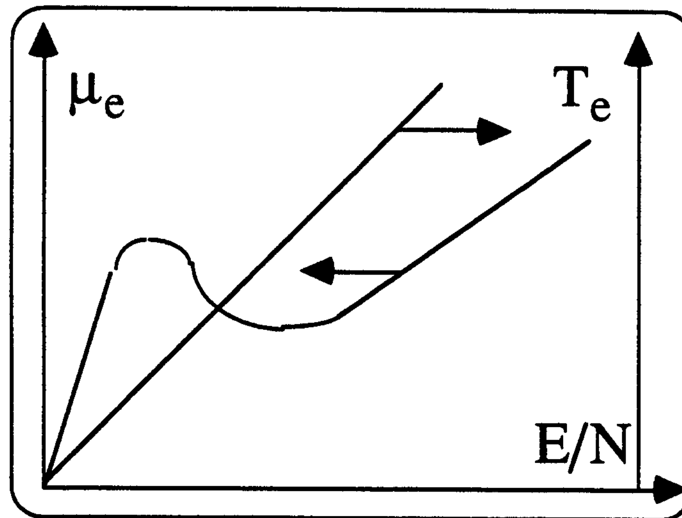

- This effect is caused by Ramzauer's minimum on the cross-section of electron-neutral elastic collision

- Then, from electron energy balance equation, assuming electron flux conservation, we find

$$ej^2 = \mu_e(T_e)\varepsilon_{inel}(T_e)$$

where ε_{inel} is the energy loss due to inelastic electron-neutral collisions, $d\varepsilon_{inel}/dT_e>0$

- Due to non-monotonic dependence $\mu_e(E/N)$ energy balance equation can allow three solutions

$$ev_g E = \nu_u T_e; \quad (\ldots$$

$$n_+ = n_e; \quad (\ldots$$

$$ev_g n_e = j_{\text{вн}} = \text{const}. \quad (\ldots$$

При заданной напряженности поля E уравнение (3.4) имее известных случаях единственное решение для T_e. Уравне (3.6) при заданном $j_{\text{вн}}$ может иметь несколько решений поля E, если дрейфовая скорость немонотонно зависит от E Такая зависимость действительно имеет место [107], наприм в смесях молекулярных газов с аргоном и ксеноном (рис.

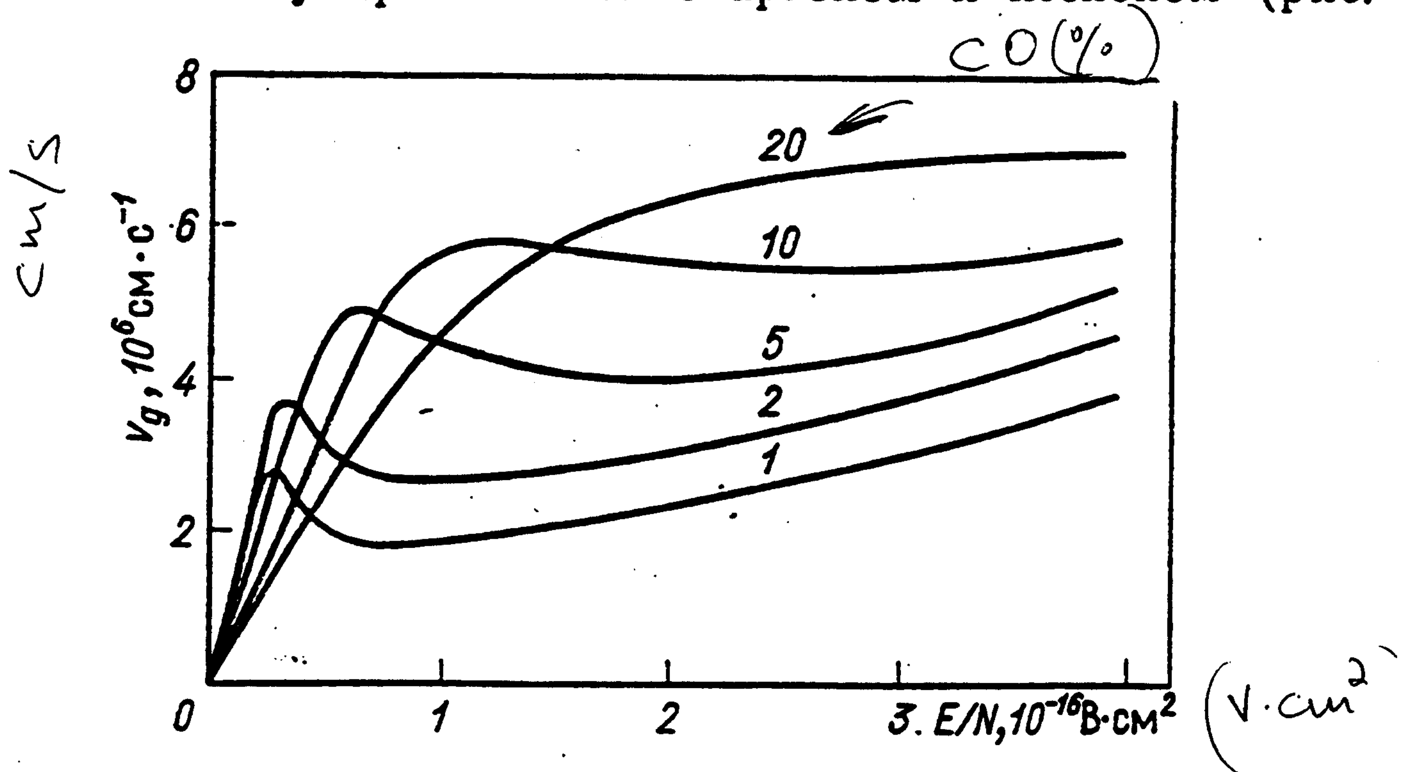

Рис. 3. Зависимость дрейфовой скорости V_g от E/N [107] для различных смесей CO : Ar (цифры у кривых — процент CO)

Немонотонная зависимость v_g от E/N связана с тем, что ср няя энергия электронов, определяемая потерями на возбу дение колебаний молекулярной компоненты, попадает в рай минимума Рамзауэра транспортного сечения рассеяния на

- In noble gases (e. g. argon, krypton) K_{ion} dependence on n_e/N due to either electron-electron collisions or multi-step processes involving metastable states is the main reason for occurrence of strats
- From plasma particle balance and current "conservation"

$$\nu_{ion}(E/N, n_e) = \nu_D \equiv D_A/L_\perp^2 = \text{const.},$$

$$n_e \mu_e E = j = \text{const., we have}$$

$$\nu_{ion}(E/N, j/\mu_e E) = \nu_D$$

- For some current densities, increasing dependence of ionization frequency with increasing n_e can compensate reduction of ν_{ion} with reduced electric field strength

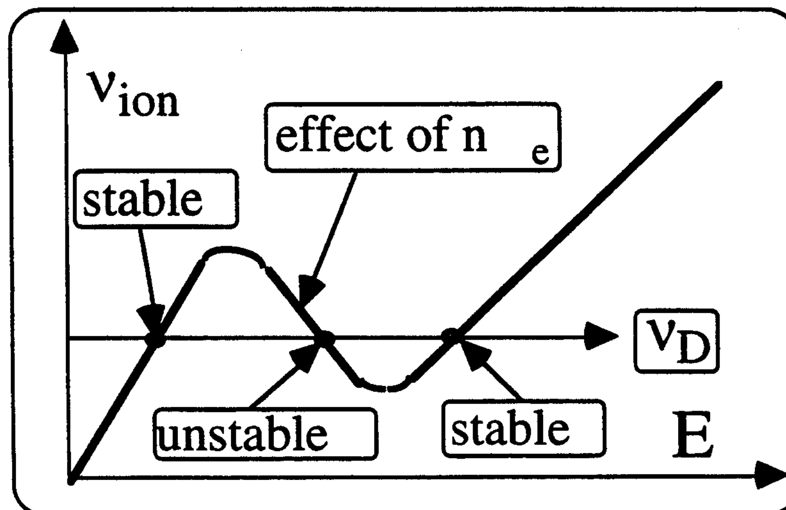

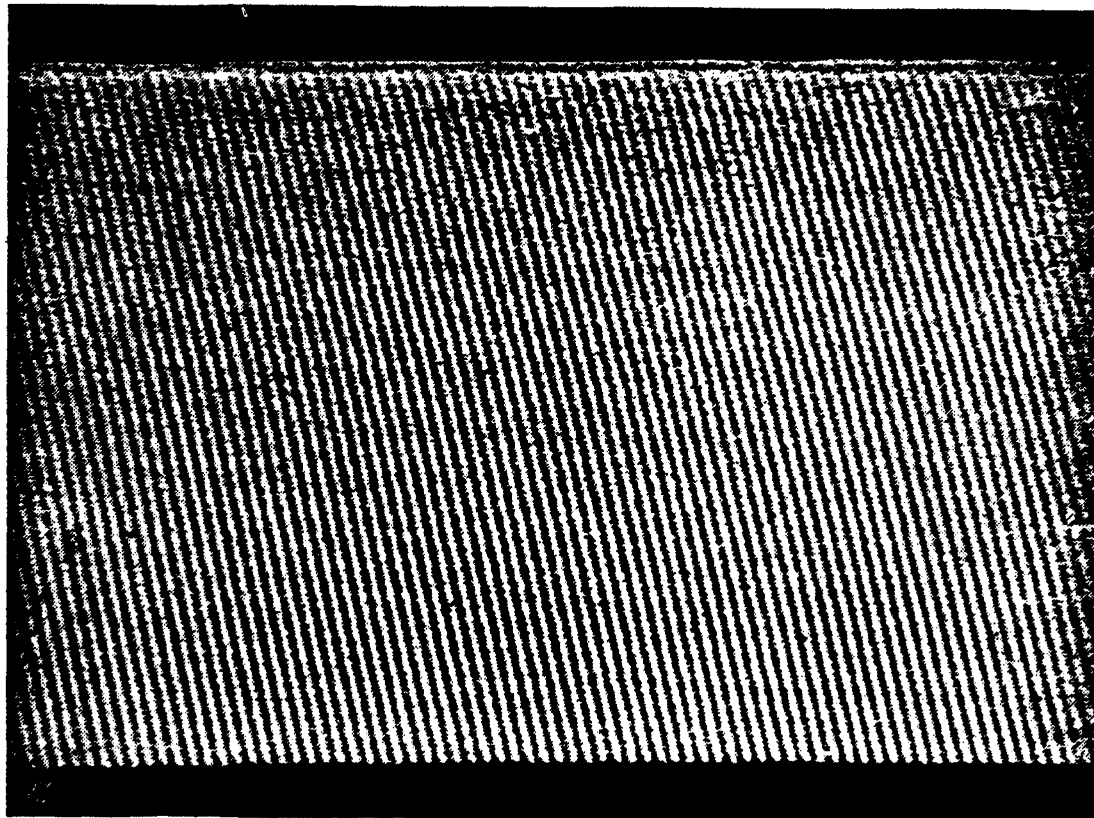

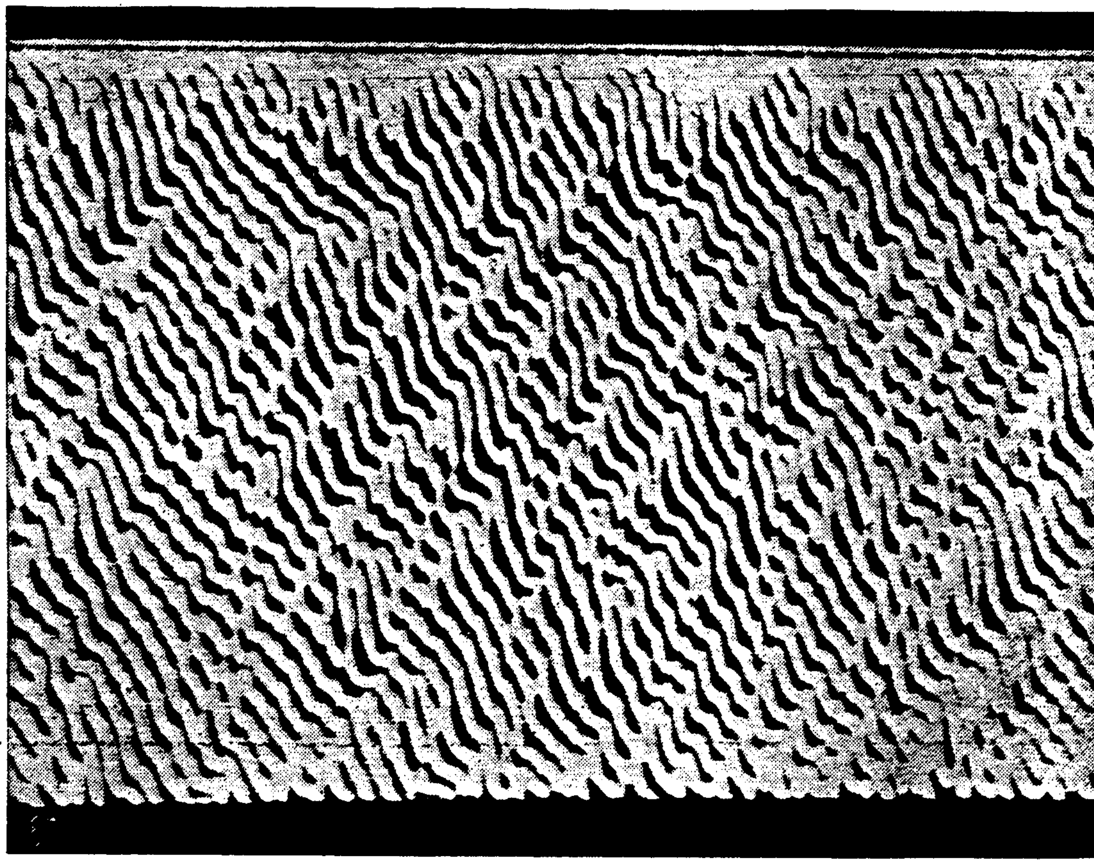

Рис. 6. Регулярные (*а*) и нерегулярные (*б*) страты

а: неон, $p = 5$ мм рт. ст., $a = 0{,}3$ см. Время — слева направо, анод наверху

glow disch. in Ne

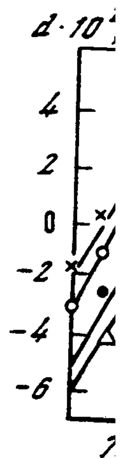

Рис. 7. Зав
буждающей

Рис. 8. Зав
границ сущ

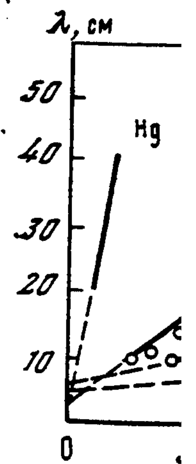

Рис. 9. Зав

Рис. 10. За
Сплошная кри

получать з
ле в газах,
мости длин
рис. 9 по д
следовали
флуктуаци
Они показа
ными ω и
Аналогичн
ции естест
достаточно

эксперимен-
поперечном
12]

мость $\langle E_x \rangle /$
12]

- расчет для

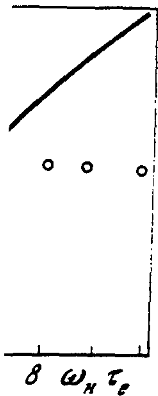

кутка падала

учить полную
го газа с до-
рование плаз-
теля с экспо-
величении на-
заполняющей
сположенные
икулярной B.
$_e)_{кр} \approx 1 \div 2$.
рат разруша-
вития неодно-
лазма стано-
я тока или
соответствии

деляются кон-
ширине плаз-

страт близка
занные с этим
азмы при ма-
стот порядка
ых неоднород-
ьших частот.
предпосылкам
йную теорию

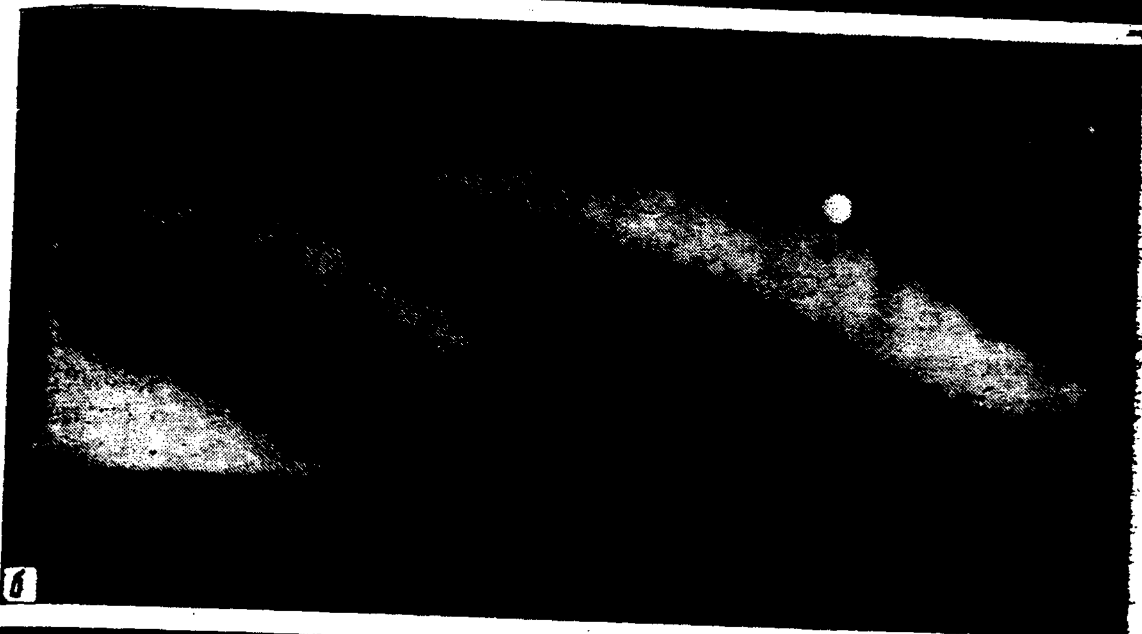

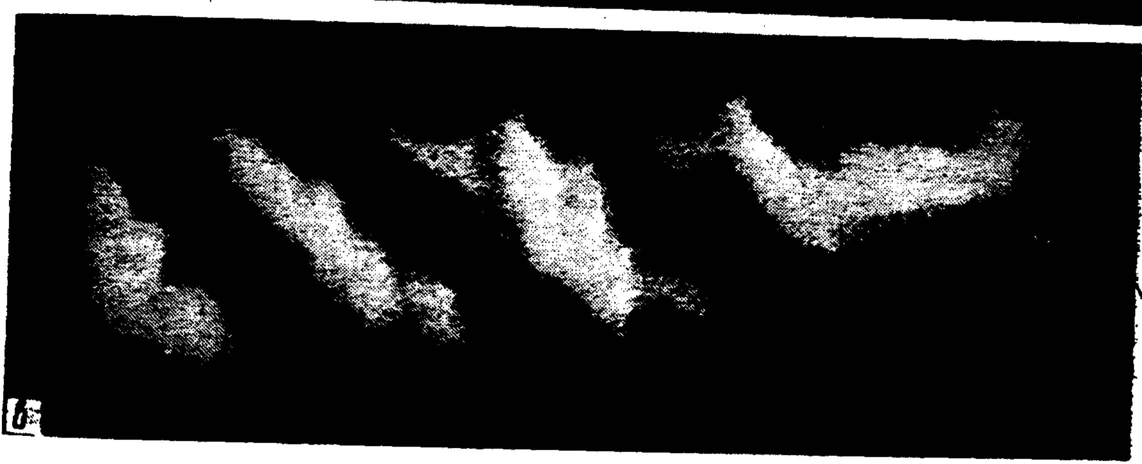

Рис. 28. Фотография разряда для разных значений $\omega_H \tau_e$
а — $\omega_H \tau_e = 0$; б — 2; в — 3

- In the discharges with magnetic field there are a large variety of instabilities associated with gas ionization and plasma-neutral collisions which result in strats, discharge filamentation, and turbulent effects
- Propagating fronts in RF discharges due to a strong increase of plasma density at the front and RF wave reflection

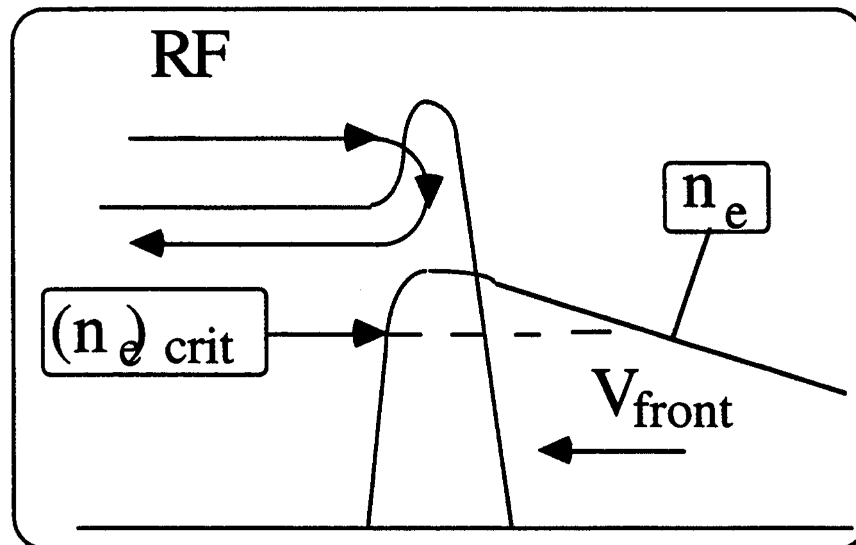

where $(n_e)_{crit} \rightarrow \omega_{pe}\left((n_e)_{crit}\right) = \omega_{RF}$

Lectures outline

L1. Introduction and atomic processes in weakly ionized plasmas

L2. Electric breakdown of a gas and steady state gas discharges

L3. Electron and vibrational kinetics in non-equilibrium plasmas

L4. Waves and instabilities in gas discharge plasmas

L5. Plasma-chemical processes in non-equilibrium weakly ionized plasmas

General remarks

- Any chemical reaction can be written as

$$\sum_i k_i A_i = 0$$

where A_i is a chemical symbol of a reactant (it can be atom, molecule, ion, electron)

- For example, reaction $2H_2 + O_2 \leftrightarrow 2H_2O$ can be written as

$$2H_2 + O_2 - 2H_2O = 0$$

and, therefore, $k_{H_2} = 2$, $k_{O_2} = 1$, and $k_{H_2O} = -2$

- From statistical physics we know that if reaction goes at constant pressure and temperature, thermodynamic potential of our system should decrease and reach minimum for equilibrium conditions, which results in equality

$$\sum_i k_i \mu_i = 0$$

where μ_i is a chemical potential

- For ideal gas (plasma) we have (see statistical physics course)

$$\mu_i = T\ell n(P_i) + \varepsilon_{0i} - c_{pi} T\ell n(T) - \zeta_i T$$

where P_i is the partial pressure, ε_{0i} is the internal energy of the reactant, c_{pi} is the specific heat at constant temperature (c_{pi}=5/2 for atom, and 9/2 for bi-atomic molecule), ζ_i is the chemical constant

- Introducing reactant concentrations, $C_i = P_i/P$, we find

$$\prod_i C_i^{k_i} = P^{-\sum_i k_i} K_p(T)$$

$$\equiv P^{-\sum_i k_i} e^{\sum_i k_i \zeta_i} T^{\sum_i k_i c_{pi}} e^{-\sum_i (k_i \varepsilon_{0i}/T)} \equiv K_c(P,T)$$

= constant of chemical equilibrium

- As a result, for equilibrium conditions the concentrations of reactants only depend on pressure and temperature

Examples

- Saha equilibrium:

chemical reaction $A \leftrightarrow e + A^+$

$$c_{pA} = c_{pe} = c_{pA^+} = 5/2, \ \zeta = \ell n\left\{g\left(m/2\pi\hbar^2\right)^{3/2}\right\}$$

$$\frac{C_A}{C_{A^+}C_e} = P\frac{g_A}{2g_{A^+}}\left(\frac{2\pi}{m}\right)^{3/2}\frac{\hbar^3}{T^{5/2}}\exp(I/T) \equiv PK_p(T)$$

$$\frac{n_e}{n_A} = \frac{1}{\sqrt{1+PK_p(T)}}$$

- Dissociation of molecule:

chemical reaction $A_2 \leftrightarrow A + A$

$$c_{pA} = 5/2, \ c_{pA_2} = 9/2, \ \zeta_A = \ell n\left\{g\left(m/2\pi\hbar^2\right)^{3/2}\right\},$$

$$\zeta_{A_2} = \ell n\left\{\left(I/\hbar^6\omega\right)(m/\pi)^{3/2}\right\}$$

$$\frac{n_{A_2}\left(n_A + n_{A_2}\right)}{\left(n_A\right)^2} = \frac{8PI(\pi/m)^{3/2}}{g^2\omega T^{1/2}}\exp(E_D/T)$$

Two ways to carry on chemical transformations

i) Equilibrium plasmas ($T_e \approx T_N$)

arch discharges, $T_e \approx T_N \approx 5000$ K

- Advantages:

high power 0.1-1 MW,

high pressure (1 atm and higher)

- Disadvantages:

close to equilibrium, tempering is needed, otherwise we may come back to initial conditions

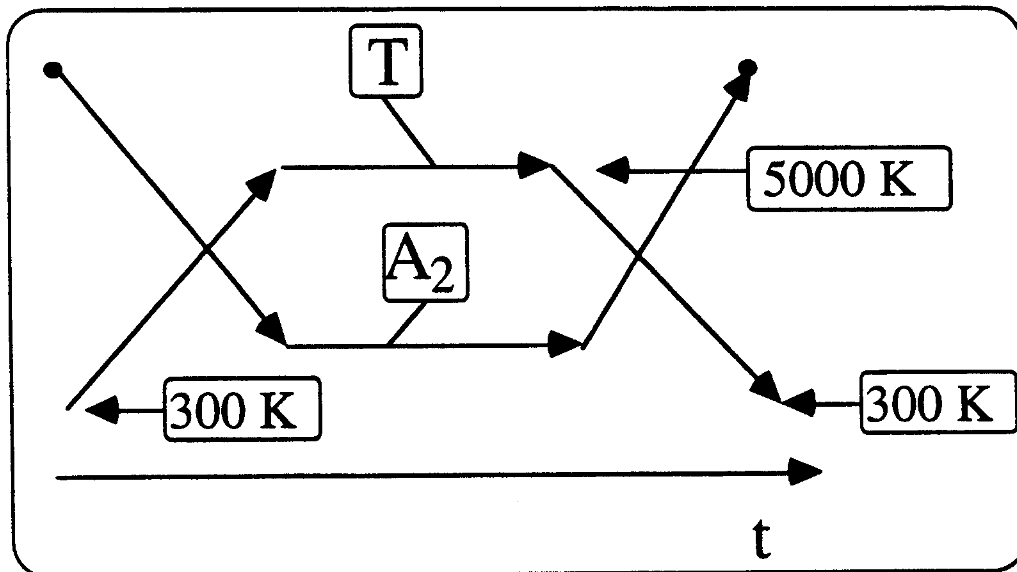

- However, applicability of equilibrium (or quasi-equilibrium) relations requires relatively slow variation of temperature
- When temperature variation is fast reactant concentrations have some delays due to a finite rate
- Moreover, usually almost all reactions (even exothermic one) require some energy to be activated (activation energy E_a)

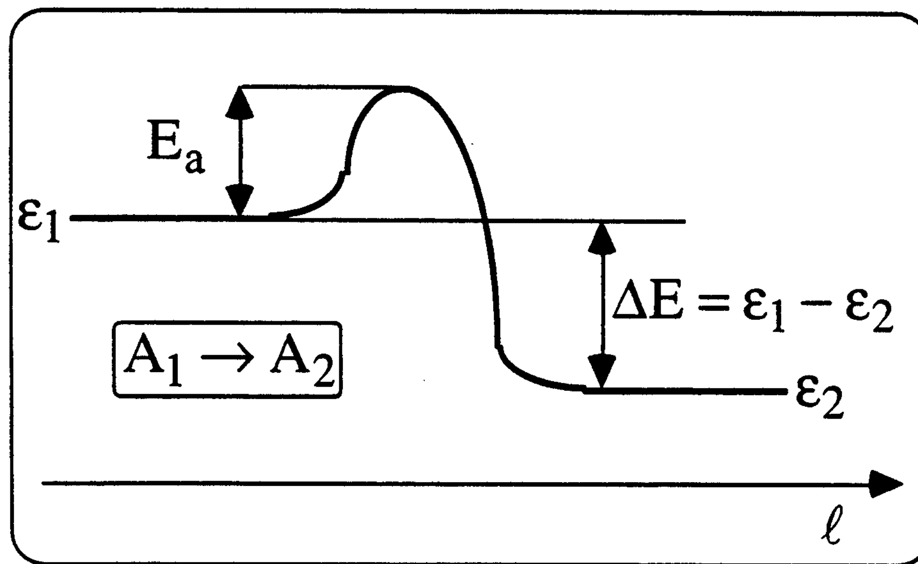

- ΔE enters in equilibrium balance equations, while E_a determines the rate of chemical reaction (Arrenius law)

$$K(T) \propto \exp(-E_a/T)$$

- Therefore, for $E_a/T>>1$ the rate of reaction can be significantly reduced by relatively small drop of temperatures
- As a result, fast reduction of temperature can lead to frozening of gas composition at a level corresponding to a higher temperature

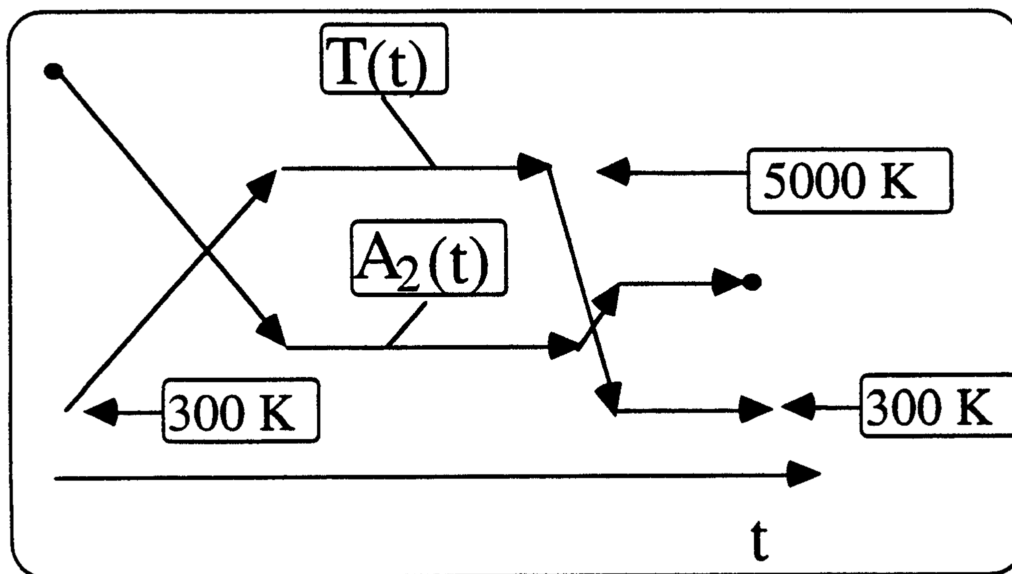

ii) Non-equilibrium plasmas ($T_e >> T_N$)

glow, RF discharges, etc.

$T_e \approx 1$ eV, $T_N \approx 300$-1000 K

- Advantages:

  tempering does not needed

  high selectivity in reaction path

  (internal degrees of freedom)

  potentially can have higher efficiency

- Disadvantages:

  low power, low pressure,

  low production rate, instabilities

- In both equilibrium and non-equilibrium plasmas, many reactions go a chain
- e. g. reaction

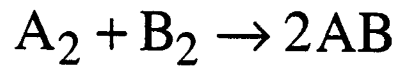

$$A_2 + B_2 \rightarrow 2AB$$

goes mainly though the channels

$$A_2 + B \rightarrow AB + A$$

$$B_2 + A \rightarrow AB + B$$

and not through

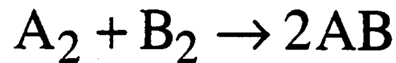

$$A_2 + B_2 \rightarrow 2AB$$

- Moreover, usually

$$n_A,\ n_B << n_{A_2},\ n_{B_2}$$

Example

- Synthesis of NO from the air

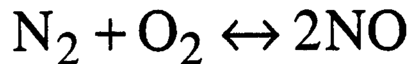

$$N_2 + O_2 \leftrightarrow 2NO$$

- This is endothermic reaction (we must supply some energy to make it happen)

$$E_D^{N_2} = 9.76 \text{ eV},\ E_D^{O_2} = 5.1 \text{ eV},\ E_D^{NO} = 6.5 \text{ eV} \Rightarrow$$

$$\Delta E = \left(E_D^{N_2} + E_D^{O_2} - 2E_D^{NO}\right)/2 \approx 0.9 \text{ eV (per NO)}$$

- It goes through the chain

$$N_2 + O \leftrightarrow NO + N, \text{ (endothermic)}$$

$$E_a \approx \Delta E \approx 3 \text{ eV}$$

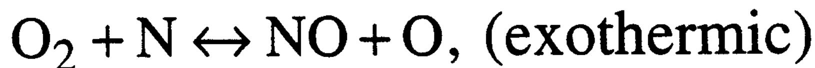

$$O_2 + N \leftrightarrow NO + O, \text{ (exothermic)}$$

$$E_a \approx 0.3 \text{ eV},\ \Delta E \approx \text{-}1 \text{ eV}$$

- In non-equilibrium plasmas endothermic reaction $N_2 + O \rightarrow NO + N$ goes due to vibrational excitation of nitrogen

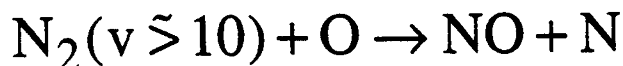

$$N_2(v \gtrsim 10) + O \rightarrow NO + N$$

- However, the presence of radicals, R, (in our case O and N) results in a departure from the Landau-Teller expression for v-T relaxation
- This is due to formation of a metastable molecules

$$M(v) + R \rightarrow (MR)^* \rightarrow M(v') + R$$

- As a result, v-T relaxation on radicals occurs much faster than it follows from Landau-Teller model
- In addition, reaction $O_2 + N \rightarrow NO + O$, being exothermic, results in a significant gas heating and accelerates conventional v-T relaxation
- As a result, the efficiency of NO synthesis in gas discharge plasmas is $\lesssim$ 30% (real energy "cost" of NO is ~ 3 eV)

Plasma Phys. Control. Fusion 36 (1994) B65–B78. Printed in the UK

Plasma Processing and Chemistry

D C Schram, J A M van der Mullen and M C M van de Sanden

Eindhoven University of Technology, Department of Physics,
P.O. Box 513, 5600 MB Eindhoven, The Netherlands

Abstract. The growing field of applications of plasma as deposition, etching, surface modification and chemical conversion has stimulated a renewed interest in plasma science in the atomic physical chemistry regime. The necessity to optimize the various plasma processing techniques in terms of rates, and material properties has made it mandatory to take a new look at the various processes, as fragmentation, plasma and radical transport and plasma surface interaction with advanced diagnostics and with modellization.
Many types of plasmas are used in the technology of plasma chemistry: varying from RF–glow, discharges, coronas to high density arcs.
The physics involved will be illustrated at the hand of important examples: etching and modification of surfaces and the deposition of thin layers of amorphous (a–C:H, a–Si:H) and crystalline (diamond, graphite) layers. Besides dissociation and ionization in the plasma, wall association, recirculation, cluster formation and energy flows are important issues.
These conclusions are also pertinent to the new field of waste destruction and are directly relevant to the economics of the plasma process.

1. Introduction

Plasma processing, deposition and etching, modification, conversion and nucleation in or with plasmas has become important in practically all aspects of high technology and more traditional industries [1–4]. The economic interest in plasma processing for microelectronics, sensors, solar cells, hard coatings is enormous and is in the order of tens of billions of dollars [3]. The development of the field has first been phenomenologically; at present it develops into a new professional sub–discipline, with systematic analysis and modellization in connection with material science, vacuum science and gaseous electronics.
The effectivity of the plasma as chemical medium is a consequence of the high reactivity related to the presence of electrons, ions, radicals and other active species. Both electron and heavy particle kinetics play a role in transferring kinetic energy to internal energy. The high energy density of the plasma medium makes it possible to obtain large radical fluxes which carry a high energy flow at low densities. The virtue of plasmas lies further in the nearly unlimited possibilities for atomic combinations. Practically everything is possible: deposition of crystalline or amorphous thin layers, etching, surface modification, chemical conversion,

0741-3335/94/000065+14$19.50 © 1994 IOP Publishing Ltd

synthesis and destruction, cluster formation and production of powders. The low inventory in the conversion process makes plasma processing inherently relatively clean and safe and is environmentally friendly if properly designed. The only but important limitation of plasma processing is the relatively high price; also this aspect is linked with the two earlier mentioned factors: high energy density and small material inventory (and thus throughput). It is for this reason that more systematic scientific support is desired, like that traditionally present in the plasma fusion community.

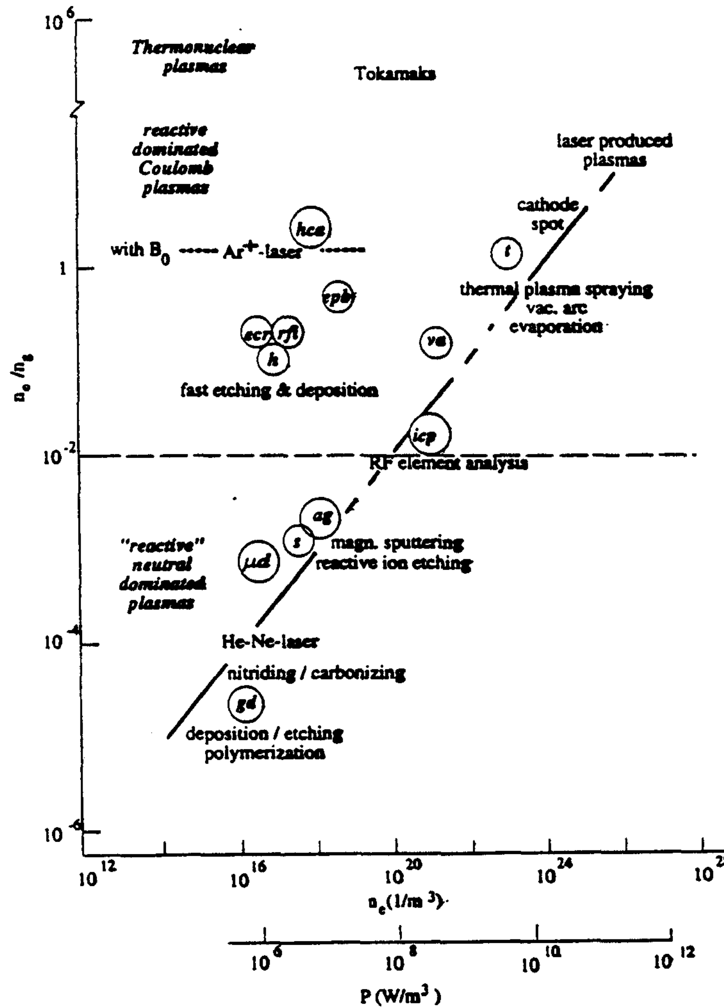

Figure 1. Plasmas characterised in terms of electron density and ionisation degree for several plasma applications and plasma types; gd glow discharge, μd: microwave discharge, s: surfatron, ag: anomalous glow, rfi: rf induction plasma, h: helicon discharge, ecr: electron cyclotron resonance discharge, icp: inductively coupled plasma, epb: expanding plasma beam; va: vacuum arc, t: thermal plasma, hca: hollow cathode arc. At the bottom the required power density is indicated. Adapted from [5].

Important applications of plasma processing are to be found in Integrated Circuit (IC) semiconductor electronic industry, polymer films, optical layers, protective

layers, membrames, biocompatible layers, corrosion– and wear resistant coatings, production of ceramics (including high T superconductors) and catalysts, conversion and destruction of chemical compounds and waste, plasma spraying, and recovery of materials from metal scrap. Plasma processing ranges from high added value processes as in IC fabrication, intermediate cost processes as large area thin films for solar cells, to low added value processes as destruction of waste materials, and in the metallurgical industry. In the first class the cost of the process is less important and the quality of the layer is the key issue. In the intermediate class of processes (as thin layer solar cell fabrication) acceptable cost figures could be \$ 10–100/m^2 for a 1 μm thin layer, which is equivalent to \$ 10–100/g. In the low added value processes prices of \$ 1–10/kg have to be reached to become economically feasible. In most cases the time duration of the process and associated depreciation cost determines the price and high power, large throughputs and high energy and material efficiencies are essential. This line, from high added value processes to the processing of larger volumes (cf. also fig. 1, [5]) will be our guideline in the description of plasma processing.

2. Plasma processing, a short summary of etching and deposition mechanisms

In the IC process industry (and in e.g. solar cell fabrication) RF excitation is the traditional technology. We will first describe the dry etching of patterned wafers, which is a crucial plasma assisted step in IC–(sub)micron technology. The process, e.g. fluorine etching of SiO_2 is relatively well understood because of detailed beam studies [6], many diagnostics studies [7] and modellization including wall processes [8]. Between two parallel plates of the size of a wafer an RF field is applied with typical conditions; pressure 10–100 Pa, 10–100 W RF power at 13.56 MHz with RF field amplitude and self bias of 100 V–200 V. Plasma etching can be performed

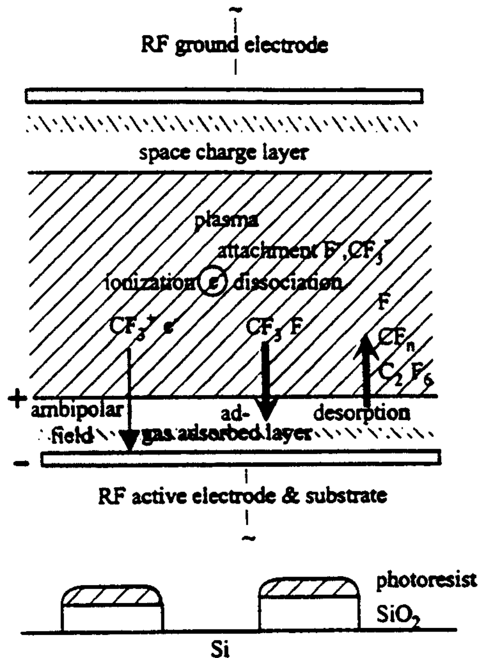

Figure 2. Etched patterned wafer (with permission reprinted from brochure "plasma assisted processes for surface engineering" of Arbeitskreis Plasma Oberflächen Technologie); sketch of RF–reactor & anisotropic and selective etching.

(e.g. SiO_2 by CF_4) with chemical selectivity (large etch rates for the material to be etched, e.g. SiO_2 and small for the photoresist mask) and anisotropy (i.e. fast etching in depth and slow lateral etching) as important figures of merit. In this way anisotropic etching will ideally lead to features of (sub) μm dimensions (fig. 2). The anisotropy and chemical selectivity are thought to arise because of the ion induced character of the etching by radicals. In this picture radicals adsorbed at the surface are stimulated to etch the surface by an incident ion. The side wall etching is inhibited because of the absence of ion irradiation and the protection by an inert (e.g. CF_2) inhibition layer (fig. 2). The etch rates are limited by the ion flux, which in turn is limited by the ionization production.

Plasma chemistry processes can all be characterized by five steps:
1. plasma production, electrons and ions serve as source for:
2. production of radicals by dissociation of injected and recirculating monomers in electron and heavy particle processes
3. transport of radicals and ions by diffusion or convection (typical transport times 10^{-4}–10^{-3} s)
4. surface interaction, adsorption, reactions, polymerization and desorption
5. recirculation of stable monomers and radicals, which add to the injected monomers (residence time 0.1–1 s).

Electrons heated in the RF–field ionize and dissociate the etchant gas: $CF_4 + e^- \longrightarrow CF_3^+ + F + 2e^-$ and $CF_4 + e^- \longrightarrow CF_n + (4-n)\,F + e^-$. Ambipolar diffusion drives ions and electrons to the substrate, with ambipolar diffusion velocities in the order of the ion acoustic speed. Large bias potentials, in the order of the large RF field amplitude (100–200 V) accelerate the ions to the substrate. Radicals diffuse collisionally to the substrate where they may reflect, adsorb or react. Desorption of radicals (F, CF_3) contributes to the radical density and desorption of stable monomers (CF_4, C_2F_6) and etching products alters the gas composition, cf. fig. 3.

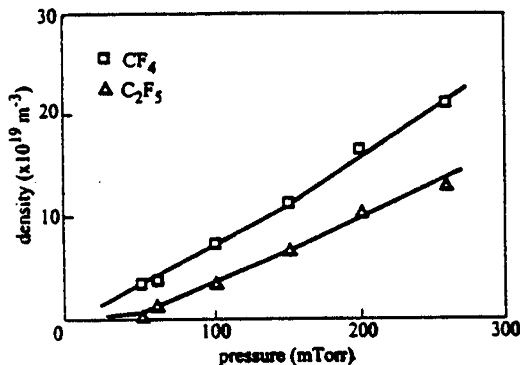

Figure 3. By IR absorption spectroscopy measured densities of CF_4 and C_2F_6 in a CHF_3 plasma as a function of the gas pressure at 80 watt RF power and 1/3 scc/s flow; from Haverlag [7].(scc/s= standard cc per second, 1 scc/s is equivalent to 2.5 10^{19} molecules per second.

As dissociation is more effective than ionization the net flux of radicals (incoming – desorbed) is somewhat higher than the ion flux (typically a factor 3–10). The incident radical flux is much higher because of radical density built up in the recycling. In the $SiO_2 - CF_4$ case the etch rate is ion flux limited and can be estimated from a global inspection of the mass and energy balances [9], i.e. the existence demands of the plasma non equilibrium system. The mass balance equates the volume ion production to the ambipolar ion flux to the substrate:

$$\iiint n_e n_{CF4}\, k^{ion}\,(\hat{T}_e^{eff})\; d\,Vol = \iint D^{amb}\,\nabla\, n_e \cdot \underline{dS} = \iint \text{ion flux} \cdot \underline{dS}$$

With typical values for the electron density ($n_e \sim 10^{16}/m^3$), neutral density ($n_{CF_4} \sim 10^{21}/m^3$), ionization rate ($k^{ion}(\hat{T}_e^{eff}) \sim 10^{-16}$ m^3/s) and distance between the electrodes (2 cm), ion fluxes of $10^{19}/sm^2$ result. The mass balance determines for given dimensions and pressure (30 Pa) the effective ionization temperature, $\hat{T}_e^{eff} \sim 3$ eV, which can be associated to the non–Maxwellian electron energy distribution function. This conclusion is independent of the value of the electron density as both the production and the flux are linear in n_e. The mass balance learns that $\hat{T}_e$ has to be large enough to guarantee sufficient production by ionization to balance the diffusive losses.

The electron density is determined by the energy balance; the dissipation results mainly from ion production and ion acceleration in the sheath and vibrational excitation of the molecular gas. Hence in the most simple form the Joule dissipation is equal to the energy carried with the ion flux and the (electron induced) vibrational heating of the molecular gas. As both losses are proportional to the electron density the allowable power density (10^6 W/m^3) and energy flux (10^4 W/m^2) limit the electron density to the quoted values at the 13.56 MHz excitation frequency. Hence the mass and energy balance determine the ion flux and thus the etch rate (or deposition rate). In the quoted example it is $10^{19}/m^2s$ equivalent to 1 monolayer per second and etch rates in the order of 1 nm/s result. From this simple picture it is already clear that low pressure and high power favours ion induced anisotropy whereas chemical slectivity is optimum in a more radical rich situation at higher pressures and smaller power. At higher frequencies the density increases somewhat and self bias decreases; thus higher rates can be achieved and ion induced damage (but also the anisotropy) decrease.

RF excitation is also used for plasma deposition of thin layers of many materials, as polymers [2], diamondlike amorphous carbon, TiN, passivation layers and diffusion barriers. A pertinent example is the deposition of amorphous hydrogenated silicon, (a–Si:H) for solar cells applications [4]. Silane (SiH_4) admixed with H_2 is dissociated (SiH_n) and ionized (SiH_3^+) see fig. 4. Is has been shown with infrared laser absorption spectroscopy (SiH_n), visible light laser absorption and laser induced fluorescence (SiH) [10] that SiH_3 is the most abundant radical, typically 10% of the parent gas. Detailed modelling with over

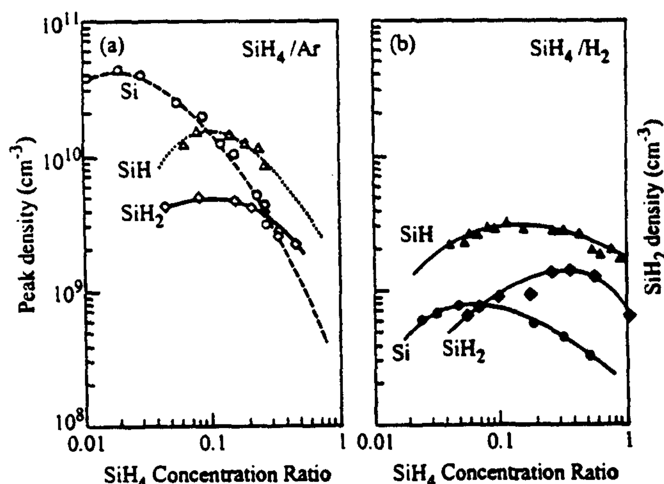

Figure 4. Densities of Si, SiH, SiH_2 (measured by LIF and Intra cavity laser absorption) in a SiH_4 plasma diluted by Ar (a) or H_2 (b) at a total pressure of 0/3 Torr, a total flow of 10 sccm and RF power of 15 W; from Tachibana et al. [10].

100 reactions has confirmed this finding. Hydrogen atoms may also participate in the radicalisation, either in the gas phase or at the wall:

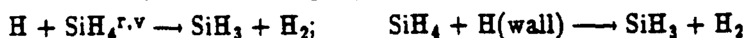

$$H + SiH_4^{r,v} \longrightarrow SiH_3 + H_2; \qquad SiH_4 + H(wall) \longrightarrow SiH_3 + H_2$$

The deposition mechanism is commonly thought to be radical controlled [11],

though other possibilities are mentioned [9], [12]. There is an influence of doping, which is different from SiH_4 feed then for SiF_4 [11]. Still many authors argue that SiH_3 is the preferred precursor as the mobility of this fragment at the surface is high, but also SiH_2 is mentioned [13]. Similar standpoint exist concerning the preference for CH_3 in diamond deposition but also here controversies exist. However it could also be that not so much the volume abundances of a specific radical is the determining factor, but rather the composition of the adsorbed layer. Of course the latter depends on the irradiation of radicals and thus the flux composition (at least the stochiometry in Si/H) but also on energy irradiation, substrate temperature and thus the effective temperature of the adsorbed layer. The fact that many plasma methods lead to similar deposited material favours this more general point of view. Hence energy irradiation in the absorbed layer is of importance too and needs to be considered.
For deposition higher frequencies may be beneficial as in that case lower ion energies and higher rates are desired. Improvement of rate and quality of the layer have been realised this way for deposition of amorphous silicon for e.g. solar cell applications [14].

As has been stated, the rates of in situ processing are limited by restraints set by the plasma mass– and energy balances, or in other words, the existence demands. To circumvent these rate limitations by the existence demands other approaches have been pursued. They all have in common that plasma production is separated geometrically from the plasma treatment. This approach is commonly referred to as the remote plasma (source) treatment. In this way both production and treatment can be optimized separately. In these remote sources dissipated power can be chosen to be substantially larger (1kW) and the fluxes and thus the rates are consequently larger too. In e.g. electron cyclotron resonance sources (ECR) the plasma is produced upstream in e.c.r. zone ($f = 2.45$ GHz, $B^{res} \simeq .0875$ Tesla) [15]. The resonance is not very critical as the plasma frequency is close to the electron cyclotron frequency. The energy density gradient and the diverging magnetic field lead to a fast flow of radicals, ions and electrons to the substrate. The final ion energy is coupled to the ambipolar acceleration process in the diverging field (and can be RF–bias enhanced) and is typically 20–200 V. These sources and related ones as helicon sources [16] operate at higher electron temperature and lower pressure. The newest type in this approach is the RFI (inductive) source, sometimes combined with minimum B magnetic confinement at sideways and upstream sides. This type of source relies on inductive dissipation and again the power density gradient and thus plasma energy density gradient leads to efficient transport of the produced ions and radicals from the upstream side to the downstream plasma treatment. For larger area deposition also non–resonant microwave excitation is used. The radiation leaks through vacuum sealed antenna slit and excites a homogeneous plasma with again downstream deposition. A still other type of source is the surface wave heated surfatron [17].
An extreme form of separation of plasma production and treatment is found in the expanding plasma beam deposition (EPBD) method [18]. In this method the plasma is produced in a thermal arc close to atmospheric pressure and is expanded in a low pressure background where deposition, etching or surface modification occurs. Plasma production at high pressure – and thus high electron density – is very efficient and large ion flows can be achieved. In the expansion process (supersonic expansion, shock and subsonic expansion) the plasma cools from the 1 eV temperature in the arc to .3 eV in the treatment chamber. Hence the electron temperature is relatively low and the heavy particle temperature is relatively high (both .3 eV). In this situation the governing radicalisation kinetics are charge exchange and dissociative recombination, rather than electron kinetics as in the previous examples. For an argon arc and injected SiH_4 the following reactions may occur [19]:

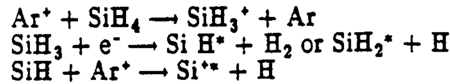

$$Ar^+ + SiH_4 \rightarrow SiH_3^+ + Ar$$
$$SiH_3 + e^- \rightarrow Si\,H^* + H_2 \text{ or } SiH_2^* + H$$
$$SiH + Ar^+ \rightarrow Si^{+*} + H$$

The example shows that very efficient transfer of the chemical energy to the formation of SiH_n radicals and even Si^+ ions may result. There is no dependence on electron energy distribution functions and strong radicalisation to even atomic ions is possible. The charge transfer rates are typically 10^{-15} m^3/s and may depend on the ro(tational)–vibrational excitation of the parent molecules. The dissociative recombination reactions have rates of 10^{-13} m^3/s also probably dependent on ro–vibrational excitation. Similar reactions are possible with metastable argon atoms; however in most cases the ion density is larger than the metastable density even in recombining plasmas and charge transfer fragmentation dominates.

These examples show the 5 steps to be distinguished in plasma chemistry processes:
1. plasma production by ionization
2. production of radicals by dissociation of injected and recirculating monomers
3. transport of radicals and ions
4. surface proces as deposition and desorption
5. recirculation of stable monomers and radicals.

3. Surface modification and deposition by the expanding plasma beam deposition (EPBD)–technique

3a. Hydrogen treatment of surfaces

Restauration of archaeological artefacts by hydrogen atom irradiation [20] may serve as an example of surface treatment processes. Other examples are etching (with F or O) [21] nitriding [22] (with N) etc.. Here the plasma serves as a dissociator; for an argon/hydrogen arc charge transfer and dissociative recombination add to the electron dissociation in the arc. Again the chemical energy is stored in ions, but even more in atoms. For hydrogen arcs the radical (H)

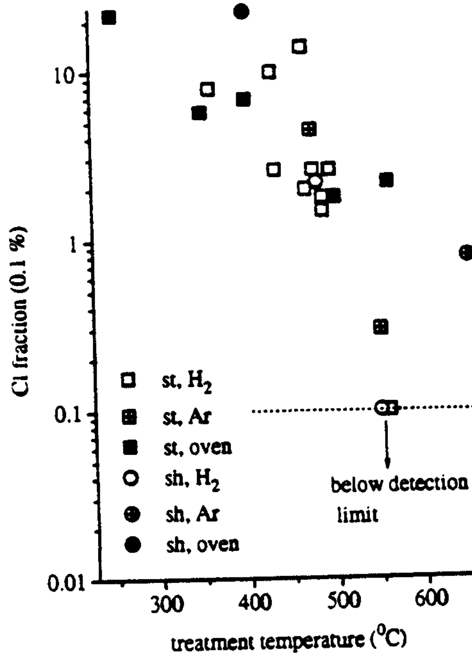

Figure 5. Overview of residual chlorine concentrations measured on both shipwreck (sh.) and standard type platelets (st.) after treatment in an oven, H_2 plasma or Ar plasma. The chlorine fraction on an untreated platelet is 5%. After M.J. de Graaf, R. Severens et al. [23].

flow may be as large as 1–3.10^{21} p/s which carry ½ dissociation energy. In expansion in 1 mbar background typical plasma beam diameters range from 3 cm at the shock to 10 cm further downstream. Thus very large fluxes in excess of 10^{23}/sm^2 are reachable. Archaeological artefacts have been treated in this particle beam during typically 30 minutes. In particular those specimens which were post treated in a nitrogen plasma and further preserved by epoxy–sealing have shown very good results. By nuclear techniques the residual O and Cl surface abundances have been analysed. The results are shown in fig. 5 [23] in which heat treatments and plasma treatments are shown indicating that the presence of hydrogen and an elevated substrate temperature give nearly full chlorine reduction.
Hydrogen plasmas may serve as the most simple plasma chemical systems. Still two major complications become evident already from observation of the above mentioned plasma cleaning.

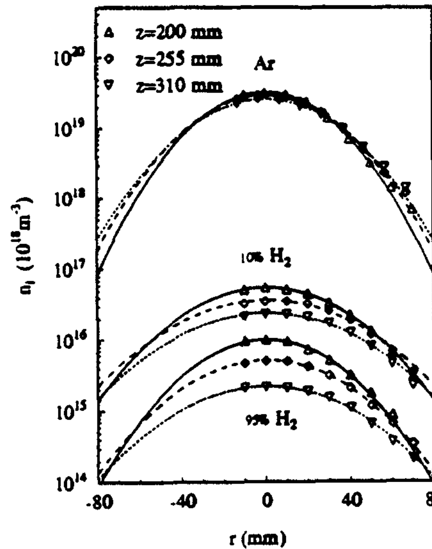

Figure 6a. Radial ion–density profiles for Ar and Ar–H_2 mixtures. The arc current is 45 A, the flow 3 slm and reactor pressure is 0.5 mbar.

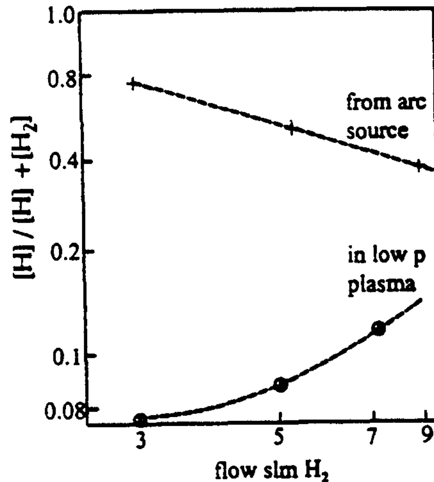

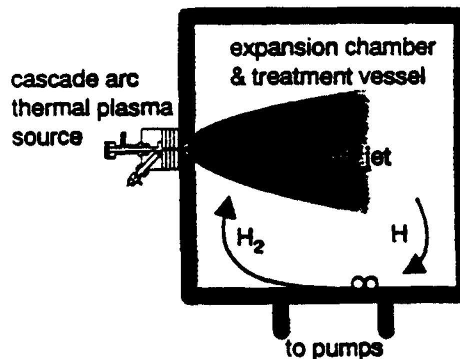

Figure 6b. Variation of dissociation degree with flow in full H_2 at constant pressure (1 Torr) and arc current 35 A). From De Graaf et al. [23], [24].

The first one is an anomalously high recombination rate of hydrogen (containing) plasmas as compared to only weakly recombining argon plasmas [24]. This anomalously high recombination is due to the earlier mentioned charge exchange (H^+, $Ar^+ + H_2^{v,r} \longrightarrow H_2^+ + H$, Ar) and dissociative recombination sequence. Hence even atomic plasmas recombine because of the presence of residual molecules. Similar effects, though less severe are observed in other molecular plasmas, as e.g. in nitrogen [25] and methane seeded plasmas. Hence, molecules (essential in plasma chemistry) influence the ionization degree of higher density plasmas. The second point of interest is the very presence of the H_2 molecules in the example. One major source is wall association of the primary H–atoms of the source with wall absorbed H–atoms. As practically always the residence time of particles in the machine is much longer than the circulation time these wall associated molecules are more abundant than the primary atoms. This is clear from fig. 6 in which the source dissociation degree and that in the expansion volume are displayed as function of flow at constant pressure and source current. It is clear that the H/H_2 abundances are primarily influenced by wall associated molecules. Similarly if SiH_4 would be injected in an argon/hydrogen plasma beam the SiH_4 concentration (and wall associated disilane (Si_2H_6) and H_2) will be determined by wall association and recirculation of molecules, rather than by the primary gas feed. Hence wall (and wall conditions) have a major influence on the molecular plasma constituents and therewith on the deposition process.

3b. Plasma deposition of amorphous and crystalline layers

Plasma deposition is a very wide area, with many material combinations and executed with many kinds of plasmas. Polymer layers from all kind of organic precursors, metal–organic layers –nitrides, –oxides with organo metallic gases or high vapour pressure fluids [2], semiconducting layers as a–Si:H and a–Ge:H [26] and hard protective layers as a–C–H, or diamondlike layers [27]. The most important issue here is an understanding of the deposition process, in order to obtain control on composition, morphology, (semi)conducting optical and electrical properties and (in particular for the intermediate added value processes) sufficiently fast rates.

Deposition of amorphous hydrogenated carbon [27] and –silicon [26] has been extensively investigated in view of application as protective coatings and in solar cells respectively. With elaborate diagnostic techniques radicals (SiH, SiH_2, SiH_3) have been measured [10]; they all point to a dominance of SiH_3 (similarly CH_3 in the case of CH_4). This has been verified by extensive modellization [28] and there is more or less consensus on the preferred role of SiH_3 and CH_3 as precursors. But still the picture is far from clear and further clarification would facilitate the achievement of further advanced layers with new properties. Here we will summarize the results for amorphous carbon obtained with the fast expanding plasma beam technique [29]. In this method, quite similar to the H–atom source (fig. 6c), a very large radical flow is obtained by seeding of monomers as C_2H_2 or C_7H_8 (toluene) in the highly ionized argon plasma beam, which expands from a high pressure thermal arc source. As explained earlier the fragmentation is in this case mainly through heavy particle kinetics and radicalisation to C^+ ions is possible. The growth rate measured by in situ ellipsometry increases linearly with monomer flow rate and values in excess of 100 nm/s over areas of 100 cm^2 have been reached. Layer properties as index of refraction, bandgap, hydrogen/carbon ratio and bonding types have been measured with ex situ spectroscopic ellipsometry, nuclear techniques and infrared absorption analysis. The results point to more dense and hard layers for the larger monomer flows (and thus larger rates). An explanation for the dependence is sought in a variation of the energy flux/deposition event, which decreases with increasing flow. Such an explanation would tend more to a thermal growth picture, but can also fit in incomplete

dissociation and thus more CH_3.
With toluene admixed with a small amount of CF_4 thin layers were deposited on cold rolled steel [30]. It appeared that the corrosion resistance of these layers is very promising. From these experiments is appears that a small admixture of fluorine containing gas is beneficial for the layer properties and leads to a smoother layer. This example again shows that the major hindrance in this field is a good picture of the growth process: it is still nearly impossible t[illegible]ict such a beneficial effect of F–admixture.

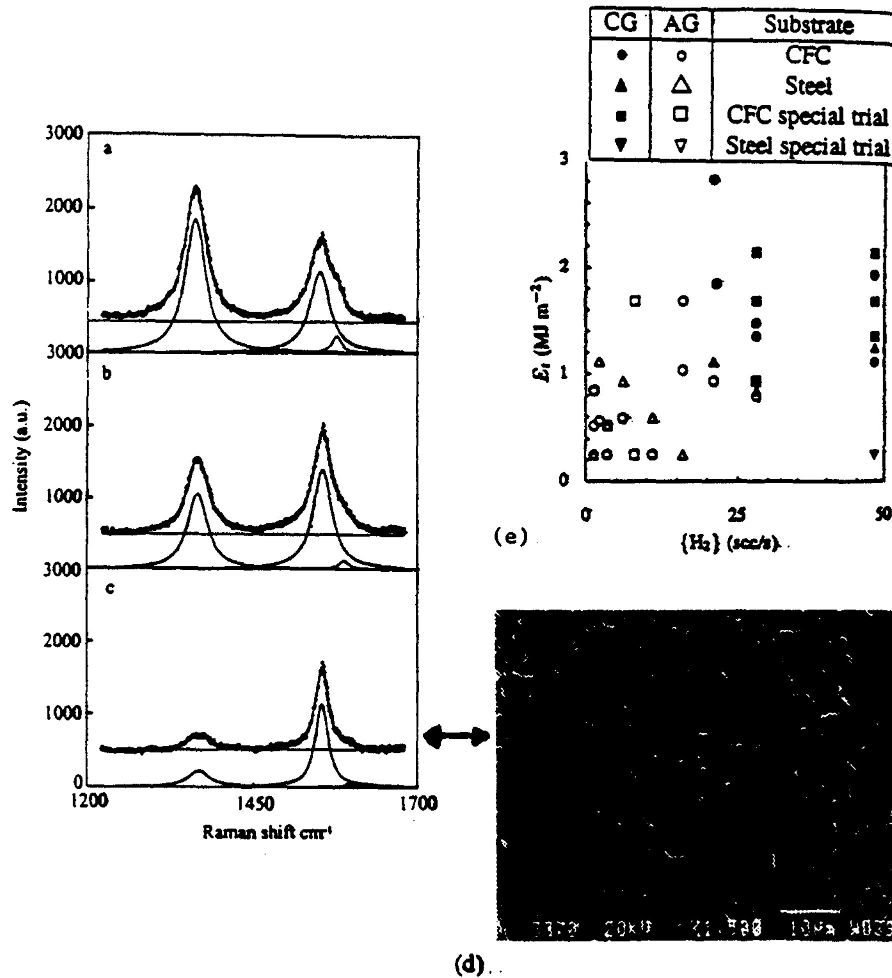

Figure 7. (a)–(c) Effect of increasing H_2 admixture on the Raman spectrum. with other reactor settings constant: $\{C_2H_2\}=1$; $P_{arc} \simeq 2.6$ kW; $p_c=10^3$ Pa; $T_{py} \simeq 840$ ^0C; increasing H_2 addition, 5, 10 and 20 scc/s respectively.
The Raman peak at 1355 cm^{-1} is called the defective graphite peak (DG), the one at 1581 cm^{-1} the graphite peak (G). Better material corresponds to a large G/DG ratio. (d) Micrograph of the film of (c). In (e) the erosion threshold for amorphous (open symbols) and crystalline (solid) graphite is shown as function of H_2 flow. (CFC denotes carbon fiber composites) From Buuron et al. [30], [31].

With the same method also crystalline layers as graphite and diamond can be deposited. Graphite is grown if the substrate temperature is above 600 ^{0}C with relatively large amounts of C_2H_2 (8 scc/s). Thick layers (up to 2 mm) were grown with deposition rates between 2 nm/s on 30 cm^2 up to 400 nm/s on 1 cm^2. The material (for divertor repair) has been tested on erosion threshold (cf. fig. 7) [31]. In fig. 7 the quality improvement of the graphite as measured with Raman spectroscopy with increased H_2 admixture (up to 20 scc/s) is also shown. With increasing H_2 admixture the graphite peak at 1581 cm^{-1} grows and narrows, whereas the defective graphite peak at 1355 cm^{-1} decreases. It is clearly an example of quality improvement with the addition of etchants, at the cost of deposition rate, which is a quite general feature of plasma deposition.

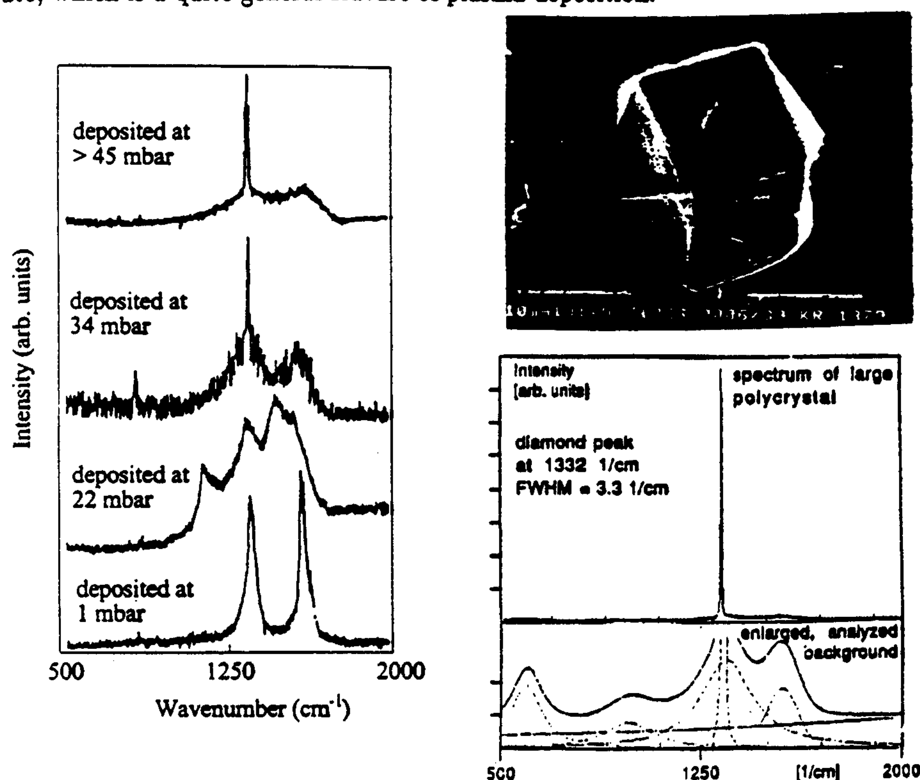

Figure 8. Raman spectra of diamond films deposited at different pressures. Note that the highest pressure film with the best Raman spectrum (diamond peak at 1332 cm^{-1} most prominent) grows also faster than the others. For comparison also a single crystal grown with the same method is shown with Raman spectrum from, Beulens [29], [32].

Diamond has been grown by various methods (hot filaments, flames, ECR plasmas, inductive coupled plasmas and thermal arcs). Again the fact that from this variety of methods similar qualities have been obtained points to a more thermal explanation of the growth process. Also with the expanding plasma beam diamond was successfully deposited. Essential are high etchant admixtures (H_2, O_2/H_2) and for CH_4/H_2 a high substrate temperature (1000 ^{0}C). In figure 8 results with Raman spectra for 3 ambient pressures are displayed. It is clear that higher pressure gives better quality in this case. The diamond Raman peak at 1332 cm^{-1} appears and becomes prominent at the highest pressure. At the same time the deposition rate increases to 10 nm/s with pressure because of the narrowing of the plasma beam with pressure [32]. It is another example of improvement of quality together with

improvement of rate.

To complete the section on deposition rate some words should be said about nucleation, cluster and dust formation in the plasma phase. Investigations in silane point to two phases: nucleation and first growth by negative ion (or cluster)–positive ion recombination agglomeration (up to 1–10 nm) and continued growth by association of radicals and monomers to the cluster [33]. Final size and dynamics depend on flow fields and electrostatic potentials. The clusters are negatively charged with charge number roughly proportional to the radius and the major forces are the electrostatic and drag forces. Clusters or powder influence the plasma state and offer an additional wall, probably at a high temperature. Powder may be detrimental e.g. for deposition; it may also be very usefull for the production of catalyst and ceramic powder. Also this aspect forms a very interesting and new area for the plasma physics community.

4. Plasma chemical conversion and waste destruction

Conversion processes and waste destruction processes require high throughputs to be economical and hence thermal plasmas at atmospheric pressure high power levels and high throughputs are common in this field [34]. Thermal plasmas have traditionally been used for plasma spraying, element analysis, C_2H_2 synthesis and for extractive metallurgy [35]. We will further shortly summarize waste destruction and effluent gas purification with plasma technology.
With plasma spraying injected ceramic or metallic powder is accelerated and heated by the plasma emanating from a high power DC plasma gun or from an inductively coupled plasma (ICP) and deposited on the workpiece. The material and energy efficiencies are high with corresponding high growth rates. The process has been investigated in detail [37] with plasma diagnostics and in flight analysis of velocity by laser anemometry and of particle temperature by pyrometry. The new development here is low pressure plasma spraying, with deposition in a lower pressure (0.1–0.3 bar) inert atmosphere. Inductively coupled plasmas (ICP) are used traditionally as excitation source for atomic emission/or ion mass spectromy) element analysis. Droplets are injected, evaporized and atomized in the inductively heated plasma; with emission spectroscopy or mass spectrometry the element concentrations of the sample (in the droplets) are measured with very high sensitivity (1–10 ppb).
Waste destruction is relevant for concentrated liquid organic waste, waste from manufacturing processes (e.g. metallic dusts) and low level radioactive waste. For the destruction of liquid organic waste commercial units exist [38] e.g. a 1 MW non–transferred plasma torch with two cylindrical electrodes which allows destruction of PCB's at a rate of 12 l/min (at 850 kW). The process is economical for intermediate amounts of waste, also as the processing unit is self contained and can be moved to the waste site. For larger amounts of waste, incineration is more economic. Combination of plasmas with thermal processing may be way to improve the economics of the total unit. Other technologies under investigation are transferred arcs also of high power combined with rotating furnaces in particular for metal scrap recovery.
Cleaning of effluent gas (De NOX/De SOX) by corona discharges [39], non–thermal plasmas at atmospheric pressure have been shown to be promising, in particular the pulsed negative corona and the silent discharge. Both types have already a history in effective and efficient ozon production.
In all these processes economics is a key factor, which also requires testing (after scaling) at high power levels. The field is still developing; a new development is the realisation that heterogeneous reactions on droplets or dust can be a key factor to reduce the energy cost per conversion and thus the economics of the process. In this area further research on cluster dynamics, electrostatic and drag forces and

(catalytic) heterogeneous reactions is necessary to investigate this promising line. It is again an example that plasma physics research needs to be complemented with flow dynamics and surface chemistry to fully exploit the potential in the field.

5. References

[1] Supano T 1985 *Applications of Plasma Processes to VLSI Technology* (New York: J Wiley)

[2] D'Agostino R *Plasma Deposition, Treatment and Etching of Polymers* (Academic Press)

[3] Shohet J L *Plasma–aided Manufacturing* p 47 in: *Industrial Applications of Plasma Physics, Int. School of Plasma Phys.*, Piero Caldirola, Varenna, 2–11 september 1992, Eds. Bonizzoni G, Hooke W and Sindoni E

[4] Luft W and Tsuo S 1993 *Hydrogenated Amorphous Silicon Alloy Deposition Process* (New York: M Dekker Inc.
cf. also *Materials for Photovoltaics* , 1993 October *MRS Bulletin*

[5] Lelevkin V M, Otorbaev D K and Schram D C 1992 *Physics of Non–Equilibrium Plasmas* (Amsterdam: North–Holland)

[6] Winters H F 1980 *Elementary Processes at Solid Surfaces Immersed in Low Pressure Plasmas* (In Topics in current Chemistry) *Plasma Chemistry III* 69
Senhorst H A J 1990 *Etching Studies in a Multiple–Beam Surface Experiment* (Eindhoven University of Technology thesis)

[7] Takahashi K, Hori M, Maruyama K, Kishimoto S and Goto T 1993 *Jpn. J. Appl. Phys.* **32** L694
Takahashi K, Hori M and Goto T 1993 *J. Appl. Phys.* **32** L1088
Kroesen G M W and Hoog De F J 1993 *Appl. Phys.* **A56** 479
Haverlag M 1991 *Plasma Chemistry of Fluorocarbon RF Discharges Used for Dry Etching* (Eindhoven University of Technology thesis)

[8] Edelson D and Flamm D 1984 *J. Appl. Phys.* **56** 1522

[9] Schram D C 1987 *Europhys. News* **18** 28
Schram D C, Hoog de F J, Bisschops T J and Kroesen G M W 1986 *Symp. Proc. SASP, Austria* p 181

[10] Tachibana K, Yuuki A and Matsui Y 1991 *Gaseous Electronics and its Appl., Tokyo* (KTK Kluwer) p 273
Kushner M J 1988 *J. Appl. Phys.* **63** 2532
Itabashi N, Nishiwaki N, Magane M, Goto T, Yamada C and Hirota E 1989 *Jpn. J. Appl. Phys.* **28** L325–328

[11] Perrin J et al. 1990 *Pure & Appl. Chem.* **62** 1681
Bruno G, Capezzuto P and Cicala G 1992 *Pure & Appl Chem.* **64**

[12] Haaland P and Targrove J 1992 *Appl. Phys. Lett.* **61** 34

[13] Veprek S and Verprek–Heijman M G J 1991 *Plasma Chem. Plasma Process* **11** 323; 1990 *Appl. Phys. Lett.* **56** 1766

[14] Bentsen A J M, Boogaard Van de M J, Sark Van W G J H M and Weg Van der W F 1992 *Mat. Res. Soc. Symp. Proc.* **258** 275
Howling A A, Dorier J L, Hollenstein Ch, Kroll U, and Finger F 1992 *J. Vac. Sci. Technol.* **A10** 1080
Matsuda 1993 *Growth Mechanisms and Control of Defects in the Deposition of a–Si:H* in ref 3 p 405

[15] Wilhelm A *Microwave plasmas for Surface Treatment and Thin Film Production* in ref 3 p 185

[16] Boswell R W *The History and Application of the Helicon Source to Plasma Processing* in ref 3 p 363

[17] Moisin M and Zakrewski 1991 *J. Appl, Phys.* **24** 1025

[18] Kroesen G M W, Timmermans C J and Schram D.C. 1988 *Pure & Appl. Chem.* 60 795–808
Buuron A J M, Meeusen G J, Beulens J J, Sanden Van de M C M and Schram D C 1993 *J. Nuclear Materials* 200 430
[19] Meeusen G J, Ershov Pavlov E A, Meulenbroeks R F G Sanden Van de M C M and Schram D C 1992 *J. Appl. Phys.* 71 9
[20] Veprek S, Patscheider J and Elmer J Th 1985 *Plasma Chem. Plasma Process* 5 201
Veprek S, Eckmann Ch and Elmer J Th 1988 *Plasma Chem. Plasma Process* 8 445
[21] Beulens J J, Wilbers A T M, Haverlag M, Oehrlein G S, Kroesen G M W and Schram D C 1992 *J. Vac. Sci. Technol.* 10 2387–2393
[22] Ricard A et al 1992 *Plasma Technology* (New York: Plenum Press)
[23] Graaf De M J, Severens R J, Sande Van de M J F, Meyer R, Kars H, Sanden Van de M C M and Schram D C 1993 *J. Nucl. Mat.* 380
Graaf De M J, Severens R J et al. to be published
[24] Graaf De M J, Meulenbroeks R F G, Sanden Van de M C M and Schram D C 1993 *Phys. Rev. E* 84 2098
Sanden Van de M C M., Regt De J M and Schram D C 1993 *Phys. Rev. E* 47 2792
[25] Dahiya R P, Graaf De M J, Severens R J, Swelsen H, Sanden Van de M C M and Schram D.C. 1994 *Phys Plasmas* 1 2086–2095
[26] Matsumoto O, Fujita T, and Uyama H 1989 *9th Int. Symp. on Plasma Chem., Pugnochioso* Proc. III p 1804
[27] Cathérine Y and Couderc P 1986 *Thin Solid Films* 144 265
[28] Möller W 1993 *Appl. Phys.* A56 527
[29] Beulens J J 1992 *Surface Modification Using a Cascade Arc Plasma Source* (Eindhoven University of Technology thesis)
[30] Buuron A J M 1993 *Plasma Deposition of Carbon Materials* (Eindhoven University of Technology thesis)
[31] Buuron A J M, Beulens J J, Schram D C, Groot P and Bakker J. 1989 *Thin Solid Films* 212 282
[32] Beulens J J, Buuron A J M and Schram D C 1991 *Surf. Coat. Technol.* 47 401
[33] Bouchoule A and Boufendi L 1993 *Plasma Sources Sci. Technol.* 2 204; 1994 *See also special issues: IEEE Trans. on Plasma Sci.* 22 2; 1994 *Plasma Sources* to appear
[34] Boulos M I 1991 *IEEE Trans. Plasma Sc.* 19 1078
[35] Drouet M G *High Temperature Processes for Industrial Waste Treatment and Valorisation* in ref 3 p 259
Akashi K 1985 *Pure Appl. Chem.* 57 1197
[36] Boulos M I *J.* 1993 *Thermal Spray Technol.* 1 33
[37] Fauchais P, Coudert J F and Vardelle M 1989 *Diagnostics in Thermal Plasma Processing* (New York: Academic Press); *Plasma Diagnostics* p 349
[38] Heberlein V R 1993 *Thermal Plasmas for the Destruction of Hazardeous Wastes* ref 3 p 219
[39] Rutgers W R 1993 *Proc. of 21e ICPIG, Bochum III* p 70
Civitano L and Sani E 1992 *DeNox, DeSOx Process by Gas Energization* (New York: Plenum Press); 1992 *Plasma Technol.* p 153